ABSTRACT

Title of dissertation: A STUDY OF EFFECTIVE THEORY APPROACHES TO PROBLEMS IN NUCLEAR PHYSICS

Panying Chen, Doctor of Philosophy, 2010

Dissertation directed by: Professor Xiangdong Ji
Department of Physics

The effective field theory is an efficient tool in dealing with physics involving separate scales. A typical effective field theory approach involves calculating the matching conditions for the desired parameters at some cutoff scale and obtain the renormalization group equation for the effective theory. In this thesis we study a collection of effective theories including the non-relativistic QED, the chiral perturbation theory, the soft-collinear effective theory, and their applications in nuclear physics.

We study the angular momentum operator in the non-relativistic QED (NRQED). We construct its gauge-invariant decomposition into spin and orbital angular momentum operators of electrons and photons and calculate the matching conditions of operators between QED and NRQED up to one loop. We perform the matching with both dimensional regularization and UV cutoff Λ. We apply the result in the Hydrogen-like system and calculate the radiation correction of the orbital angular momentum.

We study the CP-violating operators in chiral perturbation theory. We apply

our general, model-independent result onto the left-right symmetric model and relate the desired operator to the standard model penguin operators through $SU(3)_L \times SU(3)_R$ chiral symmetry. We use the lattice result for the standard model and acquire a more strict lower bound for the mass of right-hand boson in LRSM.

We study the polarized gluon distribution $\Delta g(x)$ in a longitudinally polarized proton. The first result from the MIT bag model as well as the non-relativistic quark model shows that $\Delta g(x)$ is positive at all x. The total gluon helicity ΔG from the bag model is about $0.3\hbar$ at the scale of 1 GeV, considerably smaller than previous theoretical expectations.

We study deep-inelastic scattering factorization on a nucleon in the end-point regime $x_B \sim 1 - \mathcal{O}(\Lambda_{\rm QCD}/Q)$ with an approach in soft-collinear effective theory. Refactorization of the scale $(1 - x_B)Q^2$ in the coefficient function can be made in the SCET and remains valid in the end-point regime. On the other hand, the traditional refactorization approach introduces the spurious scale $(1 - x_B)Q$ in various factors, which drives them nonperturbative in the region of our interest. We show how to improve the situation by introducing a rapidity cut-off scheme, and how to recover the effective theory refactorization by choosing appropriately the cut-off parameter. Through a one-loop calculation, we demonstrate explicitly that the proper soft subtractions must be made in the collinear matrix elements to avoid double counting.

A STUDY OF EFFECTIVE THEORY APPROACHES TO PROBLEMS IN NUCLEAR PHYSICS

by

Panying Chen

Dissertation submitted to the Faculty of the Graduate School of the
University of Maryland, College Park in partial fulfillment
of the requirements for the degree of
Doctor of Philosophy
2010

Advisory Committee:
Professor Xiangdong Ji, Chair/Advisor
Professor Elizabeth J. Beise
Professor Thomas D. Cohen
Professor Yang Tao
Professor Rabindra Mohapatra

ACKNOWLEDGEMENTS

First I would like to thank my advisor, Professor Xiangdong Ji. He is a great coach leading me on the way to adventure the physics world. His deep thoughts and broad knowledge are invaluable treasures for all his students, and I certainly benefit a lot from them. I would never finish this thesis without his guidance and encouragement.

I would like to thank my collaborators, Dr. Ahmad Idilbi, Dr. Yue Zhang and Dr. Hongwei Ke. The fun of doing physics is more than tripled with a good collaborator, and all of you certainly are.

There are many people around who have helped me during my years as a Ph.D student. Professor Tom Cohen and Professor Steve Wallace have cared for me and I would not forget that.

I would like to thank Loretta Rabinet for all the work she has done for me and for the whole group. Jane Hessing has saved me numerous times since the first day I came to this campus until the last minute before I handed in my dissertation, and I appreciate the help.

Last but not least, I would like to thank my wife, Melody Zhu. It is her love and support that gives me strength to surpass all the difficulties in my life.

Table of Contents

List of Figures v

1 Introduction 1
1.1 QCD and Its Lagrangian . . . 2
1.2 Non-Relativistic QED and Non-Relativistic QCD . . . 4
1.3 Chiral Perturbation Theory . . . 9
1.4 Spin Structure of the Proton . . . 14
1.5 Soft-Collinear Effective Theory . . . 19

2 A Decomposition of Angular Momentum Operator in Non-relativistic QED to Order α/m^2 24
2.1 Introduction . . . 24
2.2 NRQED . . . 26
2.3 Decomposition of angular momentum operator in QED . . . 27
2.4 Decomposition of Angular momentum operator in NRQED . . . 28
2.4.1 Conserved Current of NRQED Lagrangian . . . 28
2.4.2 Foldy-Wouthysen Transformation . . . 30
2.4.3 General Form of the Decomposed Operators . . . 32
2.4.4 Two-body Matching Conditions . . . 35
2.4.5 Three-body Matching Conditions . . . 41
2.4.6 Gauge Field Matching Conditions . . . 51
2.4.7 Separating QED and NRQED Cutoffs . . . 54
2.5 Application: Calculate Photon Angular Momentum in Hydrogen Atom at $\mathcal{O}(\alpha^3)$ . . . 58
2.6 Conclusions . . . 62

3 L-R model and chiral perturbation theory operators 63
3.1 Introduction . . . 63
3.2 Effective Operators from New Flavor Physics . . . 65
3.2.1 Standard Model Operators . . . 66
3.2.2 Dimension-5 and D-6 Operators . . . 68
3.2.3 Dimension-7 Operators . . . 72
3.2.3.1 $(\overline{15}, 3)$ . . . 73
3.2.3.2 $(\overline{3}, 15)$ . . . 75
3.2.3.3 $(6, 3)$ . . . 77
3.2.3.4 $(\overline{3}, \overline{6})$ . . . 78
3.3 Chiral Expansion at Leading Order . . . 79
3.3.1 ChPT and SM Operators . . . 80
3.3.2 Chiral Matching of New Operators . . . 84
3.3.3 Results at Tree Level . . . 86
3.4 Chiral Logarithms at One-Loop . . . 89
3.4.1 $K^0 \to Vacuum$ . . . 90
3.4.2 $K^+ \to \pi^+$ . . . 91

3.4.3 $K^0 \to \pi^0\pi^0$ . . . 92
3.5 An Application of the Effective Operators: Direct CP Violation in K-decay and Minimal Left-Right Symmetry Scale . . . 97
3.6 Conclusion . . . 105

4 Bag model and proton spin 107
4.1 Backgrounds and experiment status . . . 107
4.1.1 Parton helicity distributions . . . 107
4.1.1.1 Quark helicity distribution . . . 110
4.1.1.2 Gluon helicity distribution . . . 111
4.1.2 Experimental measurements . . . 114
4.2 A Bag model calculation . . . 117

5 SCET and Threshold Resummation 126
5.1 Introduction . . . 126
5.2 Validity of the standard QCD factorization at $x_B \sim 1 - \mathcal{O}(\Lambda_{\rm QCD}/Q)$ 128
5.3 Refactorization: Effective Theory Approach . . . 130
5.3.1 EFT Refactorization . . . 131
5.3.2 Collinear Contribution in SCET and Double Counting . . . 136
5.4 ReFactorization: Intuitive Approach . . . 137
5.4.1 Sterman's Method . . . 138
5.4.2 Alternative Regulator, Consistent Subtraction and Relation to SCET Factorization . . . 143
5.5 Summary . . . 149

A Noether Current with Higher Order Derivatives 151

B Leading Chiral-Logarithms in SM Operators 153

Bibliography 157

List of Figures

1.1 Coulomb-like photon exchanges between two particles in a bound state. 6

2.1 One-loop corrections to $\langle e|\mathbf{J}|e\rangle$ in QED. Here $\otimes$ can be either $\mathbf{L}_q$,$\mathbf{S}_q$, or $\mathbf{J}_\gamma$: (a) for $\mathbf{S}_q$; (a)(b) for $\mathbf{L}_q$; (c) for $\mathbf{J}_\gamma$. Wave function renormalization diagrams, mass counterterms and the mirror diagrams are not shown explicitly. . . . 39
2.2 QED tree diagrams . . . 42
2.3 NRQED tree diagrams . . . 45
2.4 One-loop contributions to $\langle e|\mathbf{J}|e\gamma\rangle$ in QED. Here $\otimes$ can be either $\mathbf{L}_q$,$\mathbf{S}_q$, or $\mathbf{J}_\gamma$: (a)-(i) for $\mathbf{L}_q$; (b)(d)(g)(i) for $\mathbf{S}_q$; (j)(k) for $\mathbf{J}_\gamma$. Wave function renormalization diagrams, mass counter terms and the mirror diagrams are not shown explicitly. . . . 47
2.5 One-loop contributions to $\langle\gamma|\mathbf{J}|\gamma\rangle$ in QED. Mirror diagrams are not shown. (a) for $\hat{S}_q$; (a)(b) for $\hat{L}_q$; (c) for $\hat{J}_\gamma$. . . . 51
2.6 One-loop corrections to $\langle e|\mathbf{L}_q^{\rm eff}|e\mathbf{A}\rangle$, (a)-(f), and $\langle e|\mathbf{J}_\gamma^{\rm eff}|e\mathbf{A}\rangle$, (g)-(k), in NRQED. . . . 56
2.7 Leading ($\mathcal{O}(\alpha_{\rm em}^2)$) electromagnetic contribution to the spin of the Coulomb-bound electron . . . 59
2.8 a) Next-to-leading order ($\mathcal{O}(\alpha_{\rm em}^3)$) EM contribution to the spin of the Coulomb-bound electron, b) subtraction needed to define the physical contribution. . . . 60
2.9 First-order expansion of EM contribution to the spin in an external Coulomb field, in the hard momentum region. . . . 61

3.1 Dimension-5 effective operators generated from the weak-interaction vertex corrections in SM (left) and in LRSM (right). The crosses on fermion lines represent mass insertion, needed to flip the chirality of the quarks. . . . 69
3.2 Feynman diagrams generating dimension-6 quark operators in SM and LRSM. . . . 70
3.3 Feynman diagrams generating scalar quark interactions through neutral-current Higgs exchanges. . . . 72
3.4 Feynman diagram for $K^0 \to$ *Vacuum* at one loop. . . . 90
3.5 Feynman diagrams for $K^+ \to \pi^+$ at one loop. . . . 92
3.6 Feynman diagrams for $K^0 \to \pi^0\pi^0$ at one loop. . . . 92
3.7 New tree-level contributions to the $\Delta S = 1$ interaction from LRSM. . 99
3.8 The new contribution in LRSM to ϵ' . . . 104

4.1 The photon-gluon scattering diagram . . . 108
4.2 The polarized gluon distributions are shown at Q^2=1 GeV^2. The uncertainty ranges are shown by the shaded band, the dotted curves, and thin solid curves for the type 1, 2 and 3, respectively.[106] . . . 111
4.3 Direct photon productions . . . 113

4.4 Current $g_1(x)$ result by various experiments[106] 114
4.5 Schematic diagram of HERMES spectrometer[13] 116
4.6 The center-of-mass energy vs. luminosity of the proposed Electron-Ion Collider eRHIC compared to other lepton scattering facilities.[14] 117
4.7 One-body and two-body contributions to the matrix element of the polarized gluon operator in the quark models of the proton. 121
4.8 $\Delta g(x)$ and $x\Delta g(x)$ calculated in the MIT bag model. 125
4.9 $x\Delta g(x)$ calculated in non-relativistic quark model by summing contributions from s, p, d, and f waves. The thin solid line is the MIT bag model result. 125

5.1 The leading reduced diagram contributing to the deep-inelastic structure function in $x \to 1$ regime. 139

Chapter 1

Introduction

The modern nuclear physics starts from Rutherford's remarkable experiment[1]. After discovering the alpha particle has a small chance to bounce back from the thin gold film, Rutherford correctly proposed the idea that there is a heavy dense particle in the center of the atom, in contrast to J.J.Thompson's pudding model. Later it was found that the atom has three building blocks, the proton, the neutron and the electron. At the time, those were named fundamental particles.

People began studying the quark model in the 1960s. At the time, many new particles were found by the accelerator and the meaning of the name "fundamental particle" became less clear, since in contrast to the three particles people learned before, these new particles have a much shorter lifetime. In 1964, Gell-Mann and Zweig independently proposed a model that the baryons and mesons are constructed by some smaller building blocks, by which Gell-Mann called quarks[2]. In the quark model, there exists an $SU(3)$ flavor symmetry; baryons and mesons are categorized into different representations of the $SU(3)_f$ group. The quantum numbers and masses of those hadrons inside the same representation is related by Gell-Mann−Nishijima formula. The model has an initial success but meets difficulties when trying to explain the component of Δ^{++} particle. By quark model it is consisted of three spin-up u quarks at ground state, which violates the Fermi-

Dirac statistics. In 1965, Han, Nambu and Greenberg independently proposed an idea that there is another $SU(3)$ gauge degree of freedom in the theory and the quark should possess a new quantum number called color. They further speculated that the quarks inside the hadrons are real particles and interact via an octet of vector gauge bosons, the gluons. In the mean time, the deep-inelastic scattering experiment in SLAC shows that there exists point-like particles inside the proton. Feynman proposed a model in which he called those point-like particles partons and explained the experiment data beautifully. In 1973, Gross, Wilczek and Politzer discovered the asymptotic freedom properties of QCD. The discovery connected the parton model with QCD and provided a strong proof of the verification of QCD at high energies. It is now clear that the partons in Feynman's parton model is indeed quarks and gluons in QCD.

1.1 QCD and Its Lagrangian

Quantum chromodynamics (QCD) is by far the most successful model to describe the strong interactions. The two major properties of QCD, confinement and asymptotic freedom, has been observed in numerous nuclear and hadronic physics experiments and are crucial in understanding the hadronic physics.

QCD is a gauge theory with a local $SU(3)_C$ symmetry. The Lagrangian is:

$$\mathcal{L}_{\text{QCD}} = \sum_f \bar{\psi}_f (i\not{D} - m)\psi_f - \frac{1}{4} G^{a,\mu\nu} G^a_{\mu\nu} \tag{1.1}$$

where ψ and $\bar{\psi}$ are the quark fields summing over all color degree of freedom. $D^\mu \equiv \partial^\mu - igT^a A^{\mu,a}$ is the covariant derivative. Here T^as are the generators of $SU(3)$

fundamental representation with normalization:

$$\mathrm{Tr}[T^a T^b] = \frac{1}{2}\delta^{ab}. \tag{1.2}$$

$G^a_{\mu\nu}$ is the field strength tensor. It lives in the adjoint representation of $SU(3)$ and has $3^2 - 1 = 8$ colors: the index a runs through it. It can be easily shown that the Lagrangian is invariant under a local gauge transformation:

$$\begin{aligned} \psi(x) &\rightarrow \hat{U}\psi(x) \\ A^a_\mu &\rightarrow \hat{U}A^a_\mu\hat{U}^\dagger - \frac{i}{g}\hat{U}\partial_\mu\hat{U}^\dagger, \end{aligned} \tag{1.3}$$

in which $\hat{U} \equiv e^{i\alpha(x)^a t^a}$ is a local $SU(3)_C$ color transformation.

The gluon field strength tensor is defined as

$$G^a_{\mu\nu}T^a \equiv \frac{i}{g}[D_\mu, D_\nu]. \tag{1.4}$$

By working out the algebra we can get the explicit form of the field strength tensor:

$$G^a_{\mu\nu} = \partial_\mu A^a_\nu - \partial_\nu A^a_\mu + g f^{abc} A^b_\mu A^c_\nu \tag{1.5}$$

in which f^{abc} is the structure constant of the Lie algebra from $SU(3)$.

The QCD contains a coupling constant $\alpha_s \equiv g^2/4\pi$ and it is a function of the renormalization scale. Under dimensional regularization and modified minimum subtraction scheme ($\overline{\mathrm{MS}}$) we will have (up to the first order of α_s):

$$\frac{d\ln\alpha_s(\mu^2)}{d\ln\mu^2} = \beta_0\alpha_s/4\pi + \mathcal{O}(\alpha_s^2) \tag{1.6}$$

where

$$\beta_0 = -\frac{11}{3}C_A + \frac{2}{3}N_f. \tag{1.7}$$

C_A is the Casimirs of the adjoint representations. For $SU(3)$, $C_A = 3$. N_f is the number of independent quarks in the theory. So far it is believed that there exists six quarks, hence $N_f = 6$ for the high energy. At lower energies, the heavy quark modes decouple from the theory and N_f has to be adjusted. Therefore, we have $\beta_0 < 0$, which means that α_s will become smaller when the energy scale μ gets larger. This is the effect of asymptotic freedom and it can be directly observed by the deep inelastic scattering process.

By solving the differential equation we can derive:

$$\alpha_s(\mu^2) = \frac{4\pi}{(11 - \frac{2}{3}N_f)\ln(\mu^2/\Lambda^2_{\rm QCD})}. \tag{1.8}$$

Here we have introduced the $\Lambda_{\rm QCD}$ parameter. It is a function of the renormalization scale. As one can see, the physics at or below $\Lambda_{\rm QCD}$ will become non-perturbative. Based on the current phenomenological observations we have a crude estimation of $\Lambda_{\rm QCD} \approx 200$MeV with $\overline{MS}$ scheme. Since the equation (1.8) is derived by a one-loop expansion in QCD it would only be held at the scale where α_s is small. Eqation (1.8) reflects the confinement property of the theory.

1.2 Non-Relativistic QED and Non-Relativistic QCD

The history of quantum mechanics starts from the understanding of a bound state, the Hydrogen atom, in a non-relativistic picture. After that, many high-energy processes have been studied with the hope to figure out the fundamental structures of our world. Relativistic quantum field theories, such as QED and QCD, have been proposed to describe the high-energy processes and are well tested. QED even

remains to be the most stringently tested theory in physics up to the time.

However, there remains a handful of processes in the high-energy region involving non-relativistic bound states. For example, the famous J/ψ, being independently discovered by two groups at Brookhaven and SLAC in 1974, is indeed a bound state of the then newly discovered heavy quark charm (c) and its antiparticle $\bar{c}$. Later on people would call it a "charmonium" state and a general name "quarkonium" for all the heavy quark-antiquark pair bound states. In 1977 bottomonium was produced at Fermilab. Lastly, the heaviest of the quarks, the top quark, was found at the Tevatron in 1995. The top quark decays too fast to form a bound state, however. All these systems are denoted as heavy quarkonia and are characterized by the heavy quark mass and the small speed of the quark relative to the speed of light. The very heavy mass of the quarks are much larger than the QCD hadronic scale Λ_{QCD}, and hence made the application of perturbative expansion in QCD possible. However, there exists lower scales in the system such as the momentum $\mathbf{P}$ and the kinetic energy E, which may or may not be much larger than the Λ_{QCD} and makes solving the dynamics of the heavy quarkonia extremely difficult.

On the other side of the spectrum, the precision tests of QED, in the hopes to see the trace of new physics, call for very high-order theoretical calculations of the muonium energy eigenstates, which is made up of an antimuon and an electron. A frequently measured quantity is the Lamb shift of the muonium. It was first calculated by Bethe in 1947 with a formalism now called Bethe-Salpeter equations. Unfortunately, in a non-relativistic bound state the higher-order corrections of Bethe-Salpeter equations with a perturbative QED expansion is prohibitively hard.

The reason that the traditional perturbative expansion cannot be directly applied to a bound state system is that the perturbative expansion might not produce a converging series at low energy scales, especially for the Coulomb-like photon (gluon) exchange. For example, consider a Coulomb interaction between two heavy quarks:

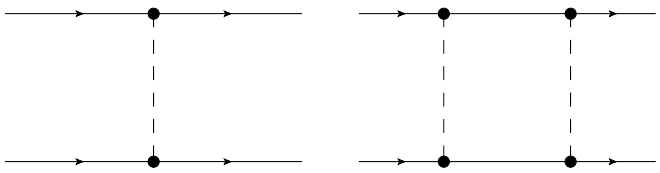

Figure 1.1: Coulomb-like photon exchanges between two particles in a bound state.

The expansion parameter is $\alpha_s/2\pi$ or $\alpha_{\rm em}/2\pi$, depending on whether it is a QCD or a QED system. The typical momentum exchange in a bound state is $\mathbf{k} \sim \mathbf{p} \sim \alpha m$, and for the inner line of the heavy quark (electron) propagator, it is $S_F(p+\mathbf{k}) \sim \frac{\not{p}+\not{k}+m}{(p+\mathbf{k})^2-m^2} \sim 1/(m\alpha^2)$. Therefore, for each added Coulomb photon loop we have the total amplitude:

$$I_{n+1} \sim I_n \times e^2 \int \frac{d^3\mathbf{k}}{(2\pi)^3} \frac{1}{\mathbf{k}^2} \frac{1}{(p+\mathbf{k})^2 - m^2} \sim I_n \times e^2 \frac{m\alpha}{m\alpha^2} \sim I_n, \qquad (1.9)$$

and the expansion fails.

In the 1980's an effective theory to handle the bound state problem have emerged[18][20]. The now-called non-relativistic QED (NRQED), as well as its QCD version NRQCD, is obtained from QED (QCD) by integrating out the hard scale m while maintaining a power counting of $\mathbf{v} \sim \mathbf{p}/m$ below m in the effective Lagrangian. There are three typical momentum scales in the effective theory: m, mv, mv^2;

v being the heavy quark (electron) velocity with $v \ll 1$ being understood. In NRQCD we would further demand $m \gg mv \gg mv^2 \gg \Lambda_{QCD}$. Therefore NRQCD is preferably applied on heavy quark systems such as top-antitop pair production and bottomonium physics.

For a simple review, we will introduce the basic idea and Feynman rules of NRQED here. The NRQED Lagrangian reads,

$$\begin{aligned}\mathcal{L}_{\rm NRQED} &= \psi^\dagger \Bigg\{ iD^0 + c_2 \frac{\mathbf{D}^2}{2m} + c_4 \frac{\mathbf{D}^4}{8m^3} + \frac{e\, c_F}{2m} \boldsymbol{\sigma} \cdot \mathbf{B} + \frac{e\, c_D}{8m^2} [\boldsymbol{\nabla} \cdot \mathbf{E}] \\ &\quad + \frac{ie\, c_S}{8m^2} \boldsymbol{\sigma} \cdot (\mathbf{D} \times \mathbf{E} - \mathbf{E} \times \mathbf{D}) \Bigg\} \psi \\ &\quad + d_1 F_{\mu\nu} F^{\mu\nu} + \frac{d_2}{m^2} F_{\mu\nu} \Box F^{\mu\nu} + \mathcal{L}_{4-\rm Fermi} + \ldots \end{aligned} \tag{1.10}$$

where ψ is the two-component electron spinor, E and B are the electronic and magnetic field of the photon. The Lagrangian is similar to another effective theory, the heavy quark effective theory (HQET). The difference is that in NRQED one must treat $D^0 \sim \mathbf{D}^2/2m$ and keep both of them in the Greens function, since in a bound state they are of the same order, $E \sim p^2/2m \sim mv^2$. Therefore the electron propagator will be different than the heavy quark operator in HQET:

$$S_F(E_p, \mathbf{p})_{\rm NRQED} = \frac{i}{E_p - \mathbf{p}^2/2m + i0}. \tag{1.11}$$

The original construction of NRQED has several caveats, though. It is realized that the photon field in the Lagrangian describes all fluctuations of frequencies below m. However, there exists two low scales in the theory: the kinetic energy of the heavy fermion $E \sim mv^2$, and the 3-momentum of the fermion $\mathbf{p} \sim mv$. The NRQE(C)D Lagrangian and its Feynman rules do not provide a clear distinction between various

contributions coming from different momentum regions. Manohar argued that under dimensional regularization this will lead to inconsistencies of power counting[23]. It can be shown by a one-loop self-energy diagram for an electron. For simplicity we will use Feynman gauge here. Taking the external electron on shell, the loop integral has the form:

$$\begin{aligned} I &\sim \int \frac{d_k^d}{(k_0^2 - \mathbf{k}^2 + i0)(E_q + k^0 - \frac{(\mathbf{p}+\mathbf{k})^2}{2m} + i0)} \\ &= \int \frac{d_k^d}{(k_0^2 - \mathbf{k}^2 + i0)(k^0 - \frac{\mathbf{k}^2+2\mathbf{p}\cdot\mathbf{k}}{2m} + i0)}. \end{aligned} \tag{1.12}$$

Finishing the contour integral for the k_0 integration and taking the pole at $k_0 = -|\mathbf{k}| + i0$, the integral will be proportional to

$$\int \frac{d^{d-1}k}{|\mathbf{k}|(2m|\mathbf{k}| + \mathbf{k}^2 + 2\mathbf{p}\cdot\mathbf{k})}. \tag{1.13}$$

Since $\mathbf{p} \ll m$, the integral will be dominated by hard momenta $\mathbf{k} \sim m$. However, the NRQED is constructed by integrating out all the hard modes at $\mathcal{O}m$. Therefore the power counting is broken, as the physics at different scales are mixed within one diagram. A three-momentum cutoff can render the problem by putting a cutoff scale $\Lambda \ll m$ yet $\Lambda \gg mv$, but it is cumbersome in calculation and explicitly breaks gauge symmetry; hence it cannot be used in NRQCD.

It is argued that the dimensional regularization can be saved by treating the term $\mathbf{D}^2/2m$ in the Greens function as a perturbation and taking an expansion in powers of $1/m$ in (1.12) before finishing the integral[23]. Labelle[22] pointed out that the Greens function from the effective theory has to be understood as a multipole expansion, in which each expanded part has its own consistent power counting (mv,

mv^2, etc). Later on it is shown that Labelle's multipole expansion method can be understood as a generalization of the $1/m$ expansion[24]. Finally the NRQE(C)D has to be written in terms of a Schrödinger theory with potentials and calculate as a time-independent perturbation theory.

All these problems inspire people to develop new effective theories based on NRQE(C)D. To date people have constructed two lower energy effective theories, namely "potential NRQCD" (pNRQCD)[29] and "velocity NRQCD" (vNRQCD)[30]. In those theories the scales are completely separated at Lagrangian level and a systematical way of running and resummation of large logarithms is established. Reviews of these two effective theories can be found in [31]. In this thesis, we will restrict ourselves within the scope of the "traditional" NRQED scheme.

1.3 Chiral Perturbation Theory

Chiral perturbation theory (ChPT) is an effective theory often used in the context of weak decays. It describes QCD at low energy, where QCD becomes non-perturbative. The idea is that at low energy the degrees of freedom is no longer single quarks and gluons, but rather hadrons, due to the QCD confinement effect. In ChPT the propagating fields are baryons and mesons, and their interactions are determined by the symmetry of the underlying QCD.

The chiral perturbation theory starts from the observation that, if we neglect the masses of three light quarks, namely u, d and s, we should achieve an $SU(3)_L \times$

$SU(3)_R$ symmetry. This can be read from the quark Lagrangian:

$$\bar{\psi} i \not{D} \psi \to \bar{\psi}_L i \not{D} \psi_L + \bar{\psi}_R i \not{D} \psi_R. \tag{1.14}$$

Here $\psi_L \equiv \frac{1-\gamma^5}{2}\psi$, $\psi_R \equiv \frac{1+\gamma^5}{2}\psi$.

If this $SU(3)_L \times SU(3)_R$ were realized in the real world, all the known hadron states would have their corresponding parity counterparts. In reality, however, only an (approximated) $SU(3)$ flavor symmetry is observed, without the parity doubling. The logical consequence is that one of the $SU(3)$ groups has broken spontaneously. By Nambu-Goldstone theorem this will produce a set of massless, spinless Goldstone bosons in the theory, with the number of them equal to the number of generators of the broken symmetry. At here what we are expecting is the spontaneous symmetry breaking $SU(3)_L \times SU(3)_R \to SU(3)_V$, where $SU(3)_V$ is the vector subgroup of $SU(3)_L \times SU(3)_R$, and the broken axial vector subgroup, $SU(3)_A$, would produce an octet of massless Goldstone bosons as pseudoscalar particles. Indeed we have the light pseudoscalar pions and kaons in an octet state. They are not massless, however, and the masses can be related to the light quark masses manifestly appearing in the QCD Lagrangian and breaking the $SU(3)_L \times SU(3)_R$ symmetry. These masses are still small compared with the typical hadronic scales such as the proton mass or the ρ meson mass: $m_\pi \sim 140$MeV, $m_K \sim 500$MeV and $m_\eta \sim 540$MeV, while $m_\rho \sim 770$MeV and $m_p \sim m_n \sim 940$MeV.

Now that we know the pions are the Goldstone bosons from the broken axial vector group, we have the current algebra:

$$\langle 0 | \bar{q}_i \gamma^\mu \gamma^5 T^a_{ij} q_j | \pi^b(p) \rangle = i f_\pi \delta^{ab} p^\mu, \tag{1.15}$$

in which a,b are indices of the octet, and the q_i can be u, d or s. The f_π is the pion decay constant, $f_\pi \approx 135$MeV, which can be determined by the decay of $\pi_\pm$ into a muon and a neutrino.

The spontaneous symmetry breaking of the $SU(3)_L \times SU(3)_R$ symmetry in QCD indicates that the QCD vacuum in not invariant under such symmetry. It can be observed by the fact that the composite operator $\bar{q}q$ has a vacuum expectation value (vev):

$$\langle 0|\bar{q}q|0\rangle \neq 0. \tag{1.16}$$

It is called the quark condensate, or the chiral condensate, in QCD. It can be related to the mass of the light quark, as it will be seen.

We may write down an effective theory based on the underlying $SU(3)_L \times SU(3)_R$ symmetry by defining a field Σ with the transformation property

$$\Sigma \to L\Sigma R^\dagger, \tag{1.17}$$

in which $L \in SU(3)_L$ and $R \in SU(3)_R$. The simplest $SU(3)_L \times SU(3)_R$ invariant Lagrangian is given by

$$\mathcal{L} = \frac{f^2}{8}\mathrm{Tr}\left[(\partial_\mu \Sigma)^\dagger(\partial^\mu \Sigma)\right] \tag{1.18}$$

where f is some constant with dimension of mass and will be determined later. We can require $\langle 0|\Sigma|0\rangle = 1$ as it will spontaneously break the $SU(3)_L \times SU(3)_R$ symmetry. Therefore we can define the field Σ in terms of the Goldstone bosons in the theory. In this thesis we will use the nonlinear sigma model:

$$\Sigma \equiv \exp\left(\frac{2i\phi}{f}\right) \tag{1.19}$$

where ϕ is the Goldstone meson matrix

$$\phi = \begin{pmatrix} \frac{\pi^0}{\sqrt{2}} + \frac{\eta}{\sqrt{6}} & \pi^+ & K^+ \\ \pi^- & -\frac{\pi^0}{\sqrt{2}} + \frac{\eta}{\sqrt{6}} & K^0 \\ K^- & \overline{K^0} & -\sqrt{\frac{2}{3}}\eta \end{pmatrix}. \tag{1.20}$$

Hence the dynamics of QCD will be determined by the Goldstone modes. For weak decays we can add $\mathcal{L}_w$ into the (1.18) describing the non-leptonic weak interactions between quark fields.

With (1.18) and (1.19) we can readily calculate the vector current and axial current from Noether's theorem. It reads,

$$V_\mu^a = if^{abc}[\pi^b, \partial_\mu \pi^c] + \mathcal{O}(f^{-1}), \quad A_\mu^a = if\partial_\mu \pi^a + \mathcal{O}(f^{-1}). \tag{1.21}$$

Comparing A_μ with (1.15), we can deduce $f = f_\pi \approx 135\text{MeV}$.

Once considering the explicit breaking of the $SU(3)_L \times SU(3)_R$ symmetry by small quark mass terms in the QCD Lagrangian, we should include an explicit mass term $M \equiv \text{diag}(m_u, m_d, m_s)$ in the ChPT effective Lagrangian as well. Now the complete ChPT Lagrangian would look like:

$$\mathcal{L}_{\chi PT} = \frac{f^2}{8}\text{Tr}\left[(\partial_\mu \Sigma)^\dagger (\partial^\mu \Sigma)\right] + \frac{v}{2}\text{Tr}[M\Sigma + (M\Sigma)^\dagger] + \mathcal{L}_w \tag{1.22}$$

We would like to keep the invariance of $\mathcal{L}_{\chi PT}$ under the $SU(3)_L \times SU(3)_R$ transformation. We can achieve this by demanding the mass term satisfying the transformation property

$$M \to RML^\dagger \tag{1.23}$$

By expanding Σ to the second order we can obtain the mass matrix of the pion

fields and get the relationship between pion and quark mass:

$$m^2_{\pi^0,\pi^\pm} = \frac{4v}{f^2}(m_u + m_d), \quad m^2_{K^\pm} = \frac{4v}{f^2}(m_u + m_s),$$
$$m^2_{K^0,\overline{K^0}} = \frac{4v}{f^2}(m_d + m_s), \quad m^2_\eta = \frac{4v}{3f^2}(m_u + m_d + 4m_s). \tag{1.24}$$

We can eliminate the quark masses and get the famous Gell-Mann−Okubo mass relations for the meson octet:

$$\frac{1}{2}\left[(m_{K^-} + m_{\overline{K^0}})^2 + (m_{K^+} + m_{K^0})^2\right] = 3m^2_\eta + \frac{1}{9}(m_{\pi^0} + m_{\pi^+} + m_{\pi^-})^2 \tag{1.25}$$

Now we can calculate the vacuum expectation value of $\bar{q}q$ under the framework of ChPT:

$$\langle 0|\bar{q}q|0\rangle = -4v \tag{1.26}$$

Therefore to keep the meson mass real the quark condensate has to be negative.

It should be pointed out that the matching process chiral perturbation theory is not the same as the NRQED, or SCET which we will discuss in the next section. As an effective theory describing the dynamics of QCD at low energy, ChPT should be matched to QCD at some intermediate scale where is the limit of ChPT. Naturally it will be the expansion parameter f_π in ChPT. However, it is related to the lower cutoff scale Λ_{QCD} of QCD, below which the perturbative expansion is not valid. Therefore the matching cannot be done in a perturbative manner and we must resort to non-perturbative methods of QCD, such as lattice calculation, to achieve the matching.

1.4 Spin Structure of the Proton

The spin structure of the nucleon has been intensely studied since the EMC experiment[36]. In the experiment people fired muons at polarized protons, and the data showed that the origin of the proton spin cannot be well explained by the naive quark model, which is the so-called "spin crisis". Over years many effects have been made both theoretically and experimentally. However, due to some technical difficulties in both experiment and theoretical calculations, the problem is far from being well understood and there are still a lot of open questions in this field.

To begin with, we have a simple sum rule for the intrinsic spin of the nucleon based on a constituent picture of the nucleon:

$$J_z^N = \frac{1}{2}\Delta\Sigma + \Delta G + L_q + L_g = \frac{1}{2}. \tag{1.27}$$

The $\frac{1}{2}\Delta\Sigma$ and ΔG correspond to the intrinsic angular momentum for quarks and the gluons inside the neutron, respectively; while the L_q and L_g stand for the orbital angular momentum for quarks and gluons.

The $SU(6)$ quark model has been thought to be quite successful since it predicted the magnetic moment of the nucleons pretty well. Therefore people were expecting that it would also well explain the spin structure of the nucleon. In this model all the spin momentum of the nucleon is carried by the constituent quarks (e.g. $\Delta\Sigma = 1$ and $\Delta G = L_q = L_g = 0$). The first measurement of the spin-dependent proton structure function $\Gamma_1^p \equiv \int_0^1 g_1^p(x)dx$ was made by SLAC in 1983[3]. The result they obtained is 0.17 ± 0.05, which agrees with the prediction of the Ellis-Jaffe sum rule[5], which is 0.171 ± 0.006. The latter is based on the SU(6) model and the

assumption of vanishing strange-sea polarization. The polarized gluon contribution was thought to be a higher correction at that time.

In 1987 the EMC experiment was using polarized muon as the probe and thus had a kinematic region in $x < 0.2$ which was not covered by the SLAC experiment[4]. The result came to be a surprise. They obtained a substantially smaller result, $\Gamma_1^p = 0.126 \pm 0.018$, which indicates that the quarks contribute very little to the total proton spin (around 20%). The "missing" part of the spin inside the proton cannot be explained by the $SU(6)$ model. After that, the spin structure has become a hot topic and a number of experiments have been built in the hopes to probe the spin structure of the nucleon.

Consider the scattering of a high-energy charged lepton off a hadron target. In the laboratory frame the differential cross section has the form:

$$\frac{d^2\sigma}{d\omega dE'} = \frac{1}{2M}\frac{\alpha^2}{q^4}\frac{E'}{E}L_{\mu\nu}W^{\mu\nu} \tag{1.28}$$

$L_{\mu\nu}$ and $W_{\mu\nu}$ are the leptonic and hadronic tensor, respectively. If we neglect the weak interaction but keep the scattered hadron polarized, considering all the constraints as gauge invariance, Lorentz covariance and Gorgon identity, the most general expression of $W^{\mu\nu}$ can be written as

$$\begin{aligned} W_{\mu\nu} &= W^S_{\mu\nu} + W^A_{\mu\nu} \\ &= F_1\left(-g_{\mu\nu} + \frac{q_\mu q_\nu}{q^2}\right) + \frac{F_2}{p\cdot q}\left(p_\mu - \frac{p\cdot q}{q^2}q_\mu\right)\left(p_\nu - \frac{p\cdot q}{q^2}q_\nu\right) \\ &\quad + i\frac{M}{p\cdot q}\epsilon_{\mu\nu\rho\sigma}q^\rho\left[s^\sigma g_1 + \left(s^\sigma - \frac{s\cdot q}{p\cdot q}p^\sigma\right)g_2\right] \end{aligned} \tag{1.29}$$

The first part, $W^S_{\mu\nu}$ containing F_1 and F_2, is the usual part of the spin-independent structure function; the second part, $W^A_{\mu\nu}$ containing g_1 and g_2, is the spin dependent

part of the structure function. All F_1, F_2, g_1, g_2 are functions of Bjorken x and energy scale $Q^2 = -q^2$.

We can calculate the spin-dependent $eq \to eq$ scattering cross section in a naive quark model. The result gives:

$$\begin{aligned} F_1(x) &= \frac{1}{2}\sum_q e_q^2[q(x) + \bar{q}(x)], \\ F_2(x) &= 2xF_1(x), \\ g_1(x) &= \frac{1}{2}\sum_q e_q^2[\Delta q(x) + \Delta\bar{q}(x)], \\ g_2(x) &= 0; \end{aligned} \tag{1.30}$$

where

$$q = q^{\uparrow} + q^{\downarrow}, \qquad \Delta q = q^{\uparrow} - q^{\downarrow}. \tag{1.31}$$

The sum is over u, d, s for three active quark flavors and the scaling is conserved in this naive parton model. The first two equations in (1.30) are the familiar Callan-Gross relation; the second two equations are a simple physical explanation to the spin-dependent structure functions g_1 and g_2 in the naive parton model. Notice that the $g_2 = 0$ in this model, which is generally not true. However, both physical interpretation and experimental measurement for g_2 are hard to achieve partially due to it being a higher twist contribution.

We can define the first moment of $g_1(x)$ and the quark distributions as:

$$\Gamma_1 \equiv \int_0^1 g_1(x)dx = \int_0^1 \frac{1}{2}\sum_q e_q^2[\Delta q(x) \quad + \quad \Delta\bar{q}(x)]dx = \frac{1}{2}\sum_q e_q^2[\Delta q + \Delta\bar{q}],$$

$$\Delta q \equiv \int_0^1 \Delta q(x)dx, \qquad \Delta\bar{q} \equiv \int_0^1 \Delta\bar{q}(x)dx. \tag{1.32}$$

With $SU(3)_f$ symmetry we can define the nucleon axial charges:

$$\begin{aligned} a_0 &= (\Delta u + \Delta\bar{u}) + (\Delta d + \Delta\bar{d}) + (\Delta s + \Delta\bar{s}) \\ a_3 &= (\Delta u + \Delta\bar{u}) - (\Delta d + \Delta\bar{d}) \\ a_8 &= (\Delta u + \Delta\bar{u}) + (\Delta d + \Delta\bar{d}) - 2(\Delta s + \Delta\bar{s}) \end{aligned} \tag{1.33}$$

Under these assumptions we have several sum rules, namely *Ellis-Jaffe sum rule*[5] and *Bjorken sum rule*[6].

In the Ellis-Jaffe sum rule it is assumed that the strange quark and sea polarizations are zero ($\Delta s = \Delta\bar{q}_i = 0$). Then from (1.33) we have $a_0 = a_8$ and

$$\Gamma_1^{p,n} = \frac{1}{9}a_0 \pm \frac{1}{12}a_3 + \frac{1}{36}a_8 = \pm\frac{1}{12}a_3 + \frac{5}{36}a_8 \tag{1.34}$$

for proton and neutron, respectively.

The Bjorken sum rule predicts the difference between Γ_1^p and Γ_1^n:

$$\Gamma_1^p - \Gamma_1^n = \int_0^1 (g_1^p - g_1^n)dx = \frac{1}{6}a_3. \tag{1.35}$$

Moreover, the spin contribution from quarks will be

$$\Delta\Sigma \equiv a_0 = (\Delta u + \Delta\bar{u}) + (\Delta d + \Delta\bar{d}) + (\Delta s + \Delta\bar{s}) \tag{1.36}$$

In the $SU(6)$ model we can write down the proton wave function as

$$|p\uparrow\rangle = \frac{1}{\sqrt{6}}\big(2|u\uparrow u\uparrow d\downarrow\rangle - |u\uparrow u\downarrow d\uparrow\rangle - |u\downarrow u\uparrow d\uparrow\rangle\big) \tag{1.37}$$

where the color indices and permutations have been suppressed. In this model we will have $\Delta u = 4/3$ and $\Delta d = -1/3$, thus $\Delta\Sigma = 1$ and all the momentum of the proton is carried by the constituent quarks. For a relativistic correction we noticed

that in this simple model $a_3 = 4/3 + 1/3 = 5/3$, while by measuring the nucleon and hyperon beta decay we get $a_3 \approx 1.25 = 5/4$. Thus we need to multiply a factor of $3/4$ on top of the total contribution of the quark spin, which leads to $\Delta\Sigma = 0.75$. The rest of the angular momentum is carried by the orbital momentum of the quarks, since the quarks are relativistic Dirac particles inside the proton.

Both a_3 and a_8 can be determined by the neutron and hyperon beta decays. The results are $a_3 \approx 1.25$ and $a_8 \approx 0.75$. By the Ellis-Jaffe sum rule we can expect that $\Gamma_1^p = 0.185 \pm 0.003$ ($= 0.171 \pm 0.006$ at $Q^2 = 10\text{GeV}^2$ after leading-order corrections).

However, the EMC result gives:

$$\Gamma^p_{1,\text{EMC}} = 0.126 \pm 0.01. \pm 0.015 \tag{1.38}$$

at $Q^2 = 10.7\text{GeV}^2$. From it we can derive:

$$\begin{aligned} \Delta u + \Delta\bar{u} &= 0.77 \pm 0.06, \\ \Delta d + \Delta\bar{d} &= -0.49 \pm 0.06, \\ \Delta s + \Delta\bar{s} &= -0.15 \pm 0.06 \end{aligned} \tag{1.39}$$

and

$$\Delta\Sigma = 0.14 \pm 0.16. \tag{1.40}$$

We can draw several conclusions:

a. The Ellis-Jaffe sum rule is severely violated;

b. The total quark spin contribution only accounts for 20% $\sim$ 30% of the total nucleous spin;

c. Sea quark contribution is non-zero and negative.

This is the origin of the "spin crisis".

There are several proposals trying to explain the missing spin contribution in the proton after the discovery of EMC experiment. One of the ideas is to attribute the large spin to the gluons inside the proton. Since by deep inelastic scattering and parton distribution functions people have already learned that about half of the proton momentum is carried by gluons, this idea has some ground. In [27] a connection between the total angular momentum carried by the gluon, ΔG, and the off-forward scattering form factor have been established. Several experiments have been launched in the hopes to measure the quantity ΔG since then. In Chapter 4 we will have a review of these attempts and give out a calculation of ΔG under the bag model and large N_C approximations. The result roughly agrees with the experimental data fitting curve and suggests a positive ΔG in the proton.

1.5 Soft-Collinear Effective Theory

Soft-collinear effective theory (SCET) is an effective theory describing fast-moving collinear particles accompanied with soft ones. It is widely used in collider physics threshold regions when resummation of large logarithms is needed. To describe the Lagrangian we first introduce the so-called "light cone" coordinates here:

we define

$$n^\mu = \frac{1}{\sqrt{2}}(1,0,0,-1), \;\; \bar{n}^\mu = \frac{1}{\sqrt{2}}(1,0,0,1). \tag{1.41}$$

Therefore the momentum p of a fast-moving particle along the z direction can be projected onto the plus- and minus- light-cone directions and we have

$$p^+ \equiv n\cdot p = \frac{1}{\sqrt{2}}(p^0+p^3), \;\; p^- \equiv \bar{n}\cdot p = \frac{1}{\sqrt{2}}(p^0-p^3), \;\; p = (p^+, p^-, \mathbf{p}_\perp) \tag{1.42}$$

The dot product becomes

$$p\cdot q = p^+q^- + p^-q^+ - \mathbf{p}_\perp\cdot\mathbf{q}_\perp, \;\; p^2 = 2p^+p^-\mathbf{p}_\perp^2 \tag{1.43}$$

The effective theory starts from the observation that in a hard process characterized by the large momentum transfer scale Q, in a Breit frame, the target particle (for example, the proton in deep-inelastic scattering process) will be moving at close to the light speed. The partons inside the particle (quarks, gluons, etc), therefore, will contain large momentum components in the $+z$ direction. For a twist-2 interference all the momentum transfer are on this fast moving parton and we can characterize its momentum scaling as

$$p = (p^+, p^-, \mathbf{p}_\perp) \sim Q(1, \lambda^2, \lambda). \tag{1.44}$$

Here λ is a small parameter relevant to the residue transverse momentum of that parton inside the target particle. Usually we have $\lambda \ll 1$, and it can serve as an expansion parameter of the effective theory. SCET is constructed based on such observations.

In SCET we have three relevant momentum scales, Q, $Q\lambda$, and $Q\lambda^2$. The

terminology goes like:

$$\begin{aligned} \text{Hard} &: p^2 \sim Q^2 \\ \text{Collinear} &: p^\mu \sim Q(1, \lambda^2, \lambda) \text{or} p^\mu \sim Q(\lambda^2, 1, \lambda) \\ \text{Soft} &: p^\mu \sim Q(\lambda, \lambda, \lambda) \\ \text{Ultrasoft} &: p^\mu \sim Q(\lambda^2, \lambda^2, \lambda^2) \end{aligned} \tag{1.45}$$

The effective theory is constructed by integrating out all the hard scales while assigning a power counting for all the remaining quark and gluon fields. Furthermore, the full momentum of a collinear particle is decomposed into a collinear "label" momentum and a residual ultrasoft momentum, $P^\mu = p^\mu + k^\mu$, where p^μ contains momentums of order Q and $Q\lambda$, and k^μ collects all the $Q\lambda^2$ momentums. The SCET Lagrangian is built up by the labeled fields and the fluctuations are therefore all at order $Q\lambda^2$. This is actually very much like the vNRQCD we mentioned before, in which the heavy quark fields are labeled by their velocity v and the residual momentums are at order mv^2.

For a field collinear to n, a redefinition in SCET from the full QCD field goes like:

$$\psi(x) = \sum_p e^{-ip\cdot x} \xi_{n,p}(x) \tag{1.46}$$

Here $\xi_{n,p}(x)$ is a collinear quark field in SCET carrying a label momentum p. The residual momentum can be acquired by a Fourier transformation. If the quark mass is neglected we will further have $\not{n}\xi_{n,p} = 0$. For a general quark field $\psi(x)$, only the collinear and the ultrasoft part enter the redefined SCET fields. All other degrees of freedom have been integrated out.

Sometimes it is convenient to define an operator $\mathcal{P}^\mu$ which acts on fields with labels:

$$\begin{aligned}\mathcal{P}^\mu(\phi^\dagger_{q_1}\cdots\phi^\dagger_{q_m}\phi_{p_1}\cdots\phi_{p_n}) \\ = \ (p_1^\mu+\cdots+p_n^\mu-q_1^\mu-\cdots-q_m^\mu)(\phi^\dagger_{q_1}\cdots\phi^\dagger_{q_m}\phi_{p_1}\cdots\phi_{p_n}).\end{aligned} \tag{1.47}$$

Now we write down the collinear quark sector of SCET Lagrangian:

$$\mathcal{L}_q=\sum_{p,p'}\bar{\xi}_{n,p'}(x)\left[n\cdot D+i\not{D}^c_\perp W_n(x)\frac{1}{in\cdot\mathcal{P}}W_n^\dagger(x)(i\not{D}^c_\perp)\right]\frac{\not{n}}{2}\xi_{n,p} \tag{1.48}$$

in which D^c contains only the collinear gluon field. The W_n, $W_n^\dagger$ are collinear Wilson lines with the form:

$$W_n(x)=P\exp\left[ig\int_{-\inf}^{x}dsn\cdot A^c(ns)\right], \tag{1.49}$$

and P is the ordering operator. By choosing the light-cone gauge $n\cdot A=0$, we can eliminate the Wilson line in the quark sector and simplify the Lagrangian. Similarly we can define another Wilson line with only ultrasoft gluon fields:

$$Y(x)=P\exp\left[ig\int_{-\inf}^{x}dsn\cdot A_{us}(ns)\right], \tag{1.50}$$

this will be used later.

The scaling of the fields are listed in Table 1.5:

A major application of SCET is to achieve a clear factorization and resummation in the inclusive process. For the leading twist the cross section can be written as a convolution of a hard scattering kernel H, a jet function J, and a soft function S:

$$\sigma\sim H\otimes J\otimes\Phi\otimes S \tag{1.51}$$

Field	*Scaling*
Collinear quark $\xi_{n,p}$	λ
Collinear gluon A^c	λ
Ultrasoft gluon A^{us}	λ^2

Table 1.1: Power counting of SCET collinear and ultrasoft fields

Here H contains all the short-distance physics at or above scale Q, the jet function describes the degrees of freedom from the particles moving almost along the light-cone, Φ is the normal parton distribution functions, and the soft function includes all the non-perturbative long-distance physics.

The reason for doing this in the effective theory is that in the hard inclusive processes there are additional collinear divergences different from the soft infrared divergences, and a factorization allows us to achieve separate running and resummation more clearly without the need to solve difficult renormalization group equations. In Chapter 5 we have an example of how to achieve this with SCET for the DIS process at $x \to 1$ threshold region.

Chapter 2

A Decomposition of Angular Momentum Operator in Non-relativistic QED to Order α/m^2

2.1 Introduction

It is a standard problem to solve the Hydrogen atom wave function in the college level quantum mechanics course. At the non-relativistic limit, the orbital angular momentum L and spin of the electron S are both conserved quantities and can be used to label the energy eigenstates. Under the relativistic Dirac Hamiltonian, neither L nor S still maintains a good quantum number, with corrections from the non-relativistic expectation value start at order $\mathcal{O}(\alpha_{\text{EM}}^2)$, in which $\alpha_{\text{EM}} \approx 1/137$ is the fine-structure constant. The radiating corrections from QED will further give an order $\mathcal{O}(\alpha_{\text{EM}}^3)$ correction[19]. Attempts to calculate these corrections in a bound state under QED are usually too hard to be done analytically and involves solving Bethe-Salpeter equations. In recent years, the development of effective theories for non-relativistic systems is proved to be a powerful tool in studying the bound state physics.

Since first being proposed in [18], the non-relativistic QED (NRQED), together with the later developed non-relativistic QCD (NRQCD) have become the standard language in treating non-relativistic two-body bound states such as hydrogen-like

systems and heavy quark-antiquark pair productions near threshold. A direct perturbative expansion in QED or QCD is not applicable in these situations: multiple energy scales are present and their ratios might be large, thus taint the expansion. For example, at near threshold, interactions between quark-antiquark pair will accompany with the famous Sommerfeld enhancement and the cross section $\Gamma \sim m\alpha_s/v$, in which v is the velocity of the heavy quark relative to center-of-mass. On the other hand, in an s-state for a non-relativistic system we have $E \sim \mu\alpha^2$ which translates to $v \sim \alpha_s$. Therefore the loop corrections to the cross section is of the same order as the tree level contributions, and the perturbative expansion fails.

The effective theory sheds a new light on the problem. By observing that the large contribution of the Coulomb interactions exchange momentums at some lower scale, one can integrate out the large scale from the beginning and get an effective Lagrangian with an expansion in powers of the inverse of the large scale. Now in NRQC(E)D the bound state problem can be solved systematically. The non-relativistic bound-state wave functions can be seen as a sum over all the leading order contributions from the Coulomb photon exchange. A clear power counting scheme with regard to the small momentum and by including all the contributions up to some order, the desired precision can be achieved.

For the angular momentum, by applying the effective theory one may calculate the expectation value of the spin (orbital) angular momentum for the heavy fermions or the gauge fields, order by order and taking into account the radiation corrections. All we have to do is to establish the form of the spin and orbital angular momentum operators in the effective theory. In this chapter we will construct a decomposition

of angular momentum operator in NRQED. The effective operator will have a scale separation between hard scale and soft scale. It turns out to vastly differ from the form in QED, with many new terms present.

2.2 NRQED

The NRQED Lagrangian is first given in [18]. Later in [20] a power counting rule is established. It reads:

$$\begin{aligned}\mathcal{L}_{\rm NRQED} &= \psi^\dagger\Big\{iD^0 + c_2\frac{\mathbf{D}^2}{2m} + c_4\frac{\mathbf{D}^4}{8m^3} + \frac{e\,c_F}{2m}\boldsymbol{\sigma}\cdot\mathbf{B} + \frac{e\,c_D}{8m^2}[\boldsymbol{\nabla}\cdot\mathbf{E}] \\ &\quad + \frac{ie\,c_S}{8m^2}\boldsymbol{\sigma}\cdot(\mathbf{D}\times\mathbf{E} - \mathbf{E}\times\mathbf{D})\Big\}\psi \\ &\quad + d_1 F_{\mu\nu}F^{\mu\nu} + \frac{d_2}{m^2}F_{\mu\nu}\Box F^{\mu\nu} + \mathcal{L}_{4-\rm Fermi} + \dots \end{aligned} \tag{2.1}$$

Here $\mathcal{L}_{4-\rm Fermi}$ represents all the four-fermi terms in the Lagrangian and will not be used in this chapter. The coefficients in the effective Lagrangian up to $\mathcal{O}(\alpha_{\rm EM})$ are well known[23]:

$$\begin{aligned} &c_2 = c_4 = 1;\;\; c_F = 1 + \frac{\alpha_{\rm EM}}{2\pi};\;\; c_D = 1 - \frac{4\alpha_{\rm EM}}{3\pi}\ln\frac{\mu^2}{m^2};\;\; c_S = 1 + \frac{\alpha_{\rm EM}}{\pi}; \\ &d_1 = 1 + \frac{\alpha_{\rm EM}}{3\pi}\ln\frac{\mu^2}{m^2};\;\; d_2 = \frac{\alpha_{\rm EM}}{60\pi}. \end{aligned} \tag{2.2}$$

In our calculation we are using the "old-fashioned" NRQED, which is roughly equivalent to the intermediate effective theory in pNRQED in which a first-step matching at $\mu = m$ has been executed. In doing the matching a $1/m$ expansion as described in [23] is understood. It is proved in [24] that such method agrees with the multi-pole expansion method in [22]. More explanation will follow when detailed calculation is presented.

2.3 Decomposition of angular momentum operator in QED

The spin decomposition itself is an interesting topic. A famous problem is the so-called "spin crisis" in the proton after the EMC experiment[36], which discovers that less than half of the total photon spin is carried by the quark spin. In [27] a connection between off-forward form factor and ΔG, the total photon angular momentum in proton, has been proposed. Since then lots of the work has been done on studying the quantity ΔG and several experiments have been designed to measure the quantity[96].

On the other hand, the non-relativistic limit of the angular momentum operator has evaded the public sight. It is partly because the proton system is a relativistic one due to the light mass of the u and d quarks, as well as the confinement of QCD. Nevertheless, a non-relativistic decomposition of the angular momentum can still be useful in many other systems, including the Hydrogen-like systems and heavy-quarkoniums. It helps to study how the total angular momentum is decomposed by the electron and the photon in such bound states. Our aim is to reconstruct the angular momentum decomposition in NRQED.

It is a textbook example to derive conserved angular momentum operator from the QED Lagrangian using a Noether current method:

$$\mathcal{L}_{\text{QED}} = -\frac{1}{4}F^{\mu\nu}F_{\mu\nu} + \bar{\Psi}(i\not{D} - m)\Psi \tag{2.3}$$

The conserved QED angular momentum is:

$$\begin{aligned}\mathbf{J}_{\rm QED} &= \int d^3x \left\{ \Psi^\dagger \frac{\mathbf{\Sigma}}{2} \Psi + \Psi^\dagger (\mathbf{x} \times \boldsymbol{\pi}) \Psi + \mathbf{x} \times (\mathbf{E} \times \mathbf{B}) \right\} \\ &\equiv \mathbf{S}_q + \mathbf{L}_q + \mathbf{J}_\gamma \end{aligned} \tag{2.4}$$

in which

$$\begin{aligned}\mathbf{S}_q &\equiv \frac{1}{2} \int d^3x \Psi^\dagger \mathbf{\Sigma} \Psi \\ \mathbf{L}_q &\equiv \int d^3x \Psi^\dagger (\mathbf{x} \times \boldsymbol{\pi}) \Psi \\ \mathbf{J}_\gamma &\equiv \int d^3x \, \mathbf{x} \times (\mathbf{E} \times \mathbf{B}) \end{aligned} \tag{2.5}$$

The decomposed operators $\mathbf{S}_q, \mathbf{L}_q, \mathbf{J}_\gamma$ are gauge invariant and can be labeled as the electron spin, electron orbital angular momentum and photon angular momentum, respectively. Alternative decompositions can be achieved in some particular gauge and frame choices. However, they are largely gauge- and frame-dependent. At this time we will consider gauge-invariant decompositions only.

Now the challenge upon us is to construct the non-relativistic counterparts to $\mathbf{S}_q, \mathbf{L}_q, \mathbf{J}_\gamma$ in NRQED. Later we will show that the decomposition in NRQED is gauge-invariant as well, with the manifest separation of physics between high scale and low scale.

2.4 Decomposition of Angular momentum operator in NRQED

2.4.1 Conserved Current of NRQED Lagrangian

We observe that the effective Lagrangian (2.1) still possesses the rotational symmetry. The authors in [33] have noticed this as well and by deriving the Poincare

operators they obtained an expression of total angular momentum in NRQED. Their result, however, is accurate only up to the order $\mathcal{O}(\alpha_{\rm EM}^0 m^0)$. As it will become clear, our $\mathbf{J}_{\rm NRQED}$ is accurate up to $\mathcal{O}(\alpha_{\rm EM} m^{-2})$ and is confirmed by an order-by-order matching to QED up to one-loop level.

Unlike QED, the NRQED Lagrangian contains higher order derivatives of the fields and needs some special treatments. In Appendix A we have listed the general form of the equation of motion and symmetric energy-momentum tensor $T^{\mu\nu}$ of a Lagrangian $\mathcal{L} = \mathcal{L}(x, \phi, \phi', \phi'')$. We give the equation of motion with regard to A^0 field below:

$$\begin{aligned} 0 &= -e\psi^\dagger\psi - \frac{e\,c_D}{8m^2}\boldsymbol{\nabla}^2(\psi^\dagger\psi) + \frac{ie\,c_S}{4m^2}\boldsymbol{\nabla}\cdot\left[\psi^\dagger\left(\boldsymbol{\sigma}\times\mathbf{D}\right)\psi\right] \\ &\quad + d_1\left(\partial_\mu F^{\mu 0}\right) - \frac{4d_2}{m^2}\Box\left(\partial_\mu F^{\mu 0}\right) \end{aligned} \tag{2.6}$$

By applying the improved Noether current method in the Appendix to the NRQED Lagrangian, we get the conserved angular momentum current:

$$\begin{aligned} \mathbf{J}_{\rm NRQED} &= \int d^3\mathbf{x}\Big\{\psi^\dagger\left(\frac{\boldsymbol{\sigma}}{2}\right)\psi + \psi^\dagger\left(\mathbf{x}\times\boldsymbol{\pi}\right)\psi + \frac{e\,c_D}{8m^2}\mathbf{x}\times\left[\mathbf{B}\times\boldsymbol{\nabla}(\psi^\dagger\psi)\right] \\ &\quad + \frac{e\,c_S}{8m^2}\mathbf{x}\times\psi^\dagger\left[\mathbf{B}\times\left(\boldsymbol{\sigma}\times\overleftrightarrow{\boldsymbol{\pi}}\right)\right]\psi + d_1\,\mathbf{x}\times\left(\mathbf{E}\times\mathbf{B}\right) \\ &\quad + \left(-\frac{4d_2}{m^2}\right)\Big[\mathbf{x}\times\left(\Box\mathbf{E}\times\mathbf{B}\right) - \dot{\mathbf{E}}^a(\mathbf{x}\times\boldsymbol{\nabla})\mathbf{E}^a - \dot{\mathbf{B}}^a(\mathbf{x}\times\boldsymbol{\nabla})\mathbf{B}^a \\ &\quad + \dot{\mathbf{E}}\times\mathbf{E} - \dot{\mathbf{B}}\times\mathbf{B}\Big]\Big\} + \ldots \end{aligned} \tag{2.7}$$

We will not consider four-quark operators in this chapter. Equation (2.7) is the total angular momentum operator in NRQED and is manifestly gauge invariant. Any decomposition of the total angular momentum in NRQED must sum up to $\mathbf{J}_{\rm NRQED}$. However, unlike the case in QED, we can't spot a clear decomposition

directly from the total angular momentum operator. Furthermore, we wish the decomposition to be in agreement with (2.4).

2.4.2 Foldy-Wouthysen Transformation

As a first try towards the problem, we apply the Foldy-Wouthysen (FW) transformation on the decomposed QED operators in (2.5). By its quantum mechanics nature the FW transformation would not give out any radiative corrections. Consequently, any term having a Wilson coefficient starting at $\mathcal{O}(\alpha_{\text{EM}})$ or higher would not show up in the transformation. It only affects the electron wave function, leaving the J_γ unchanged.

We give a quick review of the FW transformation: The Dirac Hamiltonian describes relativistic fermion particles. For an electron at low energy, the physics is dominated by the particle part and the correction from the anti-particle contributions are mixed into the particle part by the off-diagonal terms in the Hamiltonian. The FW transformation utilizes a unitary matrix to block-diagonalize the Dirac Hamiltonian. Up to $\mathcal{O}(m^{-2})$ the matrix reads:

$$U = \exp\left(\frac{\beta\boldsymbol{\alpha}\cdot\boldsymbol{\pi}}{2m}\right) = \exp\left(\frac{\boldsymbol{\gamma}\cdot\boldsymbol{\pi}}{2m}\right) \tag{2.8}$$

in which

$$\beta = \begin{pmatrix} 1 & 0 \\ 0 & -1 \end{pmatrix}, \quad \boldsymbol{\alpha} = \begin{pmatrix} 0 & \boldsymbol{\sigma} \\ \boldsymbol{\sigma} & 0 \end{pmatrix}. \tag{2.9}$$

With U we can eliminate the lower components in a Dirac spinor of electron:

$$\begin{aligned} U\cdot u(p) &\rightarrow \begin{pmatrix} u_h \\ 0 \end{pmatrix} + \mathcal{O}(m^{-3}) \\ \Psi\hat{\mathcal{O}}\Psi &\rightarrow (\Psi U^\dagger)(U\hat{\mathcal{O}}U^\dagger)(U\Psi). \end{aligned} \tag{2.10}$$

Using (2.8),(2.10) we find that

$$\begin{aligned} \int d^3\mathbf{x}\Psi^\dagger\frac{\mathbf{\Sigma}}{2}\Psi &\rightarrow \int d^3\mathbf{x}\psi^\dagger\left\{\frac{\boldsymbol{\sigma}}{2}+\frac{1}{8m^2}\left[(\boldsymbol{\sigma}\times\boldsymbol{\pi})\times\boldsymbol{\pi}-\boldsymbol{\pi}\times(\boldsymbol{\sigma}\times\boldsymbol{\pi})\right]+\frac{e\mathbf{B}}{4m^2}\right\}\psi \\ \int d^3\mathbf{x}\Psi^\dagger\mathbf{x}\times\boldsymbol{\pi}\Psi &\rightarrow \int d^3\mathbf{x}\psi^\dagger\left\{\mathbf{x}\times\boldsymbol{\pi}-\frac{1}{8m^2}\left[(\boldsymbol{\sigma}\times\boldsymbol{\pi})\times\boldsymbol{\pi}-\boldsymbol{\pi}\times(\boldsymbol{\sigma}\times\boldsymbol{\pi})\right]-\frac{e\mathbf{B}}{4m^2}\right\}\psi \\ &\quad+\int d^3\mathbf{x}\frac{e}{8m^2}\left\{\mathbf{x}\times\left[\mathbf{B}\times\boldsymbol{\nabla}(\psi^\dagger\psi)\right]+\mathbf{x}\times\psi^\dagger\left[\mathbf{B}\times(\boldsymbol{\sigma}\times\overleftrightarrow{\boldsymbol{\pi}})\right]\psi\right\} \\ \int d^3x\ \mathbf{x}\times(\mathbf{E}\times\mathbf{B}) &\rightarrow \int d^3x\ \mathbf{x}\times(\mathbf{E}\times\mathbf{B}), \end{aligned} \tag{2.11}$$

in which ψ is the non-relativistic electron field and $\overleftrightarrow{\boldsymbol{\pi}}$ is defined as:

$$\begin{aligned} \psi^\dagger_{p'}\overleftrightarrow{\boldsymbol{\pi}}\psi_p &\equiv \psi^\dagger_{p'}(\boldsymbol{\pi}\psi_p)+\left(\boldsymbol{\pi}\psi_{p'}\right)^\dagger\psi_p \\ &= \psi^\dagger_{p'}\left(\mathbf{p}+\mathbf{p}'-2e\mathbf{A}\right)\psi_p. \end{aligned} \tag{2.12}$$

To check this result we use it to calculate the electron spin in a Coulomb central potential. The solution of Dirac equation has the form:

$$\psi_{jj_3}(\mathbf{r}) = \begin{pmatrix} g_\kappa(r)\mathcal{Y}^{j_3}_{jl}(\hat{\mathbf{r}}) \\ if_\kappa(r)\mathcal{Y}^{j_3}_{jl'}(\hat{\mathbf{r}}) \end{pmatrix} \tag{2.13}$$

For a ground state $1s_{1/2}$, we have $\kappa=-1$, $j=\frac{1}{2}$, $l=0$,$l'=1$ and

$$\int d^3r\psi(\mathbf{r})^\dagger\Sigma^3\psi(\mathbf{r}) = 1+\frac{p^2}{6m^2} \tag{2.14}$$

This is in agreement with the result from the reduced operators.

2.4.3 General Form of the Decomposed Operators

The general form of the decomposed operators of angular momentum can be constructed as follows: first write down all the terms satisfying the symmetry requirements: they should be axial vector, gauge-invariant, Hermitian and Galilean invariant. Additionally, we require those operators do not contain time derivatives over the fermion fields. The lack of D^0 is the result from a field redefinition as has been shown in [23]: any operator containing D^0 can be rewritten as linear combinations of other operators by the equation of motion and have the same on-shell matrix element. There might be non-local operators in $\mathbf{L}_q$ and $\mathbf{J}_\gamma$ as well, with the form $\int d^3x \mathbf{x} \times \mathbf{G}$.

We write down the general form of the effective operators:

$$\begin{aligned}
\mathbf{S}_q \to \mathbf{S}_q^{\text{eff}} \;=\; & \int d^3x \left\{ a_\sigma \psi^\dagger \frac{\boldsymbol{\sigma}}{2} \psi + \frac{a_\pi}{8m^2} \psi^\dagger \left[(\boldsymbol{\sigma} \times \boldsymbol{\pi}) \times \boldsymbol{\pi} - \boldsymbol{\pi} \times (\boldsymbol{\sigma} \times \boldsymbol{\pi}) \right] \psi \right. \\
& \left. + \frac{e\, a_B}{4m^2} \psi^\dagger \mathbf{B} \psi \right\} \\
& + \int d^3x \left\{ \frac{a_{\gamma_1}}{m^2} \left[\dot{\mathbf{E}} \times \mathbf{E} - \dot{\mathbf{B}} \times \mathbf{B} \right] + \frac{a_{\gamma_2}}{m^2} \boldsymbol{\nabla} \times (\mathbf{E} \times \mathbf{B}) \right\} \\
& + \mathcal{O}(m^{-3}), \qquad (2.15)
\end{aligned}$$

$$
\begin{aligned}
\mathbf{L}_q \to \mathbf{L}_q^{\rm eff} &= \int d^3x \Bigg\{ d_\sigma \psi^\dagger \frac{\boldsymbol{\sigma}}{2} \psi + \frac{d_\pi}{8m^2} \psi^\dagger \left[(\boldsymbol{\sigma} \times \boldsymbol{\pi}) \times \boldsymbol{\pi} - \boldsymbol{\pi} \times (\boldsymbol{\sigma} \times \boldsymbol{\pi}) \right] \psi \\
&\quad + d_R \psi^\dagger (\mathbf{x} \times \boldsymbol{\pi}) \psi + \frac{e\, d_B}{4m^2} \psi^\dagger \mathbf{B} \psi + \frac{e\, d_D}{8m^2} \mathbf{x} \times \left[\mathbf{B} \times \boldsymbol{\nabla} (\psi^\dagger \psi) \right] \\
&\quad + \frac{e\, d_s}{8m^2} \mathbf{x} \times \psi^\dagger \left[\mathbf{B} \times (\boldsymbol{\sigma} \times \overleftrightarrow{\boldsymbol{\pi}}) \right] \psi + \frac{e\, d_s'}{8m^2} \mathbf{x} \times \psi^\dagger \left[\boldsymbol{\sigma} \times (\mathbf{B} \times \overleftrightarrow{\boldsymbol{\pi}}) \right] \psi \\
&\quad + \frac{e\, d_E}{4m} \mathbf{x} \times \psi^\dagger (\boldsymbol{\sigma} \times \mathbf{E}) \psi \Bigg\} \\
&\quad + \int d^3x \Bigg\{ d_\gamma\, \mathbf{x} \times (\mathbf{E} \times \mathbf{B}) + \frac{d_{\gamma_1}}{m^2} \left[\dot{\mathbf{E}} \times \mathbf{E} - \dot{\mathbf{B}} \times \mathbf{B} \right] \\
&\quad + \frac{d_{\gamma_2}}{m^2} \boldsymbol{\nabla} \times (\mathbf{E} \times \mathbf{B}) + \frac{d_{\gamma_3}}{m^2} \mathbf{x} \times (\Box \mathbf{E} \times \mathbf{B}) \\
&\quad + \frac{d_{\gamma_4}}{m^2} \left[\dot{\mathbf{E}}^a (\mathbf{x} \times \boldsymbol{\nabla}) \mathbf{E}^a + \dot{\mathbf{B}}^a (\mathbf{x} \times \boldsymbol{\nabla}) \mathbf{B}^a \right] \Bigg\} + \mathcal{O}(m^{-3}),
\end{aligned} \tag{2.16}
$$

and the gluon angular momentum operators:

$$
\begin{aligned}
\mathbf{J}_\gamma \to \mathbf{J}_\gamma^{\rm eff} &= \int d^3x \Bigg\{ f_\sigma \psi^\dagger \frac{\boldsymbol{\sigma}}{2} \psi + \frac{f_\pi}{8m^2} \psi^\dagger \left[(\boldsymbol{\sigma} \times \boldsymbol{\pi}) \times \boldsymbol{\pi} - \boldsymbol{\pi} \times (\boldsymbol{\sigma} \times \boldsymbol{\pi}) \right] \psi \\
&\quad + f_R \psi^\dagger (\mathbf{x} \times \boldsymbol{\pi}) \psi + \frac{e\, f_B}{4m^2} \psi^\dagger \mathbf{B} \psi + \frac{e\, f_D}{8m^2} \mathbf{x} \times \left[\mathbf{B} \times \boldsymbol{\nabla} (\psi^\dagger \psi) \right] \\
&\quad + \frac{e\, f_s}{8m^2} \mathbf{x} \times \psi^\dagger \left[\mathbf{B} \times (\boldsymbol{\sigma} \times \overleftrightarrow{\boldsymbol{\pi}}) \right] \psi + \frac{e\, f_s'}{8m^2} \mathbf{x} \times \psi^\dagger \left[\boldsymbol{\sigma} \times (\mathbf{B} \times \overleftrightarrow{\boldsymbol{\pi}}) \right] \psi \\
&\quad + \frac{e\, f_E}{4m} \mathbf{x} \times \psi^\dagger (\boldsymbol{\sigma} \times \mathbf{E}) \psi \Bigg\} + \int d^3x f_\gamma \mathbf{x} \times (\mathbf{E} \times \mathbf{B}) + \mathcal{O}(m^{-3}).
\end{aligned} \tag{2.17}
$$

There are other possible candidates such as $\frac{e}{4m} \mathbf{x} \times \psi^\dagger \mathbf{B} \psi$, etc. However, they do not show up in one-loop matching, and we do not include them explicitly in the general operators above. In the following sections we will see that all the Wilson coefficients in (2.15)-(2.17) can be determined.

The matching condition is:

$$
\langle \mathbf{J}(\mu) \rangle_{\rm QED} = \langle \mathbf{J}^{\rm eff}(\mu) \rangle_{\rm NRQED}. \tag{2.18}
$$

Although the primary application of our NRQED effective operators will be in bound states, we are not obliged to use a particular bound state to do the matching. Since all the infrared physics are captured by the effective theory itself, the Wilson coefficients will contain ultraviolet sensitivities only. Any processes can be used to perform the matching and we should choose the one as simple as possible. Throughout this work, we will use plane waves as our external states in the matching.

For the coefficients in effective theory we use the following convention:

$$w_i = w_i^{(0)} + \frac{\alpha_{\rm EM}}{2\pi} w_i^{(1)} + \mathcal{O}(\alpha_{\rm EM}^2), \tag{2.19}$$

in which $w_i^{(0)}$s represent the tree level contribution, $w_i^{(1)}$ the one-loop level, etc.

Equation (2.7) has given the total angular momentum operator originated from the underlying $SO(3)$ rotational symmetry of the NRQED Lagrangian. It has nothing to do with the perturbative expansion and must be exact. Our decomposed effective operators, on the other hand, are derived from the matching to the full theory with order-by-order expansions. They must agree or our effective theory is not self-consistent. By imposing the constraints:

$$\mathbf{S}_q^{\rm eff} + \mathbf{L}_q^{\rm eff} + \mathbf{J}_\gamma^{\rm eff} = \mathbf{J}_{\rm NRQED}, \tag{2.20}$$

we have the following sum rules for the Wilson coefficients:

$$\begin{aligned}
a_\sigma + d_\sigma + f_\sigma &= d_R + f_R = 1, \\
a_\pi + d_\pi + f_\pi &= a_B + d_B + f_B = 0, \\
d_D + f_D &= c_D, \\
d_S + f_S &= c_S, \\
d'_S + f'_S &= d_E + f_E = a_{\gamma_2} + d_{\gamma_2} = 0, \\
d_\gamma + f_\gamma &= d_1, \\
a_{\gamma_1} + d_{\gamma_1} &= d_{\gamma_3} = -2d_{\gamma_4} = -4d_2
\end{aligned} \tag{2.21}$$

We will use these sum rule as a cross-check to the matching results of the NRQED decomposed angular momentum operators.

2.4.4 Two-body Matching Conditions

We first consider the angular momentum decomposition for a free electron at non-relativistic limit. Such matching alone cannot determine all the Wilson coefficients in (2.15)-(2.17). However, the physics is easier to understand in this case and some of the important concepts will be explained.

We wish to calculate the forward matrix elements of the decomposed angular momentum operators: $\langle e_{p,s}|\mathcal{O}_J|e_{p,s}\rangle$, with $\mathcal{O}_J$ representing one of the decomposed operators $\mathbf{S}_q, \mathbf{L}_q$, and $\mathbf{J}_\gamma$. Here we will generate a non-relativistic reduction of such matrix elements, and a matching with corresponding matrix elements in NRQED will follow. Before doing any calculations we consider an interesting question first:

what is the physics of the angular momentum of a free electron?

The idea of deriving the total angular momentum of a free electron sounds bizarre; the orbital angular momentum of a plane wave is ill defined. A more realistic problem would be to calculate the angular momentum of a *distribution*, or a wave packet, of the electron. The result will not only depend on the intrinsic properties of the electron itself, but also the shape of the wave packet. Such relevance arises because the angular momentum operator is a non-local operator: it contains the position operator $\mathbf{x}$ and thus relates kinematics between two separate points in space. In a momentum frame $\mathbf{x}$ can be carried away by a partial integral as the derivative over the momentum, and the contribution to the total angular momentum can be separated into two parts: the derivative on the electron transition matrix amplitude itself and on the electron momentum distribution of the wave packet.

We will focus on the decomposition of the angular momentum and take a close look on $\mathbf{S}_q$, $\mathbf{L}_q$ and $\mathbf{J}_\gamma$, respectively. The spin operator $\mathbf{S}_q$ is local and its contribution can be calculated right away:

$$\langle \mathbf{S}_q \rangle = \langle \mathbf{p}| \left(\mathbf{\Sigma}/2\right) |\mathbf{p}\rangle. \tag{2.22}$$

The situation of the other two operators, $\mathbf{L}_q$ and $\mathbf{J}_\gamma$, is more subtle. The presence of a coordinate $\mathbf{x}$ in the decomposed operator have made the definition of a forward matrix element less clear. To see this we consider an off-forward matrix

element of the operator $\mathbf{L}_q$ first:

$$\begin{aligned}\langle \mathbf{L}_q \rangle_{p',p} &= \int d^3x \langle \mathbf{p}'|(\mathbf{x}\times\boldsymbol{\pi})|\mathbf{p}\rangle \\ &\equiv \int d^3x e^{-i\mathbf{x}\cdot(\mathbf{p}'-\mathbf{p})}\mathbf{x}\times\mathbf{f}(p',p) \\ &= (2\pi)^3[i\boldsymbol{\nabla}_{p'}\delta^3(p'-p)]_{p'=p}\times\mathbf{f}(p',p). \end{aligned} \tag{2.23}$$

The derivative over a delta function looks strange at first. However, when considering a wave packet, e.g. $|\Phi\rangle \equiv \int \frac{d^3\mathbf{p}'}{(2\pi)^3}\Phi(\mathbf{p}')|\mathbf{p}'\rangle$, we can use the partial integral and $\boldsymbol{\nabla}_{p'}$ will then act on the distribution function $\Phi(\mathbf{p}')$, as well as $\mathbf{f}(p',p)$. Integrate over the delta function and the contribution to a wave packet will look like:

$$\begin{aligned}\langle \mathbf{L}_q \rangle_\Phi &= \int d^3p \Phi^*(\mathbf{p})\Phi(\mathbf{p})[i\boldsymbol{\nabla}_{p'}\times\mathbf{f}(p',p)]_{p'=p} \\ &\quad +\frac{1}{2}\int d^3p \boldsymbol{\nabla}_p[\Phi^*(\mathbf{p})\Phi(\mathbf{p})]\times\mathbf{f}(p,p). \end{aligned} \tag{2.24}$$

Here the first term is the self-induced angular momentum and will contribute to the total electron helicity in the same way as $\langle \mathbf{S}_q \rangle$. The second term is precisely the orbital angular distribution carried by the wave packet, as we have discussed before. Similar terms exist in matrix elements of $\mathbf{J}_\gamma$ as well as all non-local effective operators. In the following, we will call the first term the *spin* contribution and the second term the *orbital* contribution. For local operators like $\mathbf{S}_q$, only the spin contribution is present, and no non-local effective operators shall appear in $\mathbf{S}_q^{\text{eff}}$. For non-local operators $\mathbf{L}_q$ and $\mathbf{J}_\gamma$ we should impose two matching conditions: by equaling both spin and orbital contributions of operators in full and effective theories, respectively, to get coefficients for both local and non-local operators.

We use the following wave function for free electrons with momentum p:

$$u(p) = \sqrt{\frac{p^0+m}{2p^0}}\begin{pmatrix} u_h \\ \frac{\mathbf{p}\cdot\boldsymbol{\sigma}}{p^0+m}u_h \end{pmatrix} \tag{2.25}$$

u_h is the non-relativistic 2-component spinor. To do a non-relativistic reduction, we rewrite the matrix amplitudes in full theory into functions of $u_h^\dagger, u_h$ and compare them with matrix amplitudes in the effective theory.

Tree level calculation yields:

$$\begin{aligned} \langle \mathbf{S}_q \rangle^{(0)}_{\text{spin}} &= u_h^\dagger \frac{\boldsymbol{\sigma}}{2} u_h + \frac{1}{4m^2} u_h^\dagger \left[(\boldsymbol{\sigma}\times\mathbf{p})\times\mathbf{p} \right] u_h + \mathcal{O}(m^{-3}) \\ \langle \mathbf{L}_q \rangle^{(0)}_{\text{spin}} &= -\frac{1}{4m^2} u_h^\dagger \left[(\boldsymbol{\sigma}\times\mathbf{p})\times\mathbf{p} \right] u_h + +\mathcal{O}(m^{-3}) \\ \mathbf{f}(p,p)^{(0)}_{L_q,\text{orbital}} &= u_h^\dagger \mathbf{p} u_h, \end{aligned} \tag{2.26}$$

The result can be compared with the one we got by FW-tranformation in (2.11). By inserting the FW operators between two non-relativistic spinor wave functions we find it indeed agrees with (2.26). Therefore we conclude:

$$a_\sigma^{(0)} = a_\pi^{(0)} = -d_\pi^{(0)} = d_R^{(0)} = 1 \tag{2.27}$$

One loop diagrams are shown in Fig 2.1. We have used dimensional regularization for both infrared and untraviolet divergencies.

The spin contributions are:

$$\begin{aligned} \langle \mathbf{S}_q \rangle^{(1)}_{\text{spin}} &= \frac{\alpha_{\text{EM}}}{2\pi} u_h^\dagger \left\{ \frac{\boldsymbol{\sigma}}{2} + \frac{1}{4m^2}(\boldsymbol{\sigma}\times\mathbf{p})\times\mathbf{p} \right\} u_h \\ \langle \mathbf{L}_q \rangle^{(1)}_{\text{spin}} &= \frac{\alpha_{\text{EM}}}{2\pi} u_h^\dagger \left\{ \left(-\frac{4}{3\epsilon_{\text{UV}}} - \frac{4}{3}\ln\frac{\mu^2}{m^2} - \frac{20}{9} \right)\frac{\boldsymbol{\sigma}}{2} - \frac{1}{4m^2}\frac{8}{3}(\boldsymbol{\sigma}\times\mathbf{p})\times\mathbf{p} \right\} u_h \\ \langle \mathbf{J}_\gamma \rangle^{(1)}_{\text{spin}} &= \frac{\alpha_{\text{EM}}}{2\pi} u_h^\dagger \left\{ \left(\frac{4}{3\epsilon_{\text{UV}}} + \frac{4}{3}\ln\frac{\mu^2}{m^2} + \frac{11}{9} \right)\frac{\boldsymbol{\sigma}}{2} + \frac{1}{4m^2}\frac{5}{3}(\boldsymbol{\sigma}\times\mathbf{p})\times\mathbf{p} \right\} u_h \end{aligned} \tag{2.28}$$

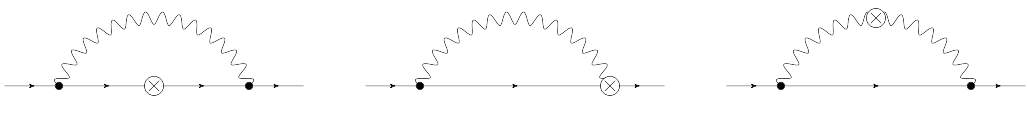

Figure 2.1: One-loop corrections to $\langle e|\mathbf{J}|e\rangle$ in QED. Here $\otimes$ can be either $\mathbf{L}_q$,$\mathbf{S}_q$, or $\mathbf{J}_\gamma$: (a) for $\mathbf{S}_q$; (a)(b) for $\mathbf{L}_q$; (c) for $\mathbf{J}_\gamma$. Wave function renormalization diagrams, mass counterterms and the mirror diagrams are not shown explicitly.

and the orbital contributions:

$$\begin{aligned}\mathbf{f}(p,p)^{(1)}_{L_q,\text{orbital}} &= -\mathbf{f}(p,p)^{(1)}_{J_\gamma,\text{orbital}} \\ &= \frac{\alpha_{\text{EM}}}{2\pi}\left(-\frac{4}{3\epsilon_{\text{UV}}}-\frac{4}{3}\ln\frac{\mu^2}{m^2}-\frac{17}{9}\right)u_h^\dagger \mathbf{p} u_h. \end{aligned} \tag{2.29}$$

As a cross check we calculate the total one-loop contribution from different operators and find:

$$\begin{aligned}\langle \mathbf{S}_q+\mathbf{L}_q+\mathbf{J}_\gamma\rangle^{(1)}_{\text{spin}} &= 0 \\ \mathbf{f}(p,p)^{(1)}_{L_q,\text{orbital}}+\mathbf{f}(p,p)^{(1)}_{J_\gamma,\text{orbital}} &= 0. \end{aligned} \tag{2.30}$$

The vanishing total first-order contribution is expected since the total angular momentum is a conserved quantity and should not depend on expansion parameters.

For the NRQED diagrams we will use dimensional regularization as well. Following the argument in [23], in dimensional regularization all loop diagrams in effective theory are zero due to scaleless integrals. The lack of scale is a natural consequence of the multipole expansion [22] applied in the calculation. In the one-loop diagram containing ultrasoft photons in NRQED, the mass m decoupled from the calculation and the relevant scales are infrared cutoff and ultraviolet cutoff in the

effective theory. However, in dimensional regularization both of them are regulated by spacetime dimension D and the only scale is μ Of course the Wilson coefficients will not depend on physics at the lower energy scale. All the infrared sensitivities that appear in the full theory calculation should be reproduced by the effective theory loop diagrams. It is achieved by setting the result of EFT loop integral in the form:

$$A_{\text{eff}} \left(\frac{1}{\epsilon_{\text{UV}}} - \frac{1}{\epsilon_{\text{IR}}} \right) \tag{2.31}$$

For a general matrix element in full theory, we have

$$\langle \mathcal{O}_{\text{QED}} \rangle^{(1)} = \frac{\alpha_{\text{EM}}}{2\pi} \left(\frac{A}{\epsilon_{\text{UV}}} + \frac{B}{\epsilon_{\text{IR}}} + (A+B) \ln \frac{\mu^2}{m^2} + C + (\text{counterterms}) \right), \tag{2.32}$$

By imposing the matching condition,

$$\begin{aligned} \langle \mathcal{O}_{\text{QED}} \rangle^{(1)}(\mu) &= \langle w_i \mathcal{O}_{i,\text{eff}} \rangle^{(1)}(\mu) \\ &= A_{\text{eff}} \left(\frac{1}{\epsilon_{\text{UV}}} - \frac{1}{\epsilon_{\text{IR}}} \right) + \frac{\alpha_{\text{EM}}}{2\pi} w_i^{(1)}(\mu) \langle \mathcal{O}_{i,\text{eff}} \rangle^{(0)} + (\text{counterterms}) \end{aligned} \tag{2.33}$$

Comparing (2.32) and (2.33), the following relationship should hold:

$$A_{\text{eff}} = -B; \;\; w_i^{(1)}(\mu) \langle \mathcal{O}_{i,\text{eff}} \rangle^{(0)} = (A+B) \ln \frac{\mu^2}{m^2} + C, \tag{2.34}$$

which is to say, the Wilson coefficients can be obtained by dropping all the $1/\epsilon$ poles while keeping logarithms and finite terms in full theory calculation. Effectively this is equivalent to "pulling up" the infrared singularities in the full theory calculation to the ultraviolet sensitivities in the Wilson coefficients of the effective theory.

A drawback of this method is that we must assume the loop diagrams in effective theory produce the same infrared divergences as in full theory. This is a bit

self-proofing since the validity of the effective theory should depend on such a check. Another problem is that the physical meaning of the cutoff scale in the dimensional regularization is unclear. Hence it is not easy to see the separation of scales (hard vs. soft) in the effective theory. We will render the problem by imposing a three-momentum cutoff Λ in the effective theory loop calculations later. At the moment we just satisfy ourselves with this "pull-up" mechanism.

The tree diagram contributions can be readily read from the operators in (2.15)-(2.17):

$$\begin{aligned}
\langle \mathbf{S}_q^{\rm eff}\rangle_{\rm spin} &= u_h^\dagger \left\{ a_\sigma \frac{\boldsymbol{\sigma}}{2} + \frac{a_\pi}{4m^2}(\boldsymbol{\sigma}\times\mathbf{p})\times\mathbf{p} \right\} u_h \\
\langle \mathbf{L}_q^{\rm eff}\rangle_{\rm spin} &= u_h^\dagger \left\{ d_\sigma \frac{\boldsymbol{\sigma}}{2} + \frac{d_\pi}{4m^2}(\boldsymbol{\sigma}\times\mathbf{p})\times\mathbf{p} \right\} u_h \\
\langle \mathbf{J}_\gamma^{\rm eff}\rangle_{\rm spin} &= u_h^\dagger \left\{ f_\sigma \frac{\boldsymbol{\sigma}}{2} + \frac{f_\pi}{4m^2}(\boldsymbol{\sigma}\times\mathbf{p})\times\mathbf{p} \right\} u_h
\end{aligned} \tag{2.35}$$

$$\begin{aligned}
\mathbf{f}(p,p)_{L_q^{\rm eff},{\rm orbital}} &= u_h^\dagger d_R \mathbf{p} u_h \\
\mathbf{f}(p,p)_{J_\gamma^{\rm eff},{\rm orbital}} &= u_h^\dagger f_R \mathbf{p} u_h
\end{aligned} \tag{2.36}$$

Comparing them with (2.28),(2.29) we could deduce:

$$\begin{aligned}
a_\sigma &= 1+\frac{\alpha_{\rm EM}}{2\pi};\ \ a_\pi = 1+\frac{\alpha_{\rm EM}}{2\pi}; \\
d_R &= 1+\frac{\alpha_{\rm EM}}{2\pi}\left(-\frac{4}{3}\ln\frac{\mu^2}{m^2}-\frac{17}{9}\right);\ \ d_\sigma = \frac{\alpha_{\rm EM}}{2\pi}\left(-\frac{4}{3}\ln\frac{\mu^2}{m^2}-\frac{20}{9}\right);\ \ d_\pi = -1-\frac{5\alpha_{\rm EM}}{6\pi} \\
f_R &= \frac{\alpha_{\rm EM}}{2\pi}\left(\frac{4}{3}\ln\frac{\mu^2}{m^2}+\frac{17}{9}\right);\ \ f_\sigma = \frac{\alpha_{\rm EM}}{2\pi}\left(\frac{4}{3}\ln\frac{\mu^2}{m^2}+\frac{11}{9}\right);\ \ f_\pi = \frac{\alpha_{\rm EM}}{3\pi}.
\end{aligned} \tag{2.37}$$

2.4.5 Three-body Matching Conditions

The two-body matching is insufficient to derive all the Wilson coefficients in the effective theory. For example, in two-body calculations operators containing

photon field $\mathbf{E}$ or $\mathbf{B}$ such as the ones proportional to c_D and c_S in (2.7) do not present: their matrix amplitude are of order $\mathcal{O}(m^{-3})$ from NRQED loop diagrams. To acquire all the coefficients up to one-loop, we consider more complicated matrix elements. The next process we will use in this section is an electron interacting with a static field. Together with the free electron case in the last section we can determine all the coefficients bilinear in fermion fields. We will discuss the matching for pure gauge terms in the next subsection.

In short, we calculate the QED amplitude $\langle e_{p'}|\mathcal{O}_J|\mathbf{A}_q e_p\rangle$ for the vector potential, as well as $\langle e_{p'}|\mathcal{O}_J|A_q^0 e_p\rangle$ for the scalar potential, with electrons on shell in both case. The virtual photon interacting with the electron carries a small momentum q comparing to the electron mass, $\mathbf{q}^2 \ll m^2$.

The tree diagrams are shown in Fig. 2.2. In Fig. 2.2(a) the contribution is

Figure 2.2: QED tree diagrams

from the gauge part of L_q and in Fig. 2.2(b) the contribution is from L_q or S_q. To make our matching easier we have set $p^0 = p'^0 = \mathbf{p}^2 + m^2$ in the calculation. In this case, the incident photon momentum $q^\mu = (0, \mathbf{q})$ in which $\mathbf{q} = \mathbf{p}' - \mathbf{p}$.

Clearly the diagrams such as Fig. 2.2(b) will diverge when using physical external states since the intermediate propagator carries a momentum on mass shell.

This is not surprising as it represents the part of the contribution to angular momentum from a free electron. When doing matching this divergency will be exactly canceled by the corresponding effective operators we have already calculated in the previous section. However, in QED there exists another scenario: the intermediate state can be an antiparticle with negative energy. In this case the antiparticle will be deeply off-shell with order $\mathcal{O}(m^{-1})$. Such modes shall be already integrated out in NRQED diagrams. Therefore the antiparticle contribution in QED will shrink to a point and match to the effective operator contributions like those in Fig. 2.3(a). In order to catch all these subtleties, we introduce a small off-shellness by letting the photon momentum q^μ carry a time component: $q^\mu \to (q^0, \mathbf{q})$. Meanwhile we rewrite the operator as $\hat{\mathcal{O}} \to \hat{\mathcal{O}} e^{-iq^0 x^0}$ to maintain the four-momentum conservation. In effect, the additional small momentum $(q^0, 0)$ flows inward from the interacting photon line and outward at the operator, and now the intermediate fermion propagator is no longer on-shell. In the end we let $q^0 \to 0$ go back to the desired operator expansion. When calculating the matrix element we separate the q^0 pole and the finite part to differentiate the contribution purely from the free electron contributions and the contributions from the interaction with the static field. In the following we will only match the finite part between full theory and NRQED. Matching with terms carrying q^0 poles is not necessary since it is merely a replica of the two-body matchings we did before.

After introducing the q^0, the denominator of the intermediate electron propa-

gator in Fig. 2.2(b) can be expanded as:

$$\frac{1}{(p+q)^2-m^2} = \frac{1}{2mq^0}-\frac{1}{4m^2}+\frac{q^0}{8m^3}-\frac{\mathbf{p}^2}{4m^3q^0}+\dots \tag{2.38}$$

Here we have used the on-shell kinematics $p^2=p'^2=m^2$, $\mathbf{p}'=\mathbf{p}+\mathbf{q}$ and $p'^0=p^0\approx m+\mathbf{p}^2/2m$. Later on we should make expansion on powers of q^0 in loop calculations as well.

In calculating the matrix element we make the replacement $\mathbf{x}\to i\boldsymbol{\nabla}_q$, i.e. a derivative with respect to the external momentum of the current. This has several advantages: the result would be symmetric between incoming and outgoing electron momentums; we won't need to consider the derivative over the wave functions since the exchange photon's wave function does not depend on momentum $\mathbf{q}$ and it will greatly simplify the calculation. Of course, the final result will not depend on taking the derivative over which momentum. Finally, the three-momentum conservation relation $\mathbf{p}'=\mathbf{p}+\mathbf{q}$ should be understood only after $\mathbf{x}\to i\boldsymbol{\nabla}_q$ has taken place.

The tree diagram contributions from Fig. 2.2 in full theory are presented below:

$$\begin{aligned}
\langle\mathbf{S}_q\rangle^{(0)}_{\rm spin} &= \frac{e}{4m^2}u_h^\dagger\left[i\mathbf{q}\times\mathbf{A}+(\mathbf{P}\cdot\mathbf{A})\boldsymbol{\sigma}-(\mathbf{P}\cdot\boldsymbol{\sigma})\mathbf{A}\right]u_h\\
\langle\mathbf{L}_q\rangle^{(0)}_{\rm spin} &= \frac{e}{4m^2}u_h^\dagger\left[-i\mathbf{q}\times\mathbf{A}-(\mathbf{P}\cdot\mathbf{A})\boldsymbol{\sigma}+(\mathbf{P}\cdot\boldsymbol{\sigma})\mathbf{A}\right]u_h\\
\mathbf{f}(p',p,p'-p)^{(0)}_{L_q,\rm orbital} &= u_h^\dagger\left[1-\frac{|\mathbf{q}|^2}{8m^2}+\frac{i}{8m^2}(\mathbf{q}\times\mathbf{P})\cdot\boldsymbol{\sigma}\right](-e\mathbf{A})u_h,
\end{aligned} \tag{2.39}$$

in which $\mathbf{P}\equiv\mathbf{p}'+\mathbf{p}$ and $\mathbf{q}\equiv\mathbf{p}'-\mathbf{p}$. Terms of order $\mathcal{O}(m^{-3})$ are dropped.

Now we consider the tree diagrams in NRQED as shown in Fig.2.3. The inner

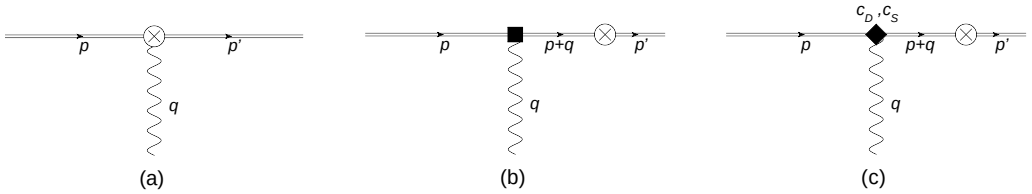

Figure 2.3: NRQED tree diagrams

line fermion propagator in Fig.2.3(b),(c) will be:

$$\frac{1}{E_p - \frac{(\mathbf{p}+\mathbf{q})^2}{2m} + i0} \sim \frac{1}{E_{p'} - \frac{\mathbf{p}'^2}{2m} + i0} \tag{2.40}$$

and will again diverge after applying the relation $E^0_{p'} = E^0_p = \mathbf{p}^2/2m$ for on-shell external states. By introducing a small non-zero q^0, the fermion propagator in Fig. 2.3(b),(c) will become $\frac{i}{q^0+i\epsilon}$. Since our operators do not contain time derivatives, the q^0 pole can only be canceled by Dirac and spin-orbit interactions: in an effective Lagrangian the c_D, c_S terms contain $E^i = -F^{0i} \sim i(q^0 A^i - q^i A^0)$ containing positive powers of q^0. We will calculate $\langle e|\mathbf{x}\times\boldsymbol{\pi}|e\mathbf{A}\rangle^{\rm eff,Tree}_{\rm Spin}$ below as an example.

We can readily write down the spin contribution from Fig. 2.3:

$$\begin{aligned}
\langle e|\mathbf{x}\times\boldsymbol{\pi}|e\mathbf{A}\rangle^{(0)}_{\rm Spin,Tree} &= i\boldsymbol{\nabla}_q \times u_h^\dagger \left\{ (-e\mathbf{A}) + \left(\frac{i\mathbf{p}}{q^0+i0} + \frac{i\mathbf{p}'}{-q^0+i0} \right) \right. \\
&\quad \cdot \left[\frac{iec_D}{8m^2}\mathbf{q}\cdot(\mathbf{q}A^0 - q^0\mathbf{A}) + \frac{ec_S}{8m^2}A^0\sigma\cdot(\mathbf{P}\times\mathbf{q}) \right] \\
&\quad \left. + \frac{ec_S}{8m^2}q^0 \left(\frac{i\mathbf{p}\,[(2\mathbf{p}'-\mathbf{q})\cdot\mathbf{A}\times\boldsymbol{\sigma}]}{q^0+i0} + \frac{i\mathbf{p}'\,[(2\mathbf{p}+\mathbf{q})\cdot\mathbf{A}\times\boldsymbol{\sigma}]}{-q^0+i0} \right) \right\} u_h \\
&= u_h^\dagger \left[\frac{(\mathbf{p}'-\mathbf{p})}{q^0} \times \frac{iec_D}{8m^2}(-q^0\mathbf{A}) + \frac{(\mathbf{p}+\mathbf{p}')}{q^0} \times \frac{ec_S}{8m^2}q^0(\mathbf{A}\times\boldsymbol{\sigma}) \right] u_h \\
&= u_h^\dagger \left[-\frac{iec_D}{8m^2}\mathbf{q}\times\mathbf{A} - \frac{ec_S}{8m^2}\mathbf{P}\times(\boldsymbol{\sigma}\times\mathbf{A}) \right] u_h + (q^0 \text{ poles})
\end{aligned} \tag{2.41}$$

As mentioned before, we keep finite terms only and have dropped all the terms containing q^0 poles.

In a similar fashion we calculate all the tree diagrams contributing to the spin and orbital part of the angular momentum for the effective operators appearing in (2.15)-(2.17). The results are listed in Table 2.4.5.

operator	*spin*	*orbital*
$\psi^\dagger(\boldsymbol{\sigma}/2)\psi$	$\frac{e}{8m^2}c_S u_h^\dagger(\mathbf{P}\times\mathbf{A})\times\boldsymbol{\sigma}u_h$	-
$\psi^\dagger\mathbf{x}\times\boldsymbol{\pi}\psi$	$-\frac{e}{8m^2}u_h^\dagger\left[c_D(i\mathbf{q}\times\mathbf{A})\right.$ $\left.+c_S\mathbf{P}\times(\boldsymbol{\sigma}\times\mathbf{A})\right]u_h$	$\frac{e}{8m^2}u_h^\dagger\left[c_D(\mathbf{q}\cdot\mathbf{A})\mathbf{q}\right.$ $\left.+ic_S\boldsymbol{\sigma}\cdot(\mathbf{P}\times\mathbf{A})\mathbf{q}\right]u_h$
$\psi^\dagger\left[\mathbf{x}\times(\boldsymbol{\sigma}\times\mathbf{E})\right]\psi$	$2u_h^\dagger(A^0\boldsymbol{\sigma})u_h$	$-\mathbf{x}\times u_h^\dagger(A^0\boldsymbol{\sigma}\times i\mathbf{q})u_h$
$\psi^\dagger\left[(\boldsymbol{\sigma}\times\boldsymbol{\pi})\times\boldsymbol{\pi}\right.$ $\left.-\boldsymbol{\pi}\times(\boldsymbol{\sigma}\times\boldsymbol{\pi})\right]\psi$	$u_h^\dagger\left[\mathbf{P}\times(\boldsymbol{\sigma}\times\mathbf{A})\right.$ $\left.+\mathbf{A}\times(\boldsymbol{\sigma}\times\mathbf{P})\right]u_h$	-
$\psi^\dagger\mathbf{B}\psi$	$u_h^\dagger i\mathbf{q}\times\mathbf{A}u_h$	-
$\mathbf{x}\times\left[\mathbf{B}\times\boldsymbol{\nabla}(\psi^\dagger\psi)\right]$	$u_h^\dagger i\mathbf{q}\times\mathbf{A}u_h$	$u_h^\dagger\left[\mathbf{q}^2\mathbf{A}-(\mathbf{q}\cdot\mathbf{A})\mathbf{q}\right]u_h$
$\mathbf{x}\times\psi^\dagger\left[\boldsymbol{\sigma}\times(\mathbf{B}\times\overleftrightarrow{\boldsymbol{\pi}})\right]\psi$	$u_h^\dagger\left[(\sigma\cdot\mathbf{P})\mathbf{A}+(\mathbf{A}\cdot\mathbf{P})\boldsymbol{\sigma}\right]u_h$	$u_h^\dagger\left[(i\mathbf{q}\cdot\mathbf{P})\boldsymbol{\sigma}\times\mathbf{A}\right.$ $\left.-(\mathbf{A}\cdot\mathbf{P})\boldsymbol{\sigma}\times i\mathbf{q}\right]u_h$
$\mathbf{x}\times\psi^\dagger\left[\mathbf{B}\times(\boldsymbol{\sigma}\times\overleftrightarrow{\boldsymbol{\pi}})\right]\psi$	$u_h^\dagger\mathbf{A}\times(\boldsymbol{\sigma}\times\mathbf{P})u_h$	$u_h^\dagger\left[\boldsymbol{\sigma}\cdot(i\mathbf{q}\times\mathbf{P})\mathbf{A}\right.$ $\left.+\boldsymbol{\sigma}\cdot(\mathbf{P}\times\mathbf{A})i\mathbf{q}\right]u_h$

Table 2.1: Spin and orbital contributions to $\langle e|\mathcal{O}^{\rm eff}|e\gamma\rangle_{\rm Tree}$

From (2.39), (2.15), (2.16) we get:

$$a_\sigma^{(0)} = a_\pi^{(0)} = a_B^{(0)} = 1;$$

$$d_\sigma^{(0)} = -d_\pi^{(0)} = -d_B^{(0)} = d_D^{(0)} = d_S^{(0)} = 1; \tag{2.42}$$

all other Wilson coefficients in $\mathbf{S}_q^{\text{eff}}$ and $\mathbf{L}_q^{\text{eff}}$ will be of order $\mathcal{O}(\alpha_{\text{EM}})$ or higher. This agrees with the non-relativistic decomposition obtained by the FW transformation method in (2.11).

In the following we will calculate the one-loop contributions for the angular momentum in QED. To collect all the diagrams one can draw a scattering diagram first, then insert angular momentum operators at all possible positions. Furthermore, we will not put $\mathbf{J}_\gamma$ on the external photon line; matching of the gauge part will be done with photons as external states in the next subsection.

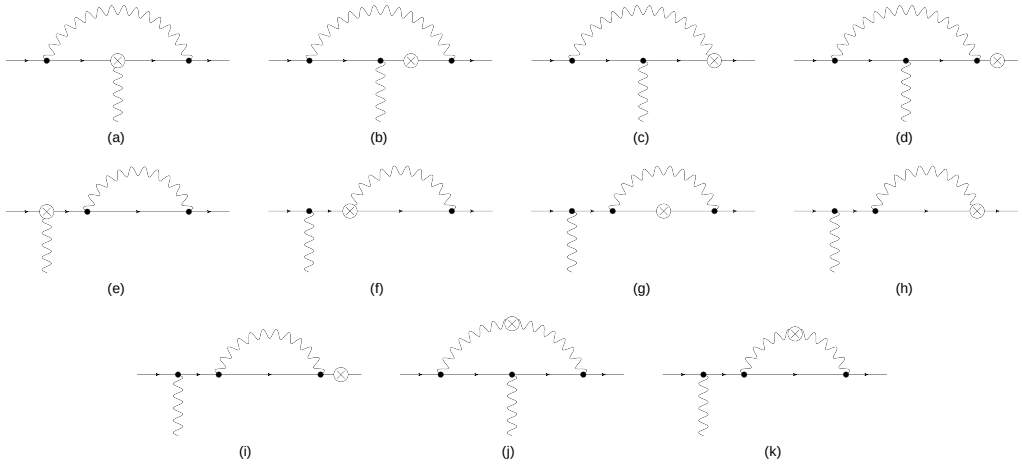

Figure 2.4: One-loop contributions to $\langle e|\mathbf{J}|e\gamma\rangle$ in QED. Here $\otimes$ can be either $\mathbf{L}_q$,$\mathbf{S}_q$, or $\mathbf{J}_\gamma$: (a)-(i) for $\mathbf{L}_q$; (b)(d)(g)(i) for $\mathbf{S}_q$; (j)(k) for $\mathbf{J}_\gamma$. Wave function renormalization diagrams, mass counter terms and the mirror diagrams are not shown explicitly.

The loop diagrams are considerably more complicated. For the spin part,

again we apply $\mathbf{x} \to -i\boldsymbol{\nabla}_q$ but we cannot apply three-momentum conservation at the operator before $\boldsymbol{\nabla}_q$ has taken place. The matrix element should be expanded in powers of q^0, and only the finite part under the limit $q^0 \to 0$ are relevant for our matching purpose. A non-relativistic expansion of the matrix element in full theory into two-component spinors, similar to the two-body case, is proceeded as well.

With vector external potential $\mathbf{A}$, the spin part:

$$\langle \mathbf{S}_q \rangle^{(1)}_{\rm spin} = \frac{\alpha_{\rm EM}}{2\pi}\frac{e}{4m^2} u_h^\dagger \left[7i\mathbf{q}\times\mathbf{A} + (\mathbf{P}\cdot\mathbf{A})\boldsymbol{\sigma} + (\boldsymbol{\sigma}\cdot\mathbf{A})\mathbf{P} - 2(\mathbf{P}\cdot\boldsymbol{\sigma})\mathbf{A}\right] u_h \quad (2.43)$$

$$\begin{aligned}\langle \mathbf{L}_q \rangle^{(1)}_{\rm spin} = \frac{\alpha_{\rm EM}}{2\pi}\frac{e}{4m^2} u_h^\dagger \Bigg[&\left(\frac{8}{\epsilon_{\rm IR}} + 8\ln\frac{\mu^2}{m^2} + \frac{50}{3}\right) i\mathbf{q}\times\mathbf{A} + \frac{2}{3}(\mathbf{P}\cdot\mathbf{A})\boldsymbol{\sigma} \\ &-2(\boldsymbol{\sigma}\cdot\mathbf{A})\mathbf{P} + \frac{8}{3}(\mathbf{P}\cdot\boldsymbol{\sigma})\mathbf{A}\Bigg] u_h \end{aligned} \quad (2.44)$$

$$\begin{aligned}\langle \mathbf{J}_\gamma \rangle^{(1)}_{\rm spin} = \frac{\alpha_{\rm EM}}{2\pi}\frac{e}{4m^2} u_h^\dagger \Bigg[&\left(-\frac{8}{\epsilon_{\rm IR}} - 8\ln\frac{\mu^2}{m^2} - \frac{71}{3}\right) i\mathbf{q}\times\mathbf{A} - \frac{5}{3}(\mathbf{P}\cdot\mathbf{A})\boldsymbol{\sigma} \\ &+(\boldsymbol{\sigma}\cdot\mathbf{A})\mathbf{P} - \frac{2}{3}(\mathbf{P}\cdot\boldsymbol{\sigma})\mathbf{A}\Bigg] u_h, \end{aligned} \quad (2.45)$$

as well as the orbital contributions:

$$\begin{aligned}&\mathbf{f}(p', p, p'-p)^{(1)}_{L_q,\rm orbital} \\ &= \frac{\alpha_{\rm EM}}{2\pi}\frac{e}{4m^2} u_h^\dagger \Bigg[\left(\frac{4}{3\epsilon_{\rm UV}} + \frac{4}{3}\ln\frac{\mu^2}{m^2} + \frac{17}{9}\right)(4m^2)\mathbf{A} - \frac{2}{3}i(\mathbf{P}\cdot\mathbf{A})(\boldsymbol{\sigma}\times\mathbf{q}) \\ &\quad -\frac{5}{3}i[\boldsymbol{\sigma}\cdot(\mathbf{P}\times\mathbf{A})]\mathbf{q} + \left(\frac{2}{3\epsilon_{\rm UV}} + \frac{2}{3}\ln\frac{\mu^2}{m^2} - \frac{31}{18}\right) i[\boldsymbol{\sigma}\cdot(\mathbf{q}\times\mathbf{P})]\mathbf{A} \\ &\quad -\frac{7}{9}(\mathbf{q}\cdot\mathbf{A})\mathbf{q} + \left(-\frac{2}{3\epsilon_{\rm UV}} - \frac{4}{3\epsilon_{\rm IR}} - 2\ln\frac{\mu^2}{m^2} - \frac{1}{6}\right)|\mathbf{q}|^2\mathbf{A}\Bigg] u_h \end{aligned} \quad (2.46)$$

$$
\begin{aligned}
&\mathbf{f}(p',p,p'-p)^{(1)}_{J_\gamma,\text{orbital}} \\
&= \frac{\alpha_{\text{EM}}}{2\pi}\frac{e}{4m^2}u_h^\dagger\left[\left(-\frac{4}{3\epsilon_{\text{UV}}}-\frac{4}{3}\ln\frac{\mu^2}{m^2}-\frac{17}{9}\right)(4m^2)\mathbf{A}+\frac{2}{3}i(\mathbf{P}\cdot\mathbf{A})(\boldsymbol{\sigma}\times\mathbf{q})\right. \\
&\quad +\frac{5}{3}i[\boldsymbol{\sigma}\cdot(\mathbf{P}\times\mathbf{A})]\mathbf{q}+\left(-\frac{2}{3\epsilon_{\text{UV}}}-\frac{2}{3}\ln\frac{\mu^2}{m^2}+\frac{13}{18}\right)i[\boldsymbol{\sigma}\cdot(\mathbf{q}\times\mathbf{P})]\mathbf{A} \\
&\quad \left.+\frac{7}{9}(\mathbf{q}\cdot\mathbf{A})\mathbf{q}+\left(\frac{2}{3\epsilon_{\text{UV}}}+\frac{2}{3}\ln\frac{\mu^2}{m^2}+\frac{1}{6}\right)|\mathbf{q}|^2\mathbf{A}\right]u_h. \qquad (2.47)
\end{aligned}
$$

For scalar potential A^0, the spin part is

$$
\begin{aligned}
\langle\mathbf{S}_q\rangle^{(1)}_{\text{spin}} &= \mathcal{O}(m^{-3}) \\
\langle\mathbf{L}_q\rangle^{(1)}_{\text{spin}} &= \frac{\alpha_{\text{EM}}}{2\pi}\frac{e}{4m^2}u_h^\dagger\left[\frac{4m}{3}A^0\boldsymbol{\sigma}\right]u_h \\
\langle\mathbf{J}_\gamma\rangle^{(1)}_{\text{spin}} &= \frac{\alpha_{\text{EM}}}{2\pi}\frac{e}{4m^2}u_h^\dagger\left[-\frac{4m}{3}A^0\boldsymbol{\sigma}\right]u_h, \qquad (2.48)
\end{aligned}
$$

and the orbital part is

$$
\begin{aligned}
\mathbf{f}(p',p,p'-p)^{(1)}_{L_q,\text{orbital}} &= \frac{\alpha_{\text{EM}}}{2\pi}\frac{e}{4m^2}u_h^\dagger\left[-\frac{2m}{3}A^0 i(\boldsymbol{\sigma}\times\mathbf{q})\right]u_h \\
\mathbf{f}(p',p,p'-p)^{(1)}_{J_\gamma,\text{orbital}} &= \frac{\alpha_{\text{EM}}}{2\pi}\frac{e}{4m^2}u_h^\dagger\left[\frac{2m}{3}A^0 i(\boldsymbol{\sigma}\times\mathbf{q})\right]u_h. \qquad (2.49)
\end{aligned}
$$

Again we conduct a cross check over all the results. By summing up spin and orbital angular momentum contributions from different parts of the decomposition we have:

$$
\begin{aligned}
\langle e|\mathbf{S}_q+\mathbf{L}_q+\mathbf{J}_\gamma|e\mathbf{A}\rangle^{(1)}_{\text{spin}} &= \langle e|\mathbf{S}_q+\mathbf{L}_q+\mathbf{J}_\gamma|eA^0\rangle^{(1)}_{\text{spin}}=0, \\
\langle e|\mathbf{S}_q+\mathbf{L}_q+\mathbf{J}_\gamma|e\mathbf{A}\rangle^{(1)}_{\text{orbital}} &= \frac{\alpha_{\text{EM}}}{2\pi}\frac{e}{4m^2}\mathbf{x}\times u_h^\dagger\left[-2i[\boldsymbol{\sigma}\cdot(\mathbf{q}\times\mathbf{P})]\mathbf{A}\right. \\
&\quad \left.+\left(-\frac{4}{3\epsilon_{\text{IR}}}-\frac{4}{3}\ln\frac{\mu^2}{m^2}\right)|\mathbf{q}|^2\mathbf{A}\right]u_h \\
\langle e|\mathbf{S}_q+\mathbf{L}_q+\mathbf{J}_\gamma|eA^0\rangle^{(1)}_{\text{orbital}} &= 0 \qquad (2.50)
\end{aligned}
$$

It can be observed that all the first-order contributions, except $\langle e|\mathbf{S}_q+\mathbf{L}_q+\mathbf{J}_\gamma|e\mathbf{A}\rangle^{(1)}_{\text{orbital}}$, are summed up to zero. The non-zero first-order expansion for $\langle e|\mathbf{J}_{\text{NRQED}}|e\mathbf{A}\rangle^{(1)}_{\text{orbital}}$ roots in the non-zero one-loop contributions from $F_1(q^2)$ and $F_2(q^2)$ to the current. In the calculation we didn't include the diagram with operator J_γ placing on the outgoing photon line. Had we included that, the orbital contribution $\langle e|\mathbf{J}_\gamma|e\mathbf{A}\rangle^{(1)}_{\text{orbital}}$ would have additional terms and the sum of the orbital contribution would sum up to zero. We leave the matching of gauge part angular momentum operators to the next section.

Again in NRQED we calculate the tree diagram only, with the understanding that under dimensional regularization, loop diagrams in NRQED have no scale and contain pole structures as described in the previous two-body matching case.

By applying the matching condition (2.18) together with Table 2.4.5, all the Wilson coefficients of the effective operators for bi-quark operators can be determined:

$$
\begin{aligned}
&a_\sigma = 1+\frac{\alpha_{\text{EM}}}{2\pi},\ \ a_\pi = 1+\frac{\alpha_{\text{EM}}}{2\pi},\ \ a_B = 1+\frac{7\alpha_{\text{EM}}}{2\pi}; a_{\gamma_1} = -\frac{\alpha_{\text{EM}}}{3\pi}; a_{\gamma_2} = \frac{2\alpha_{\text{EM}}}{3\pi};\\
&d_R = 1+\frac{\alpha_{\text{EM}}}{2\pi}\left(-\frac{4}{3}\ln\frac{\mu^2}{m^2}-\frac{17}{9}\right),\ \ d_\sigma = \frac{\alpha_{\text{EM}}}{2\pi}\left(-\frac{4}{3}\ln\frac{\mu^2}{m^2}-\frac{20}{9}\right),\ \ d_\pi = -1-\frac{5\alpha_{\text{EM}}}{6\pi},\\
&d_D = 1+\frac{\alpha_{\text{EM}}}{2\pi}\left(\frac{4}{3}\ln\frac{\mu^2}{m^2}-\frac{1}{3}\right),\ \ d_S = 1+\frac{\alpha_{\text{EM}}}{2\pi}\left(-\frac{4}{3}\ln\frac{\mu^2}{m^2}+\frac{31}{9}\right),\\
&d'_S = \frac{2\alpha_{\text{EM}}}{3\pi},\ \ d_E = \frac{\alpha_{\text{EM}}}{3\pi},\ \ d_B = -1+\frac{\alpha_{\text{EM}}}{2\pi}\left(-8\ln\frac{\mu^2}{m^2}+\frac{157}{9}\right);\\
&f_R = \frac{\alpha_{\text{EM}}}{2\pi}\left(\frac{4}{3}\ln\frac{\mu^2}{m^2}+\frac{17}{9}\right),\ \ f_\sigma = \frac{\alpha_{\text{EM}}}{2\pi}\left(\frac{4}{3}\ln\frac{\mu^2}{m^2}+\frac{11}{9}\right),\ \ f_\pi = \frac{\alpha_{\text{EM}}}{3\pi},\\
&f_D = \frac{\alpha_{\text{EM}}}{2\pi}\left(\frac{4}{3}\ln\frac{\mu^2}{m^2}+\frac{1}{3}\right),\ \ f_S = -\frac{\alpha_{\text{EM}}}{2\pi}\left(-\frac{4}{3}\ln\frac{\mu^2}{m^2}+\frac{13}{9}\right),\\
&f'_S = -\frac{2\alpha_{\text{EM}}}{3\pi},\ \ f_E = -\frac{\alpha_{\text{EM}}}{3\pi},\ \ f_B = \frac{\alpha_{\text{EM}}}{2\pi}\left(8\ln\frac{\mu^2}{m^2}-\frac{220}{9}\right).
\end{aligned}
\tag{2.51}
$$

2.4.6 Gauge Field Matching Conditions

Now we calculate $\langle\gamma|\hat{\mathcal{O}}|\gamma\rangle$ up to $\mathcal{O}(\alpha_{\rm EM})$ with offshell photons carrying momentum q. Both $\mathbf{S}_q$ and $\mathbf{L}_q$ will contribute to the amplitude at one-loop.

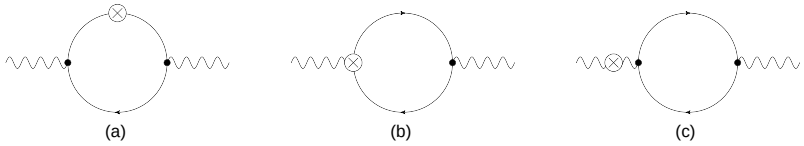

Figure 2.5: One-loop contributions to $\langle\gamma|\mathbf{J}|\gamma\rangle$ in QED. Mirror diagrams are not shown. (a) for $\hat{S}_q$; (a)(b) for $\hat{L}_q$; (c) for $\hat{J}_\gamma$.

The tree level matching is straightforward. At tree level the gauge field part of the Lagrangian of NRQED is the same as in QED, and so is the contribution. Therefore we have

$$f_\gamma^{(0)} = 1, \quad d_\gamma^{(0)} = 0. \tag{2.52}$$

Furthermore, since there is no photon-photon interaction in QED, the one-loop contribution from $\mathbf{J}_\gamma$ can only arise from Fig. 2.5(c). Immediately we can see that the form of the photon angular momentum $\mathbf{J}_\gamma$ will just match to itself since the vacuum loop contribution is replicated by the d_1 and d_2 terms in the effective Lagrangian. All the contributions in full theory will be matched by the wave-function renormalization in NRQED; thus we conclude:

$$f_\gamma^{(1)} = 0, \tag{2.53}$$

and there should be no $\mathcal{O}(\alpha_{\rm EM}^0 m^{-2})$ order terms in (2.17).

Starting from one loop, $\mathbf{S}_q$ and $\mathbf{L}_q$ enter the matching scheme with contributions in QED as:

$$\langle\gamma|\mathbf{S}_q|\gamma\rangle^{(1)}_{\rm spin} = \frac{\alpha_{\rm EM}}{2\pi}\frac{i}{m^2}\frac{2}{3}\left[(\mathbf{A}\times\mathbf{A}^*)q^0q^2-(\mathbf{A}\times\mathbf{q})q^2A^{*0}-(\mathbf{q}\times\mathbf{A}^*)q^2A^0\right] \quad (2.54)$$

$$\begin{aligned}\langle\gamma|\mathbf{L}_q|\gamma\rangle^{(1)}_{\rm spin} &= \frac{\alpha_{\rm EM}}{2\pi}\left(\frac{\mu^2}{m^2}\right)^{\epsilon}\frac{2i}{3\epsilon_{\rm UV}}\left[(\mathbf{A}\times\mathbf{A}^*)q^0+(\mathbf{A}\times\mathbf{q})A^{*0}+2(\mathbf{q}\times\mathbf{A}^*)A^0\right]\\ &+\frac{\alpha_{\rm EM}}{2\pi}\frac{i}{m^2}\frac{1}{15}\left[(\mathbf{A}\times\mathbf{A}^*)q^0q^2+3(\mathbf{A}\times\mathbf{q})q^2A^{*0}+13(\mathbf{q}\times\mathbf{A}^*)q^2A^0\right.\\ &\left.+4(\mathbf{A}\times\mathbf{q})(q\cdot A^*)q^0+4(\mathbf{q}\times\mathbf{A}^*)(q\cdot A)q^0\right] \quad (2.55)\end{aligned}$$

$$\begin{aligned}\mathbf{f}(q,q)^{(1)}_{L_q,\rm orbital} &= \frac{\alpha_{\rm EM}}{2\pi}\left(\frac{\mu^2}{m^2}\right)^{\epsilon}\frac{2}{3\epsilon_{\rm UV}}\left[-2(A\cdot A^*)q^0\mathbf{q}+(q\cdot A)q^0\mathbf{A}^*+(q\cdot A^*)q^0\mathbf{A}\right]\\ &+\frac{\alpha_{\rm EM}}{2\pi}\frac{1}{m^2}\frac{2}{15}\left[-4(A\cdot A^*)q^0q^2\mathbf{q}+(q\cdot A)q^0q^2\mathbf{A}^*+(q\cdot A^*)q^0q^2\mathbf{A}\right.\\ &+(q\cdot A)A^{*0}q^2\mathbf{q}+(q\cdot A^*)A^0q^2\mathbf{q}-(q^2)^2(A^0\mathbf{A}^*+A^{*0}\mathbf{A})\\ &\left.+2(q\cdot A)(q\cdot A^*)q^0\mathbf{q}\right]. \quad (2.56)\end{aligned}$$

Here A and A^* represent the incoming and outgoing photon wave function, respectively.

In NRQED the only contribution is from the tree diagram since all the physics at scale $\mathcal{O}(m)$ has been integrated out and no vacuum polarization diagram shall appear in the effective theory. Notice that this is different from the situation at bilinear term matchings in previous sections: there the loop diagrams vanish due to the scaleless integrals in dimensional regularization, and it should be understood as containing both UV and IR poles. We collect spin and orbital contributions from effective operators in (2.15), (2.16) and (2.17) into Table 2.4.6:

Comparing the contributions from the full theory and the NRQED, we con-

operator	*spin*	*orbital*
$\mathbf{x}\times(\mathbf{E}\times\mathbf{B})$	$i\left[(\mathbf{A}\times\mathbf{A}^*)q^0+(\mathbf{A}\times\mathbf{q})A^{*0}\right.$ $\left.+2(\mathbf{q}\times\mathbf{A}^*)A^0\right]$	$\mathbf{x}\times[-2(A\cdot A^*)q^0\mathbf{q}$ $+(q\cdot A)q^0\mathbf{A}^*+(q\cdot A^*)q^0\mathbf{A}]$
$\left[\dot{\mathbf{E}}\times\mathbf{E}-\dot{\mathbf{B}}\times\mathbf{B}\right]$	$-2i\left[q^0q^2\mathbf{A}\times\mathbf{A}^*\right.$ $-(q\cdot A^*)q^0\mathbf{A}\times\mathbf{q}$ $\left.-(q\cdot A)q^0\mathbf{q}\times\mathbf{A}^*\right]$	-
$\boldsymbol{\nabla}\times(\mathbf{E}\times\mathbf{B})$	$-i\left[(q^2A^0-q\cdot Aq^0)\mathbf{q}\times\mathbf{A}^*\right.$ $\left.+(q^2A^{*0}-q\cdot A^*q^0)\mathbf{A}\times\mathbf{q}\right]$	-
$\mathbf{x}\times(\Box\mathbf{E}\times\mathbf{B})$	$-i\left[4q^2A^0\mathbf{q}\times\mathbf{A}^*-q^2A^{*0}\mathbf{A}\times\mathbf{q}\right.$ $\left.+q^0q^2\mathbf{A}\times\mathbf{A}^*-2q\cdot Aq^0\mathbf{q}\times\mathbf{A}^*\right]$	$\mathbf{x}\times[(q^2)^2(A^{*0}\mathbf{A}+A^0\mathbf{A}^*)$ $+2q^0q^2(A\cdot A^*)\mathbf{q}$ $-q^2(q\cdot A)(q^0\mathbf{A}^*+A^{*0}\mathbf{q})$ $-q^2(q\cdot A^*)(q^0\mathbf{A}+A^0\mathbf{q})]$
$\left[\dot{\mathbf{E}}^a(\mathbf{x}\times\boldsymbol{\nabla})\mathbf{E}^a\right.$ $\left.+\dot{\mathbf{B}}^a(\mathbf{x}\times\boldsymbol{\nabla})\mathbf{B}^a\right]$	$4iq^0(q\cdot A)\mathbf{q}\times\mathbf{A}^*$	$\mathbf{x}\times[-4q^0q^2(A\cdot A^*)\mathbf{q}$ $+4q^0(q\cdot A)(q\cdot A^*)\mathbf{q}]$

Table 2.2: Spin and orbital contributions of $\langle\gamma|\mathcal{O}^{\rm eff}|\gamma\rangle_{\rm Tree}$

clude:

$$a_{\gamma_1}=-\frac{\alpha_{\rm EM}}{3\pi};a_{\gamma_2}=\frac{2\alpha_{\rm EM}}{3\pi};$$
$$d_\gamma=\frac{\alpha_{\rm EM}}{3\pi}\ln\frac{\mu^2}{m^2};d_{\gamma_1}=\frac{\alpha_{\rm EM}}{15\pi};d_{\gamma_2}=-\frac{2\alpha_{\rm EM}}{3\pi};d_{\gamma_3}=-\frac{4\alpha_{\rm EM}}{15\pi};d_{\gamma_4}=\frac{2\alpha_{\rm EM}}{15\pi};$$
$$f_\gamma=1. \quad (2.57)$$

2.4.7 Separating QED and NRQED Cutoffs

In previous sections we have seen that the decomposed angular momentum operators in NRQED are scale-dependent with logarithms containing μ. We expect the high-energy physics is completely contained in the Wilson coefficients of the effective operators, and they shall have the same running scheme as the full theory operators at high energy. In other words, they should satisfy the renormalization group (RG) evolution equations derived from the full theory[28]:

$$\frac{d}{dt}\begin{pmatrix}\mathbf{J}_q^{\text{eff}}\\ \mathbf{J}_\gamma^{\text{eff}}\end{pmatrix} = \frac{\alpha_{\text{EM}}}{2\pi}\begin{pmatrix}-\frac{4}{3} & \frac{1}{3}+\frac{1}{3}\\ \frac{4}{3} & -\frac{1}{3}+\frac{1}{3}\end{pmatrix}\begin{pmatrix}\mathbf{J}_q^{\text{eff}}\\ \mathbf{J}_\gamma^{\text{eff}}\end{pmatrix} \tag{2.58}$$

where $t = \ln \mu^2/m^2$. Here $\mathbf{J}_q^{\text{eff}} \equiv \mathbf{S}_q^{\text{eff}} + \mathbf{L}_q^{\text{eff}}$ represents the total angular momentum carried by the electron. The additional $\frac{1}{3}$ in the evolution equation stems from the scale dependence of the redefined photon fields in the effective theory, the d_1 term.

Our effective operator (2.15)-(2.17) with Wilson coefficients in (2.51) and (2.57) fail to satisfy (2.58), however. The main issue here is that in deriving the Wilson coefficients we have made arguments that the effective theory would produce infrared divergencies via loop diagrams and effectively "pull" the infrared divergencies to be ultraviolet by the mechanisms described before. Those ultraviolet divergencies, however, are in effective theory and should not run above the matching scale. However, we have used the same cutoff μ throughout our calculation and the result should only be valid at some matching scale. By introducing different cutoff schemes in QED and in NRQED, we might be able to restore the relationship in (2.58) and see the physics in different scales more clearly.

We will reconstruct the calculation with a three-momentum cutoff Λ in NRQED.

In addition, We let the photon acquire a small mass λ in both QED and effective theory to regulate the infrared divergencies. By [25] the Wilson coefficient in NRQED Lagrangian is now:

$$c_2 = c_4 = 1;\;\; c_F = 1 + \frac{\alpha_{\rm EM}}{2\pi};\;\; c_D = 1 - \frac{8\alpha_{\rm EM}}{3\pi}\left(\ln\frac{2\Lambda}{m} - \frac{5}{6}\right);\;\; c_S = 1 + \frac{\alpha_{\rm EM}}{\pi};$$
$$d_1 = 1 + \frac{\alpha_{\rm EM}}{3\pi}\ln\frac{\mu^2}{m^2};\;\; d_2 = \frac{\alpha_{\rm EM}}{60\pi}. \tag{2.59}$$

The separation of scales is shown explicitly here: all the infrared sensitivities are contained in the effective operators and the coefficients will not depend on the artificial photon mass regulator λ, as we proposed.

The full theory amplitude under the photon mass regulator can be acquired by making the replacement in (2.43)-(2.47):

$$\left(\frac{1}{\epsilon_{\rm IR}} + \ln\frac{\mu^2}{m^2}\right) \to 2\ln\frac{\lambda}{m}. \tag{2.60}$$

For the effective theory, we should now consider not only the tree diagrams but also loop diagrams. Since both quantities we are calculating are gauge-invariant in full-theory and in effective theory, we can choose Coulomb gauge in calculating the effective diagrams. Similar to the full theory calculation, the three-momentum conservation $\mathbf{p} + \mathbf{q} = \mathbf{p}'$ should be understood only after $\mathbf{x} \to i\boldsymbol{\nabla}$ has taken place. The Fermion propagator is a little different than the conventional field theory: it should be understood as a multipole expansion in powers of m after using the relation $E_p = |\mathbf{p}|^2/2m$. For example, a Fermion propagator with momentum $(p + k)$ should be written as:

$$S_F^{\rm eff}(p+k) = \frac{1}{E_p + k^0 - \frac{(\mathbf{p}+\mathbf{k})^2}{2m} + i0} = \frac{1}{k^0 + i0} + \frac{2\mathbf{p}\cdot\mathbf{k} + \mathbf{k}^2}{2m(k^0 + i0)^2} + \ldots \tag{2.61}$$

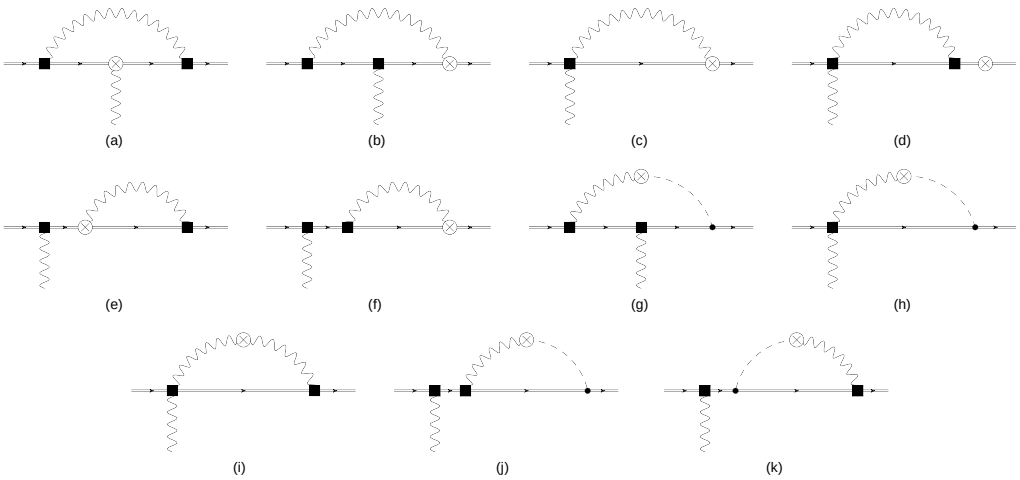

Figure 2.6: One-loop corrections to $\langle e|\mathbf{L}_q^{\text{eff}}|e\mathbf{A}\rangle$, (a)-(f), and $\langle e|\mathbf{J}_\gamma^{\text{eff}}|e\mathbf{A}\rangle$, (g)-(k), in NRQED.

By power counting we can eliminate many diagrams in effective theory. One point worth being mentioned is there shall be no diagrams with a Coulomb propagator connecting two points on the Fermion line directly. The reason is that the process we are considering is a time-ordered one and the Coulomb interaction does not contain an energy part, i.e., an instantaneous interaction. All the diagrams we should consider in NRQED are listed in Fig. 2.6. In the diagram the filled box represents the vertex interaction from term $-\frac{\mathbf{D}^2}{2m}$ in the NRQED Lagrangian. In the diagram the filled box represents the vertex interaction from term $-\frac{\mathbf{D}^2}{2m}$ in the NRQED Lagrangian and the dot represents the D^0 vertex. The dashed line is for the Coulomb photon propagator while the waving line is for the transverse photon propagator. Wave function renormalization diagrams, mass counterterms and the mirror diagrams are not shown explicitly.

The one-loop effective theory matrix elements now reads (with three-momentum

NRQED cutoff Λ):

$$\begin{aligned}
\langle \mathbf{L}_q^{\rm eff}\rangle^{(1)}_{\rm spin} &= \frac{\alpha_{\rm EM}}{2\pi}\frac{-4ie}{m^2} d_R^{(0)} \left(\ln\frac{2\Lambda}{\lambda}-\frac{5}{6}\right) u_h^\dagger \mathbf{q}\times\mathbf{A} u_h \\
\langle \mathbf{J}_\gamma^{\rm eff}\rangle^{(1)}_{\rm spin} &= \frac{\alpha_{\rm EM}}{2\pi}\frac{4ie}{m^2} f_\gamma^{(0)} \left(\ln\frac{2\Lambda}{\lambda}-\frac{5}{6}\right) u_h^\dagger \mathbf{q}\times\mathbf{A} u_h \\
\langle \mathbf{L}_q^{\rm eff}\rangle^{(1)}_{\rm orbital} &= \frac{\alpha_{\rm EM}}{2\pi}\frac{2}{3m^2} d_R^{(0)} \left(\ln\frac{2\Lambda}{\lambda}-\frac{5}{6}\right) \mathbf{x}\times u_h^\dagger |\mathbf{q}|^2 \mathbf{A} u_h
\end{aligned} \tag{2.62}$$

The one-loop amplitude $\langle \mathbf{S}_q^{\rm eff}\rangle_{\rm spin}$ and $\langle \mathbf{J}_\gamma^{\rm eff}\rangle_{\rm orbital}$ as well as the diagrams with scalar potential A^0 contribute to $\mathcal{O}(m^{-3})$ order in NRQED. By applying $d_R^{(0)} = f_\gamma^{(0)} = 1$, the infrared divergence in full theory and effective theory calculations are exactly the same, as we have expected.

Now the matching condition (2.18) should be rewritten as:

$$\langle \mathbf{J}(\mu)\rangle_{\rm QED} = \langle \mathbf{J}^{\rm eff}(\mu,\Lambda)\rangle_{\rm NRQED} \tag{2.63}$$

The sum rule of the Wilson coefficients (2.21) does not change. However, the coefficients of the effective Lagrangian appearing in (2.21) should be understood as the coefficients under the cutoff scheme, (2.59).

With the new matching conditions we find another set of Wilson coefficients as functions of both three-momentum cutoff Λ and QED scale μ. We list the ones different from (2.51) only, and address them with an asterisk:

$$\begin{aligned}
d_D^* &= 1+\frac{\alpha_{\rm EM}}{2\pi}\left(-\frac{4}{3}\ln\frac{\mu^2}{m^2}+\frac{16}{3}\ln\frac{m}{2\Lambda}+\frac{37}{9}\right), \\
d_B^* = -1+\frac{\alpha_{\rm EM}}{2\pi}\left(-16\ln\frac{m}{2\Lambda}+\frac{23}{9}\right),&\quad f_B^* = \frac{\alpha_{\rm EM}}{2\pi}\left(16\ln\frac{m}{2\Lambda}-\frac{86}{9}\right),
\end{aligned} \tag{2.64}$$

As we can see, by separating the NRQED and QED scale, $\mathbf{J}_q^{\rm eff}$ and $\mathbf{J}_\gamma^{\rm eff}$ will satisfy the RG equations in (2.58).

2.5 Application: Calculate Photon Angular Momentum in Hydrogen Atom at $\mathcal{O}(\alpha^3)$

As an application, let us consider the orbital angular momentum of the electron in the ground state of the hydrogen atom. In non-relativistic theory, the electron is in s-wave with vanishing orbital motion. However, in relativistic framework, the electron's wave function is a four-component Dirac spinor,

$$\Psi_{nljm} = \begin{pmatrix} \frac{iG_{lj}(r)}{r}\psi^l_{jm} \\ \\ \frac{F_{lj(r)}}{r}(\sigma\cdot r)\psi^l_{jm} \end{pmatrix} . \tag{2.65}$$

In the ground state ($n=1, l=0, j=1/2$), the upper component is an s-wave, but the lower component is a p-wave. Therefore, there is an orbital angular momentum contribution to the ground state spin of the hydrogen atom (we ignore the spin of the proton) which can be calculated directly through the above Dirac wave function. In effective NRQED, this angular momentum contribution can be calculated as the matrix elements of the

$$-\frac{d_\pi}{8m^2}\int d^3r\psi^\dagger[(\boldsymbol{\sigma}\times\boldsymbol{\pi})\times\boldsymbol{\pi}-\boldsymbol{\pi}\times(\boldsymbol{\sigma}\times\boldsymbol{\pi})]\psi \ , \tag{2.66}$$

in the Coulomb wave function, which yields easily $\langle L_z\rangle = \alpha^2_{\rm em}/6$, consistent with the full theory. This contribution is balanced by the equal amount of depletion of the electron spin contribution $\langle\Sigma_z/2\rangle = 1/2-\alpha^2_{\rm em}/6$.

A more interesting question is: what is the amount of hydrogen spin carried by radiative photons? This question is particularly relevant in the spin structure of the nucleon [27, 7] since, due to strong coupling, the QCD gluon could contribute

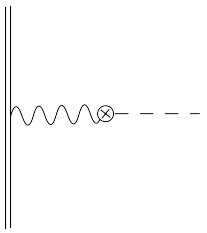

Figure 2.7: Leading ($\mathcal{O}(\alpha_{\rm em}^2)$) electromagnetic contribution to the spin of the Coulomb-bound electron

significantly to the nucleon spin [43, 45]. The spin program at the Relativistic Heavy-Ion Collider is largely motivated by this possibility [41]. Here to simplify the problem, we take the proton mass to infinity and are left with essentially an electron in a static Coulomb potential.

To answer this question, let us first consider the calculation in the full QED theory. The leading order contribution comes from the diagram in Fig. 2.5. The cross represents the photon angular momentum operator; the dashed line an external Coulomb field and the wavy line an off-shell photon field. This contribution can be easily shown to be zero because of the Coulomb nature of the static potential [112], $\mathbf{E} = \boldsymbol{\nabla} e/(4\pi r)$,

$$\int d^3r \ \mathbf{r} \times (\mathbf{E} \times \mathbf{B}) = 0 \ . \tag{2.67}$$

Therefore, the magnetic field generated by the electron current does not contribute to the hydrogen's angular momentum. This contribution, were it non-zero, would have been of order $\alpha_{\rm em}^2$.

Thus, the first non-vanishing electromagnetic contribution comes from radiative photons shown by Fig. 2.5(a), which will be at least order $\alpha_{\rm em}^3$. The loop integral is ultraviolet divergent by simple power counting. One can interpret this divergence

in two ways: First, define photon and electron in terms of a certain renormalization (or cut-off) scheme, and the answer is finite within the scheme. But the result is then scheme and scale dependent [27]. This, however, is the preferred approach in QCD because there are no free quarks and gluons due to color confinement. A second approach is to define the electron and photon using the asymptotic physical states. In this case, the physical electron spin acquires the same radiative corrections and therefore one must subtract off the contribution in which the intermediate electron is a free-space one, as shown by Fig. 2.5(b). The subtraction will produce a finite contribution, i.e., free of ultraviolet divergence. This situation is similar to the famous Lamb shift calculation for the energy shift.

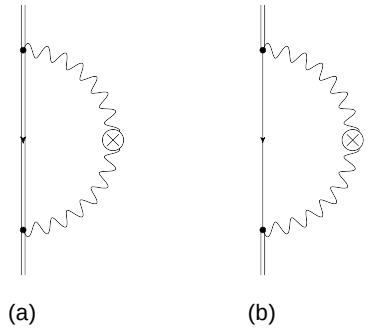

Figure 2.8: a) Next-to-leading order ($\mathcal{O}(\alpha_{\rm em}^3)$) EM contribution to the spin of the Coulomb-bound electron, b) subtraction needed to define the physical contribution.

To calculate the contribution from Fig. 2a, we use the NRQED approach similar to the calculation of the Lamb shift outlined in Ref. [47]. We split the loop momentum in Fig. 2a into small and large regions. When the loop-momentum is large, we can expand the bound state electron wave function in terms of its successive interactions with the static Coulomb field. After subtracting off the free

contribution, we are left with Fig. 2.5 in the large loop momentum region. This contribution can be matched to local operators made of the quark fields in Eq. (2.17), related to the matching coefficients f_E. Therefore, the large momentum contribution is

$$\left\langle \int d^3r \mathbf{r} \times (\mathbf{E} \times \mathbf{B}) \right\rangle = \left\langle \frac{f_E}{4m} \int d^3r \psi^\dagger [\mathbf{r} \times (\boldsymbol{\sigma} \times e\mathbf{E})] \psi \right\rangle = \frac{\alpha_{\rm em}^3}{18\pi} \ . \tag{2.68}$$

There is no logarithm associated with this, in contrast to the Lamb shift.

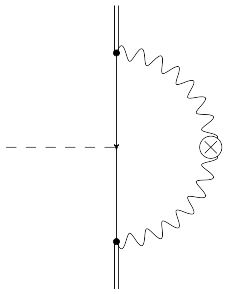

Figure 2.9: First-order expansion of EM contribution to the spin in an external Coulomb field, in the hard momentum region.

In the low-momentum region, we calculate the matrix elements of $\int d^3r \mathbf{r} \times (\mathbf{E} \times \mathbf{B})$ using the time-independent first-order perturbation theory. It is easy to see that the contribution is zero, including the free intermediate state contribution. This is because Figs. 2.5(a) and 2.5(b) in NRQED are independent of the electron spin. Therefore, Eq. (2.68) is the total radiative photon contribution to the spin of the Coulomb bound electron. It is interesting to note that the result is positive. Future atomic physics experiments might be able to measure this small quantity. To maintain the total spin 1/2, this photon contribution is balanced by the electron's orbital motion, as is clear from Eq. (2.16).

2.6 Conclusions

A gauge-invariant angular momentum decomposition in the framework of NRQED Lagrangian has been computed to order (α/m^2). The effective operators can be used in computations of higher order spin/orbital angular momentum contribution in non-relativistic bound states such as hydrogen atoms. The operators we obtained satisfy the RG evolving equations (2.58) originally derived in full theory. A natural expansion to angular momentum decompositions with NRQCD Lagrangian can be readily achieved with a similar matching in QCD.

Chapter 3

L-R model and chiral perturbation theory operators

3.1 Introduction

Non-leptonic kaon decay has been a focus for both theoretical and experimental physics for over 40 years since the discovery of CP violation by Christenson, Cronin, Fitch and Turlay [48] in $K_L \to 2\pi$. Since then the origin of CP violation has long been a challenge to many theoretical models. The recent data from various experiments have yielded a clear non-vanishing direct CP-violation parameter [49, 50]:

$$\mathrm{Re}(\epsilon'/\epsilon) = (16.7 \pm 2.6) \times 10^{-4} \,, \tag{3.1}$$

which ruled out the so-called superweak theory where no direct CP violation appears in the decay [51]. At present, a full theoretic explanation to the origin of this phenomenon is still lacking. In the framework of the standard model (SM), direct CP violation can be generated by the non-zero phase in the quark flavor-mixing matrix (CKM matrix), as was suggested by Kobayashi and Maskawa [52]. A precision calculation of the effect, however, is extremely hard due to the non-perturbative nature of the strong interactions at low energy. Results from several groups utilizing different methods differ widely, with error bars much larger than that of the experimental result [53]. The unsatisfying situation of the theoretical calculations have attracted much interest in attributing part of the phenomenon to physics beyond

SM.

To be able to pin down the contribution to ϵ' from models containing new physics, one has to make precision calculations of the strong-interaction physics associated with the non-perturbative structure of kaons and pions. Various methods have been used to calculate the hadronic matrix elements, such as lattice [55, 54], QCD-inspired models [56, 57], chiral expansion together with large-N_c [58], and parametrizations [59]. At present, the lattice field theory is the only approach based on first principles, with controllable systematic errors. There are difficulties in lattice calculations which are associated with the fact that the final state contains more than one particle. By Maiani-Testa theorem [60], it is impossible to extract the physical kaon decay matrix elements by taking the limit $\tau \to \infty$ in the Euclidean space. In practise, there are several ways to avoid it: one can either work with an unphysical choice of momenta [61, 62], utilize an unphysical set of meson masses [63, 64], or derive the physical matrix elements by unphysical, but calculable ones. All of these methods need chiral perturbation theory (ChPT).

ChPT assumes an approximate chiral symmetry exists in $SU(3)_f$ and describes the low-energy QCD physics under a chiral breaking scale $\Lambda_\chi \sim m_\rho$ by the pseudo-Goldstone particles, namely pions, kaons and eta. Then the low-energy physics can be perturbatively expanded in powers of the particles' external momenta and masses. It further assumes that, the Wilson coefficients of the QCD operators expanded in terms of meson operators are independent of the external states. Therefore the amplitudes of a large number of reactions can be determined by a relatively small set of coefficients, which gives us the predicting power. In the case of kaon decay, ChPT is

used to connect the desired matrix element $\langle\pi\pi|\mathcal{O}|K\rangle$ with some unphysical quantities, such as $\langle\pi|\mathcal{O}|K\rangle$ and $\langle 0|\mathcal{O}|K\rangle$. The results in ChPT are needed before doing relevant lattice calculations. Here we will neglect some subtleties in the ChPT (such as quadratic divergence cancelations, zero pion mass corrections, etc) and focus on possible operator structures as well as their chiral logarithm corrections for the kaon decay process. It is the goal of this work to examine the chiral structures of possible QCD operators responsible for $\Delta s = 1, \Delta d = -1$ decay in generic beyong-SM theories and to calculate the large chiral logarithms associated with them. Previous calculations have been made for operators present in the SM [65, 66, 67, 68, 69, 70]. Our work extends these studies to all possible operators in new physics models.

In this chapter, we start from the operator basis in SM for the kaon decay, as well as possible new operators coming from physics beyond SM. A chiral perturbation theory calculation will be presented in the following section, with all corresponding operators and their one-loop corrections of the matrix elements. We end this chapter by applying our general result to the Left-Right Symmetric Model.

3.2 Effective Operators from New Flavor Physics

In this section, we consider effective QCD operators contributing to CP-violating $K \to \pi\pi$ decay in a generic weak-interaction theory. There is an extensive literature on this topic in the context of SM [71, 73]. Our focus is on new operators arising from novel CP-violating mechanisms beyond SM. We classify the effective operators in terms of their flavor symmetry properties under chiral group

$SU(3)_L \times SU(3)_R$ when up, down, and strange quarks are taken as light.

The direct CP violation parameter ϵ' for $K \to \pi\pi$ decay is defined as [71]:

$$\epsilon' = \frac{1}{\sqrt{2}} e^{\left(\frac{\pi}{2}+\delta_2-\delta_0\right)} \frac{\mathrm{Re}A_2}{\mathrm{Re}A_0} \left(\frac{\mathrm{Im}A_0}{\mathrm{Re}A_0} - \frac{\mathrm{Im}A_2}{\mathrm{Re}A_2} \right) , \tag{3.2}$$

where δ_I is the strong-interaction $\pi\pi$ scattering phase shifts, and A_I is the weak kaon decay amplitudes:

$$A_I e^{i\delta_I} = \langle \pi\pi(I=0,2)|(-i\mathcal{H}_W)|K^0\rangle , \tag{3.3}$$

where $\mathcal{H}_W$ is the effective weak-interaction hamiltonian which depends on the underlying theory of kaon decay. The small ratio $\omega \equiv \mathrm{Re}A_2/\mathrm{Re}A_0 \approx 1/22$ reflects the well-known $\Delta I = 1/2$ rule. Accurate calculations of ϵ' depend on reliable evaluations of the effective QCD operators present in $\mathcal{H}_W$. Our goal is to classify these QCD operators and study their chiral behavior.

3.2.1 Standard Model Operators

The standard procedure for calculating ϵ' utilizes an effective field theory approach. The physics at high energy (or short distance) can be calculated perturbatively and is included in Wilson coefficients. The physics at low-energy scales is included in the effective QCD operators composed of light flavor quark fields (u, d, s) as well as gluons. Large QCD radiative corrections or large logarithms are resumed by solving renormalization group equations. In addition, the effective operators responsible for the neutral kaon decay have the flavor quantum numbers $\Delta s = 1$, $\Delta d = -1$. In the SM, it is well-known that $\mathcal{H}^{\mathrm{eff}}$ consists of following 10

operators [72, 73]:

$$
\begin{aligned}
Q_1 &= (\overline{s}_i u_j)_{V-A}(\overline{u}_j d_i)_{V-A} \ , \\
Q_2 &= (\overline{s}_i u_i)_{V-A}(\overline{u}_j d_j)_{V-A} \ , \\
Q_{3,5} &= (\overline{s}_i d_i)_{V-A} \sum_q (\overline{q}_j q_j)_{V\mp A} \ , \\
Q_{4,6} &= (\overline{s}_i d_j)_{V-A} \sum_q (\overline{q}_j q_i)_{V\mp A} \ , \\
Q_{7,9} &= \frac{3}{2}(\overline{s}_i d_i)_{V-A} \sum_q e_q (\overline{q}_j q_j)_{V\pm A} \ , \\
Q_{8,10} &= \frac{3}{2}(\overline{s}_i d_j)_{V-A} \sum_q e_q (\overline{q}_j q_i)_{V\pm A} \ ,
\end{aligned}
\tag{3.4}
$$

where $(\bar{q}q')_{V\pm A} = \bar{q}_{L,R}\gamma_\mu q_{L,R}$ with $q_{L,R}$ representing the left-(right-) handed quark fields. The summation in q is over the light-quark flavors; u, d, s; i and j are color indices; and e_q is the algebraic charge factor for flavor q. The $Q_{1,2}$ come from the single W_L-boson exchange tree diagram, and $Q_{3-6},\ Q_{7-10}$ are derived from one-loop gluon and electro-weak penguin diagrams, respectively. In the SM, $(\mathrm{Im}A_0/\mathrm{Re}A_0)$ is dominated by the QCD penguin operators, whereas $(\mathrm{Im}A_2/\mathrm{Re}A_2)$ receives contribution from the electro-weak penguin operators only, because the gluon interaction is flavor-singlet and cannot contribute in $\Delta I = 3/2$ channel.

A chiral structure analysis of the above ten operators will be useful if we wish to use lattice QCD to calculate the relevant matrix elements in kaon decays. Using (m, n) to denote a representation of group $SU_L(3)\times\ SU_R(3)$, where m and n are the dimensions of SU(3) representations, it is then easy to see that $Q_{1,2}$ and $Q_{9,10}$ belong to $(8, 1)$ and $(27, 1)$, $Q_{3\sim6}$ to $(8, 1)$, and $Q_{7,8}$ to $(8, 8)$ [73]. ChPT calculations have been made to uncover the large logarithms associated with these operators, which in

turn help to establish relations of different matrix elements useful for lattice QCD calculations. For the reader's convenience, we have collected the standard chiral results in the Appendix.

The question is what is the general chiral structure of all possible weak operators that might emerge in theories beyond SM? The rest of this section is devoted to addressing this question.

3.2.2 Dimension-5 and D-6 Operators

Let us systematically consider the possible operators and their chiral structures in a general low-energy description of kaon decay, independent of the underlying short-distance flavor physics that can be taken into account by Wilson coefficients. The lowest dimensional operator is a dimension-5 chromo-magnetic operator,

$$Q_M = \bar{s}(\sigma^{\mu\nu})t^a d\ G^a_{\mu\nu}\ . \tag{3.5}$$

This operator does appear in the standard model through penguin diagram as shown in left-panel Fig. 1, although it is proportional to the strange or down quark masses, which is chirally suppressed. It also appears naturally in the left-right symmetric model (LRSM) with left-right handed gauge-boson mixing, proportional to charm or top quark masses [74], as shown on the right panel in Fig.1. Under chiral symmetry, this operator transforms as $(\overline{3}, 3) + (3, \overline{3})$. The chiral logarithms appearing with the matrix elements of this operator has been studied before in the literature, and is collected in the Appendix.

Next, consider dimension-6 four-quark operators. We define the following

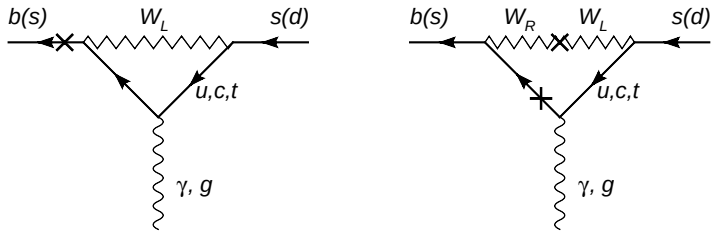

Figure 3.1: Dimension-5 effective operators generated from the weak-interaction vertex corrections in SM (left) and in LRSM (right). The crosses on fermion lines represent mass insertion, needed to flip the chirality of the quarks.

flavor tensor

$$\Theta_{ik}^{jl} = (\bar{q}^i \Gamma q_j)(\bar{q}^k \Gamma' q_l) \ , \tag{3.6}$$

where the flavor indices i, j, k, l go through 1, 2, and 3, or up, down and strange quarks. Γ and Γ' are possible Dirac matrix structures. In addition, there are two independent color structures $(\mathbf{1})(\mathbf{1})$ and $(t^a)(t^a)$ which are not essential for the following discussion. Assuming that all fields are projected to their helicity states, the possible helicities are as follows:

- All four quark fields have the same chiral projection
- Both $\bar{q}^i$ and $\bar{q}^k$ (also j and l) have the opposite chiral projection
- Both $\bar{q}^i$ and $\bar{q}^k$ (also j and l) have the same chiral projection

These are only possibilities because the operators must be Lorentz scalars, and the numbers of left and right-handed fields apart from the first case must be exactly 2, respectively. In the first and second case, the operators are the ones appearing in the SM weak interactions, as shown in Eq. (3.4), and their parity partners. They

correspond to chiral structures (8,1), (1,8), (27, 1), and (1,27) from the first case, and (8,1), (1,8) and (8,8) from the second case. The new (1,8) and (1,27) structures will appear in, for example, LR symmetric models where the right-handed gauge boson plays the same role as left-handed one in the SM. Since the strong interactions conserve parity, the new operators in LRSM have the same matrix elements as Q_i's in SM up to a parity sign. The corresponding Feynman diagrams in both SM and LRSM for the first and second cases are shown in Fig. 3.2.

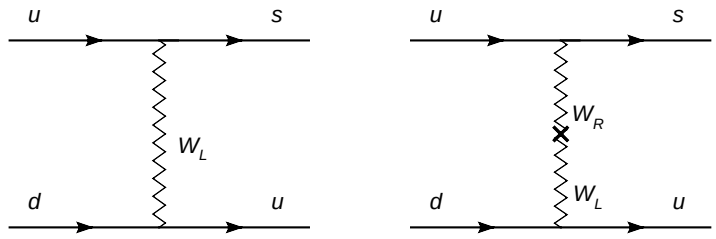

Figure 3.2: Feynman diagrams generating dimension-6 quark operators in SM and LRSM.

In the last case, there are new chiral structures arising from operators of type

$$(\bar{s}_L \Gamma d_R)(\bar{q}_L \Gamma q_R), \quad (\bar{s}_R \Gamma d_L)(\bar{q}_R \Gamma q_L) \ . \tag{3.7}$$

where two $\Gamma's$ must be the same. The new chiral structures are $(\overline{6}, 6)$, $(\overline{6}, \overline{3})$, $(3, 6)$, and their parity conjugates. However, $(\overline{6}, \overline{3})$ and $(3, 6)$ involve symmetrization of two flavor indices and, at the same time, anti-symmetrization of the other two. It is easy to check that the result vanishes, and we are left with just $(\overline{6}, 6)$ and $(6, \overline{6})$.

Let us consider the following tensor with up (and hence lower) indices symmetrized

$$\Theta^{kl}_{(ij)} = \frac{1}{2}(\bar{q}^i_L \Gamma q_{Rk})(\bar{q}^j_L \Gamma q_{Rl}) + \frac{1}{2}(\bar{q}^j_L \Gamma q_{Rk})(\bar{q}^i_L \Gamma q_{Rl}) \ , \tag{3.8}$$

where the upper indices represents the left-handed fields and the lower indices the right-handed. Without loss of generality, we take $i = 3$. If $j = 3$, and k or l is 3 and the other indices must be a 2, one get an isospin-1/2 operator

$$\Theta^{(\overline{6},6)}_{1/2,A} \equiv \Theta^{23}_{33} = \bar{s}_L \Gamma d_R \bar{s}_L \Gamma s_R \ . \tag{3.9}$$

If we define a tensor T^{ij}_{kl} which multiplies the quark operator Θ^{kl}_{ij} to generate the above operator, $T^{ij}_{kl}\Theta^{kl}_{ij}$, we have

$$T^{33}_{23} = T^{33}_{32} = 1/2 \ , \tag{3.10}$$

and other components zero.

On the other hand, if j, k, l take 1's and 2's, one can subtract the trace with respect to j and k, and j and l, and one obtain an isospin-3/2 operator

$$\begin{aligned} \Theta^{(\overline{6},6)}_{3/2} &\equiv \Theta^{12}_{(31)} + \Theta^{21}_{(31)} - \Theta^{22}_{(32)} \\ &= \bar{s}_L \Gamma u_R \bar{u}_L \Gamma d_R + \bar{s}_L \Gamma d_R \bar{u}_L \Gamma u_R - \bar{s}_L \Gamma d_R \bar{d}_L \Gamma d_R \ , \end{aligned} \tag{3.11}$$

with corresponding non-zero tensor components

$$T^{31}_{12} = T^{31}_{21} = T^{13}_{12} = T^{13}_{21} = -T^{32}_{22} = -T^{23}_{22} = 1/2 \ . \tag{3.12}$$

Another isospin-1/2 operator will can be obtained its trace part,

$$\begin{aligned} \Theta^{(\overline{6},6)}_{1/2,S} &\equiv \Theta^{12}_{(31)} + \Theta^{21}_{(31)} + 2\Theta^{22}_{(32)} \\ &= \bar{s}_L \Gamma u_R \bar{u}_L \Gamma d_R + \bar{s}_L \Gamma d_R \bar{u}_L \Gamma u_R + 2\bar{s}_L \Gamma d_R \bar{d}_L \Gamma d_R \ , \end{aligned} \tag{3.13}$$

and the corresponding tensor components are,

$$T^{31}_{12} = T^{31}_{21} = T^{13}_{12} = T^{13}_{21} = 1/2; \quad T^{32}_{22} = T^{23}_{22} = 1 \ . \tag{3.14}$$

An example of these new operators in LRSM through flavor-changing neutral and charged currents is shown in Fig. 3.3. The relevant QCD four-quark operator will be:

$$\begin{aligned} \mathcal{O}^{\Delta s=1} &= (\bar{s}_L d_R) \sum_q (\bar{q}_L q_R) \\ &= \frac{1}{2}\left[\Theta^{(\overline{6},6)}_{1/2,S} + 2\Theta^{(\overline{6},6)}_{1/2,A} - \Theta^{(3,\overline{3})}\right] \end{aligned} \tag{3.15}$$

where $\Theta^{(3,\overline{3})} \equiv (\bar{s}_L u_R)(\bar{u}_L d_R) - (\bar{s}_L d_R)(\bar{u}_L u_R)$.

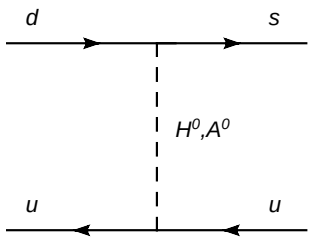

Figure 3.3: Feynman diagrams generating scalar quark interactions through neutral-current Higgs exchanges.

3.2.3 Dimension-7 Operators

Dimension-7 operators come in two types. The first is the chromomagnetic operators with an insertion of two additional derivatives, which does not change the original chiral structure. The second type is an insertion of one derivative into four-quark operators discussed above. Since the covariant derivative has one Lorentz index, it must be contracted with another Lorentz index appearing on a

Dirac matrix. An example of this type of operators is

$$\begin{aligned}\mathcal{O}^{LR}_{P,g} &= \bar{s}_{i,L}(i\sigma^{\mu\nu})d_{j,R}\sum_q \bar{q}_{j,L}(\gamma_\mu D_\nu)q_{i,L} \ , \\ \mathcal{O}^{LR}_{P,EW} &= \bar{s}_{i,L}(i\sigma^{\mu\nu})d_{i,R}\sum_q e_q\bar{q}_{j,L}(\gamma_\mu D_\nu)q_{j,L} \ , \end{aligned} \tag{3.16}$$

which comes from the gluon and electromagnetic penguin diagram in LRSM as shown in Fig. 3.1. These operators contain either 3 left-handed fields and 1 right-handed one, or 3 right-handed fields and 1 left handed one. They have novel chiral structures $(15,\overline{3})$, $(\overline{15},3)$, $(6,3)$, $(\overline{6},\overline{3})$, and parity partners. Let us classify them all in details.

3.2.3.1 $(\overline{15},3)$

Let us use Θ^{kl}_{ij} to represent an operator $\bar{q}^i_L\Gamma q_{Lk}\bar{q}^j_L\Gamma' q_{Rl}$, where l is flavor index of the right-handed field, and Γ and Γ' are not just Dirac matrices. We first construct $\hat{\Theta}^{kl}_{ij}$ which forms $(\overline{15},3)$ after symmetrizing the up two indices and subtracting the traces,

$$2\hat{\Theta}^{kl}_{ij} = \Theta^{kl}_{ij} + \Theta^{kl}_{ji} - \frac{1}{4}\delta^k_i\left[\Theta^{\alpha l}_{\alpha j} + \Theta^{\alpha l}_{j\alpha}\right] - \frac{1}{4}\delta^k_j\left[\Theta^{\alpha l}_{\alpha i} + \Theta^{\alpha l}_{i\alpha}\right] \ , \tag{3.17}$$

where α sums over 1, 2, and 3. Clearly, i, or equivalently j, has to be an $\bar{s}$. One isospin-1/2 operator that one can immediately identity is when j is 3, k is 2, and l is 3, namely

$$\Theta^{(\overline{15},3)}_{1/2} \equiv \hat{\Theta}^{23}_{33} = \Theta^{23}_{33} = \bar{s}_L\Gamma d_L\bar{s}_L\Gamma' s_R \ , \tag{3.18}$$

where the only non-zero tensor component is

$$T^{33}_{23} = 1 \ . \tag{3.19}$$

Other independent operators can be obtained by considering j, k, and l as up and down quarks. Others, such as $\hat{\Theta}^{32}_{33}$, can be related to these through traceless conditions.

One can get an isospin-3/2 operator by symmetrizing k and l while taking away SU(2) traces between j and k, and j and l. Thus we have the following combination,

$$\hat{\Theta}^{kl}_{3j} + \hat{\Theta}^{lk}_{3j} - \frac{1}{3}\delta^k_j \left(\hat{\Theta}^{al}_{3a} + \hat{\Theta}^{la}_{3a}\right) - \frac{1}{3}\delta^l_j \left(\hat{\Theta}^{ak}_{3a} + \hat{\Theta}^{ka}_{3a}\right) \ , \tag{3.20}$$

where a sums over 1 and 2 only, and j, k and l can take value in 1 or 2. There is only one independent operator

$$\begin{aligned}
\Theta^{(\overline{15},3)}_{3/2} &\equiv 2\left(\hat{\Theta}^{21}_{31} + \hat{\Theta}^{12}_{31} - \hat{\Theta}^{22}_{32}\right) \\
&= \bar{s}_L\Gamma u_L\bar{u}_L\Gamma' d_R + \bar{s}_L\Gamma d_L\bar{u}_L\Gamma' u_R + \bar{u}_L\Gamma u_L\bar{s}_L\Gamma' d_R \\
&\quad + \bar{u}_L\Gamma d_L\bar{s}_L\Gamma' u_R - \bar{s}_L\Gamma d_L\bar{d}_L\Gamma' d_R - \bar{d}_L\Gamma d_L\bar{s}_L\Gamma' d_R \ .
\end{aligned} \tag{3.21}$$

The corresponding tensor components are

$$T^{31}_{12} = T^{13}_{12} = T^{31}_{21} = T^{13}_{21} = -T^{32}_{22} = -T^{23}_{22} = 1 \ . \tag{3.22}$$

The trace part of the above operator produces an $I = 1/2$ operator, $\hat{\Theta}^{a2}_{3a} + \hat{\Theta}^{2a}_{3a}$. We can subtract from the result with another isospin-1/2 operator, $\hat{\Theta}^{33}_{32}$, to cancel the unwanted trace part $-\frac{1}{4}\delta^k_i[\Theta^{\alpha l}_{\alpha j}] - \frac{1}{4}\delta^k_j[\Theta^{\alpha l}_{\alpha i}]$ in Eq. (3.17). The resulting $I = 1/2$ operator is

$$\begin{aligned}
\Theta^{(\overline{15},3)}_{1/2,S} &\equiv 2\left(\hat{\Theta}^{12}_{31} + \hat{\Theta}^{21}_{31} + 2\hat{\Theta}^{22}_{32}\right) - 3\hat{\Theta}^{32}_{33} \\
&= \bar{s}_L\Gamma u_L\bar{u}_L\Gamma' d_R + \bar{u}_L\Gamma u_L\bar{s}_L\Gamma' d_R + \bar{s}_L\Gamma d_L\bar{u}_L\Gamma' u_R \\
&\quad + \bar{u}_L\Gamma d_L\bar{s}_L\Gamma' u_R + 2\bar{s}_L\Gamma d_L\bar{d}_L\Gamma' d_R + 2\bar{d}_L\Gamma d_L\bar{s}_L\Gamma' d_R - 3\bar{s}_L\Gamma s_L\bar{s}_L\Gamma' d_R \ .
\end{aligned} \tag{3.23}$$

with the following tensor components,

$$T^{31}_{21} = T^{13}_{21} = T^{31}_{12} = T^{13}_{12} = \frac{1}{2}T^{32}_{22} = \frac{1}{2}T^{23}_{22} = \frac{1}{3}T^{33}_{32} = 1 \ . \tag{3.24}$$

Finally, one can antisymmetrize k and l to generator another isospin 1/2 operator. Again we add $\hat{\Theta}^{32}_{33}$ to cancel the unwanted trace part:

$$\begin{aligned}
\Theta^{(\overline{15},3)}_{1/2,A} &\equiv 2\left(\hat{\Theta}^{21}_{31} - \hat{\Theta}^{12}_{31}\right) + \hat{\Theta}^{32}_{33} \\
&= \bar{s}_L\Gamma d_L\bar{u}_L\Gamma' u_R + \bar{u}_L\Gamma d_L\bar{s}_L\Gamma' u_R - \bar{s}_L\Gamma u_L\bar{u}_L\Gamma' d_R \\
&\quad -\bar{u}_L\Gamma u_L\bar{s}_L\Gamma' d_R + \bar{s}_L\Gamma s_L\bar{s}_L\Gamma' d_R \ ,
\end{aligned} \tag{3.25}$$

with the following tensor components

$$T^{31}_{21} = T^{13}_{21} = -T^{31}_{12} = -T^{13}_{12} = T^{33}_{32} = 1 \ . \tag{3.26}$$

Note that the operators in $(3, \overline{15})$ can be obtained from the above through parity transformation.

3.2.3.2 $(\overline{3}, 15)$

Define $\Theta^{kl}_{ij} = \bar{q}^i_L\Gamma q_{Rk}\bar{q}^j_R\Gamma' q_{Rl}$, and construct the general $(\overline{3}, 15)$ operators,

$$2\hat{\Theta}^{kl}_{ij} = \Theta^{kl}_{ij} + \Theta^{lk}_{ij} - \frac{1}{4}\delta^k_j\left[\Theta^{\alpha l}_{i\alpha} + \Theta^{l\alpha}_{i\alpha}\right] - \frac{1}{4}\delta^l_j\left[\Theta^{\alpha k}_{i\alpha} + \Theta^{k\alpha}_{i\alpha}\right] \ , \tag{3.27}$$

where the α trace is over 1, 2, and 3. Either index i or j can be identified as the strange quark field. In either case, one can construct isospin-3/2 operators by subtracting SU(2) trace. With the left-handed strange quark, we have

$$\begin{aligned}
\Theta^{(\overline{3},15)}_{3/2,L} &\equiv \hat{\Theta}^{12}_{31} + \hat{\Theta}^{21}_{31} - \hat{\Theta}^{22}_{32} = \Theta^{12}_{31} + \Theta^{21}_{31} - \Theta^{22}_{32} \\
&= \bar{s}_L\Gamma u_R\bar{u}_R\Gamma' d_R + \bar{s}_L\Gamma d_R\bar{u}_R\Gamma' u_R - \bar{s}_L\Gamma d_R\bar{d}_R\Gamma' d_R \ ,
\end{aligned} \tag{3.28}$$

with tensor components,

$$T_{12}^{31} = T_{21}^{31} = -T_{22}^{32} = 1 \ . \tag{3.29}$$

With the right-handed strange quark,

$$\begin{aligned} \Theta_{3/2,R}^{(\overline{3},15)} &\equiv \hat{\Theta}_{13}^{12} + \hat{\Theta}_{13}^{21} - \hat{\Theta}_{23}^{22} = \Theta_{13}^{12} + \Theta_{13}^{21} - \Theta_{23}^{22} \\ &= \bar{u}_L \Gamma u_R \bar{s}_R \Gamma' d_R + \bar{u}_L \Gamma d_R \bar{s}_R \Gamma' u_R - \bar{d}_L \Gamma d_R \bar{s}_R \Gamma' d_R \ , \end{aligned} \tag{3.30}$$

with tensor components,

$$T_{12}^{13} = T_{21}^{13} = -T_{22}^{23} = 1 \ . \tag{3.31}$$

There are also two isospin-1/2 operators. The first one with left-handed strange quark,

$$\begin{aligned} \Theta_{1/2,L}^{(\overline{3},15)} &\equiv 4\left(\hat{\Theta}_{31}^{12} + \hat{\Theta}_{31}^{21} + 2\hat{\Theta}_{32}^{22}\right) \\ &= \bar{s}_L \Gamma u_R \bar{u}_R \Gamma' d_R + \bar{s}_L \Gamma d_R \bar{u}_R \Gamma' u_R + 2\bar{s}_L \Gamma d_R \bar{d}_R \Gamma' d_R \\ &\quad -3\bar{s}_L \Gamma s_R \bar{s}_R \Gamma' d_R - 3\bar{s}_L \Gamma d_R \bar{s}_R \Gamma' s_R \end{aligned} \tag{3.32}$$

with tensor components

$$T_{12}^{31} = T_{21}^{31} = \frac{1}{2} T_{22}^{32} = -\frac{1}{3} T_{32}^{33} = -\frac{1}{3} T_{23}^{33} = 1 \ . \tag{3.33}$$

And the second one has the right-handed strange quark,

$$\begin{aligned} \Theta_{1/2,R}^{(\overline{3},15)} &\equiv \hat{\Theta}_{13}^{12} + \hat{\Theta}_{13}^{21} + 2\hat{\Theta}_{23}^{22} = \Theta_{13}^{12} + \Theta_{13}^{21} + 2\Theta_{23}^{22} \\ &= \bar{u}_L \Gamma u_R \bar{s}_R \Gamma' d_R + \bar{u}_L \Gamma d_R \bar{s}_R \Gamma' u_R + 2\bar{d}_L \Gamma d_R \bar{s}_R \Gamma' d_R \end{aligned} \tag{3.34}$$

with tensor components

$$T_{12}^{13} = T_{21}^{12} = \frac{1}{2} T_{22}^{23} = 1 \ . \tag{3.35}$$

The $\hat{\Theta}_{33}^{32}$ is not independent by the same reason as for $(\overline{15}, 3)$.

3.2.3.3 $(6,3)$

Define $\Theta^{kl}_{ij} = \bar{q}^i_L \Gamma q_{Lk} \bar{q}^j_L \Gamma' q_{Rl}$, and construct the $(6,3)$ operator,

$$\hat{\Theta}^{kl}_{ij} = \epsilon_{ijm} \hat{\Theta}^{(mk)l} = \frac{1}{2} \epsilon_{ijm} \left(\epsilon^{\alpha\beta m} \Theta^{kl}_{\alpha\beta} + \epsilon^{\alpha\beta k} \Theta^{ml}_{\alpha\beta} \right) \ . \tag{3.36}$$

where k, m are symmetric, and α, β run over 1 to 3. To get the $\Delta s = -\Delta d = 1$ operators, none of the m, k and l can be a 3: when 3 is on the ϵ, it prevents both i and j from being a strange quark, and when 3 is a lower index, both i and j must be 3 which is impossible because of the antisymmetry. In fact, the only possible combination for m, k and l is 2, 2, 1.

To get an isospin 3/2 operator, one must symmetrize m, k and l, yielding

$$\begin{aligned} \Theta^{(6,3)}_{3/2} &\equiv \hat{\Theta}^{221} + \hat{\Theta}^{212} + \hat{\Theta}^{122} = \hat{\Theta}^{21}_{31} + \hat{\Theta}^{12}_{31} + \hat{\Theta}^{22}_{23} \\ &= \bar{s}_L \Gamma d_L \bar{u}_L \Gamma' u_R + \bar{s}_L \Gamma u_L \bar{u}_L \Gamma' d_R - \bar{u}_L \Gamma d_L \bar{s}_L \Gamma' u_R \\ &\quad - \bar{u}_L \Gamma u_L \bar{s}_L \Gamma' d_R - \bar{s}_L \Gamma d_L \bar{d}_L \Gamma' d_R + \bar{d}_L \Gamma d_L \bar{s}_L \Gamma' d_R \ . \end{aligned} \tag{3.37}$$

The corresponding tensor components are

$$T^{31}_{12} = -T^{13}_{12} = T^{31}_{21} = -T^{13}_{21} = -T^{32}_{22} = T^{23}_{22} = 1 \ . \tag{3.38}$$

There is also an isospin-1/2 operator by anti-symmetrizing k and l

$$\begin{aligned} \Theta^{(6,3)}_{1/2} &\equiv 2\hat{\Theta}^{221} - \hat{\Theta}^{212} - \hat{\Theta}^{122} = 2 \left(\hat{\Theta}^{21}_{31} - \hat{\Theta}^{12}_{31} \right) \\ &= 2\bar{s}_L \Gamma d_L \bar{u}_L \Gamma' u_R - 2\bar{u}_L \Gamma d_L \bar{s}_L \Gamma' u_R - \bar{s}_L \Gamma u_L \bar{u}_L \Gamma' d_R \\ &\quad + \bar{u}_L \Gamma u_L \bar{s}_L \Gamma' d_R - \bar{d}_L \Gamma d_L \bar{s}_L \Gamma' d_R + \bar{s}_L \Gamma d_L \bar{d}_L \Gamma' d_R \ , \end{aligned} \tag{3.39}$$

The tensor components are

$$\frac{1}{2} T^{31}_{21} = -\frac{1}{2} T^{13}_{21} = -T^{31}_{12} = T^{13}_{12} = T^{32}_{22} = -T^{23}_{22} = 1 \ . \tag{3.40}$$

3.2.3.4 $(\overline{3},\overline{6})$

Define $\Theta^{kl}_{ij} = \bar{q}^i_L \Gamma q_{Rk} \bar{q}^j_R \Gamma' q_{Rl}$, and construct the $(\overline{3},\overline{6})$ operator,

$$\hat{\Theta}^{kl}_{ij} = \epsilon^{klm}\hat{\Theta}_{i(jm)} = \frac{1}{2}\epsilon^{klm}\left(\epsilon_{\alpha\beta m}\Theta^{\alpha\beta}_{ij} + \epsilon_{\alpha\beta j}\Theta^{\alpha\beta}_{im}\right) \ , \tag{3.41}$$

where j, m are symmetric, and α, β run from 1 to 3. The only choices which will generate the $\Delta s = -\Delta d = 1$ operators is i, j and m takes $3, 3, 1$. If i is 3, and j and m take 3 and 1, we have the isospin 1/2 operator

$$\begin{aligned}\Theta^{(\overline{3},\overline{6})}_{1/2,L} &\equiv \hat{\Theta}_{313} + \hat{\Theta}_{331} = 2\hat{\Theta}^{12}_{31} \\ &= \bar{s}_L\Gamma u_R \bar{u}_R \Gamma' d_R - \bar{s}_L \Gamma d_R \bar{u}_R \Gamma' u_R + \bar{s}_L \Gamma d_R \bar{s}_R \Gamma' s_R - \bar{s}_L \Gamma s_R \bar{s}_R \Gamma' d_R \ ,\end{aligned} \tag{3.42}$$

with the following tensor components,

$$T^{31}_{12} = -T^{31}_{21} = T^{33}_{23} = -T^{33}_{32} = 1 \ . \tag{3.43}$$

On the other hand, if i takes 1, one gets another isospin 1/2 operator

$$\begin{aligned}\Theta^{(\overline{3},\overline{6})}_{1/2,R} &\equiv \hat{\Theta}_{133} = \hat{\Theta}^{12}_{13} \\ &= \bar{u}_L \Gamma u_R \bar{s}_R \Gamma' d_R - \bar{u}_L \Gamma d_R \bar{s}_R \Gamma' u_R \ ,\end{aligned} \tag{3.44}$$

with the following tensor components

$$T^{13}_{12} = -T^{13}_{21} = 1 \ . \tag{3.45}$$

One could consider operators with dimension 8 and higher. However, generally they are suppressed by $1/\Lambda^2$ relative to those we have considered, where Λ is some weak interaction scale. We summarize the above result in the following table:

Table 3.1: Chiral representations appearing in dimension-5, 6 and 7 operators.

	dimension-5	dimension-6	dimension-7
(L,R)	$(3,\overline{3}),(\overline{3},3)$	(8,1),(1,8) $(27,1),(1,27)$ (8,8) $(6,\overline{6}),(\overline{6},6)$ $(3,\overline{3}),(\overline{3},3)$	$(15,\overline{3}),(\overline{3},15),(\overline{15},3),(3,\overline{15})$ $(\overline{6},\overline{3}),(\overline{3},\overline{6}),(6,3),(3,6)$ $(3,\overline{3}),(\overline{3},3)$

We emphasize that these operators are completely general, independent of the underlying mechanisms (supersymmetry, large-extra dimension, or little Higgs, etc) for flavor and CP-violations in beyond SM theories.

3.3 Chiral Expansion at Leading Order

Chiral perturbation theory (ChPT) for kaon decay is useful for two reasons: First, it allows one to connect the physical matrix elements $\langle K|\mathcal{O}|\pi\pi\rangle$ to some unphysical, but easier-to-calculate matrix elements on lattice. Second, it yields dependence of the matrix elements on meson masse parameters. Since lattice calculations are usually done at larger and unphysical meson masses because of limited computational resources, this dependence can be used to extrapolate the calculated matrix elements to physical ones. In this section, we will build a set of effective operators in ChPT up to the lowest order, and use an example to illustrate how to connect the unphysical processes to the physical process $K \to \pi\pi$ we are interested in.

In lattice calculations the quenched approximation to QCD has usually been applied in the past, where valance quark fields are "quenched" by corresponding ghost quark fields with the same masses and quantum numbers but opposite statistics. The ChPT can be adapted with the quenched QCD by introducing the "super-η'" field into the effective lagrangian [75]. At here we will work with the full dynamical QCD only.

3.3.1 ChPT and SM Operators

The standard ChPT starts with the nonlinear Goldstone meson field Σ by:

$$\Sigma \equiv \exp\left(\frac{2i\phi}{f}\right) \ , \tag{3.46}$$

where ϕ is the Goldstone meson matrix

$$\phi = \begin{pmatrix} \frac{\pi^0}{\sqrt{2}} + \frac{\eta}{\sqrt{6}} & \pi^+ & K^+ \\ \pi^- & -\frac{\pi^0}{\sqrt{2}} + \frac{\eta}{\sqrt{6}} & K^0 \\ K^- & \overline{K^0} & -\sqrt{\frac{2}{3}}\eta \end{pmatrix} , \tag{3.47}$$

and $f \approx 135$ MeV is the bare pion decay constant. We separate the effective ChPT Lagrangian into two parts:

$$\mathcal{L}_{\rm ChPT} = \mathcal{L}_s + \mathcal{L}_w \ , \tag{3.48}$$

where $\mathcal{L}_s$ corresponds the QCD strong interaction which preserves the flavor symmetry; the $\mathcal{L}_w$ is an effective Lagrangian for non-leptonic weak interaction, and is responsible for the $\Delta s = 1$ processes. The lowest-order terms for the strong interaction part is:

$$\mathcal{L}_s^{(2)} = \frac{f^2}{8}{\rm Tr}(\partial_\mu \Sigma \partial^\mu \Sigma) + v{\rm Tr}\left[M\Sigma + (M\Sigma)^\dagger\right] , \tag{3.49}$$

where $M \equiv \mathrm{diag}(m_u, m_d, m_s)$ is the quark mass matrix; and $v \sim -\frac{1}{2}\langle \bar{u}u \rangle$ is proportional to the quark chiral condensate at chiral limit. We demand the fields transform under $SU(3)_L \times SU(3)_R$ as:

$$\Sigma \to L\Sigma R^\dagger, \quad M \to R\Sigma L^\dagger, \tag{3.50}$$

to keep the Lagrangian invariant under an $SU(3)_L \times SU(3)_R$ transformation. Higher order terms in the effective Lagrangian contain higher derivatives, and can be written in systematic derivative and mass expansion. For our purpose here, however, only the leading large logarithms are calculated, and the higher order terms are irrelevant.

At one loop, the physical masses and wave-function renormalizations are given by [76]

$$\begin{aligned}
m_\pi^2 &= m_{\pi,0}^2 \left[1 + L(m_\pi) - \frac{1}{3} L(m_\eta) + \dots \right] , && (3.51)\\
m_K^2 &= m_{K,0}^2 \left[1 + \frac{2}{3} L(m_\eta) + \dots \right] , && (3.52)\\
Z_\pi &= 1 + \frac{4}{3} L(m_\pi) + \frac{2}{3} L(m_K) + \dots , && (3.53)\\
Z_K &= 1 + \frac{1}{4} L(m_\pi) + \frac{1}{2} L(m_K) + \frac{1}{4} L(m_\eta) + \dots , && (3.54)\\
f_\pi &= f \left[1 - 2L(m_\pi) - L(m_K) + \dots \right] , && (3.55)\\
f_K &= f \left[1 - \frac{3}{4} L(m_\pi) - \frac{3}{2} L(m_K) - \frac{3}{4} L(m_\eta) + \dots \right] , && (3.56)
\end{aligned}$$

for the pion and kaon fields, respectively. $L(m)$ is the chiral logarithm defined as:

$$L(m) \equiv \frac{m^2}{(4\pi f)^2} \ln \frac{m^2}{\mu_\chi^2} , \tag{3.57}$$

with μ_χ the cutoff scale. The dots represent non-logarithm contributions from $\mathcal{O}(p^4)$ and higher order Lagrangian terms. In this work we focus only on the large chiral

logarithmic corrections and will not, for simplicity, include the dots explicitly in the results.

In the standard electroweak theory, there are 7 independent four-quarks operators which can be classified into $(8,1)$, $(27,1)$, and $(8,8)$. Define $\Theta = T^{ik}_{jl}\bar{q}^i_L\gamma_\mu q_{Lj}\bar{q}^k_L\gamma^\mu q_{Ll}$, we can obtain four-independent quark operators with the following tensor components

$$(27,1)_{3/2} \;:\; T^{31}_{21} = T^{31}_{12} = T^{13}_{21} = T^{13}_{12} = -T^{32}_{22} = -T^{23}_{22} = \frac{1}{2}\ , \tag{3.58}$$

$$(27,1)_{1/2} \;:\; T^{31}_{21} = T^{31}_{12} = T^{13}_{21} = T^{13}_{12} = \frac{1}{2}, T^{32}_{22} = T^{23}_{22} = 1, T^{33}_{23} = T^{33}_{32} = -\frac{3}{2} \tag{3.59}$$

$$(8,1)_{1/2,S} \;:\; T^{31}_{21} = T^{13}_{12} = T^{31}_{12} = T^{13}_{21} = \frac{1}{2}, T^{32}_{22} = T^{23}_{22} = T^{33}_{23} = T^{33}_{32} = 1\ ,$$

$$(8,1)_{1/2,A} \;:\; T^{31}_{21} = T^{13}_{12} = -T^{31}_{12} = -T^{13}_{21} = \frac{1}{2}\ . \tag{3.60}$$

On the other hand, defining a (8,8) operator $\Theta = T^{ik}_{jl}\bar{q}^i_L\gamma_\mu q_{Lj}\bar{q}^k_R\gamma^\mu q_{Rl}$, we have three quark operators with following tensor components,

$$(8,8)_{3/2} \;:\; T^{31}_{21} = T^{31}_{12} = -T^{32}_{22} = 1\ , \tag{3.61}$$

$$(8,8)_{1/2,S} \;:\; T^{31}_{21} = T^{31}_{12} = T^{32}_{22}/2 = -T^{33}_{23}/3 = 1\ , \tag{3.62}$$

$$(8,8)_{1/2,A} \;:\; T^{31}_{21} = -T^{31}_{12} = -T^{33}_{23} = 1\ . \tag{3.63}$$

One can similarly defined other (8,8) operators with a different color indices contractions. For the sake of convenience, we have broken the operators into representations of definite isospins. This has the advantage of easily building up reducible operators from linear combinations of these simple ones. For example, the SM electromagnetic penguin operators $Q_{7,8}$:

$$Q_7 = \frac{1}{2}\left[\Theta^{(8,8)}_{3/2} + \Theta^{(8,8)}_{1/2,A}\right]\ , \tag{3.64}$$

and Q_8 is similar to Q_7 but with different color indices contraction.

In ChPT, one can match the above QCD operators to the hadronic operators made of Goldstone boson fields [78, 77, 70]:

$$\begin{aligned}
\tilde{\Theta}_1^{(8,1)} &\equiv \mathrm{Tr}\left[\Lambda\partial_\mu\Sigma\partial^\mu\Sigma^\dagger\right] \ , \\
\tilde{\Theta}_2^{(8,1)} &\equiv \frac{8v}{f^2}\mathrm{Tr}\left[\Lambda\Sigma M+\Lambda(\Sigma M)^\dagger\right] \ , \\
\tilde{\Theta}_{\Delta I}^{(27,1)} &\equiv [T_{\Delta I}^{(27,1)}]_{kl}^{ij}(\Sigma\partial_\mu\Sigma^\dagger)^k{}_i(\Sigma\partial^\mu\Sigma^\dagger)^l{}_j \ , \\
\tilde{\Theta}_{\Delta I}^{(8,8)} &\equiv [T_{\Delta I}^{(8,8)}]_{kl}^{ij}(\Sigma)^k{}_j(\Sigma^\dagger)^l{}_i \ , \\
\tilde{\Theta}^{(\overline{3},3)} &\equiv \mathrm{Tr}[\Lambda\Sigma^\dagger] \ ,
\end{aligned} \tag{3.65}$$

where $\Lambda=\delta_{i,3}\delta_{j,2}$ and T's are tensor structures defined above. The expansions go like

$$\begin{aligned}
\Theta_i^{(8,1)} &= \alpha_{1i}^{(8,1)}\tilde{\Theta}_1^{(8,1)}+\alpha_{2i}^{(8,1)}\tilde{\Theta}_2^{(8,1)}+\dots \ , \\
\Theta_{\Delta I}^{(27,1)} &= \alpha^{(27,1)}\tilde{\Theta}_{\Delta I}^{(27,1)}+\dots \ , \\
\Theta_{\Delta I}^{(8,8)} &= \alpha^{(8,8)}\tilde{\Theta}_{\Delta I}^{(8,8)}+\dots \ ,
\end{aligned} \tag{3.66}$$

where $\alpha^{(L,R)}$s are "Wilson coefficients" which are universal in different processes, and dots represent higher dimensional operators. The subscript i on the $(8,1)$ operator indicates different quark operators in the same chiral representation, including ones with two right-handed fields coupled to the singlet.

The one loop results of these operators in various processes can be found in [65, 66, 67, 68, 69, 70]. Due to the different definitions of the operators and the nonlinear meson fields, there might be sign differences among these results. Overall speaking, the (8,1) and (27,1) operators dominate in the CP-conserve process. The

(8,8) operators, corresponding to the $Q_{7,8}$ operators, play a significant role in CP-violation processes [70, 79]. The lowest-order mass-dependent term $\Theta_2^{(8,1)}$ will vanish in physical process $K \to \pi\pi$ to all orders. This property was pointed out by [78] first and has been well-studied by [80, 81]. We will come back to this issue later.

3.3.2 Chiral Matching of New Operators

Now we can proceed in constructing new hadronic operators for new interactions arising from physics beyond SM. We label operators by the irreducible representatives and their isospin quantum numbers. Similar to the case in SM, we define the effective operators at their lowest order as:

Dimension-6:

$$\tilde{\Theta}_{\Delta I}^{(\overline{6},6)} = [T_{\Delta I}^{(\overline{6},6)}]_{kl}^{ij}(\Sigma^\dagger)^k{}_i(\Sigma^\dagger)^l{}_j \ , \tag{3.67}$$

Dimension-7:

$$\tilde{\Theta}_{\Delta I}^{(\overline{15},3)} = [T_{\Delta I}^{(\overline{15},3)}]_{kl}^{ij}(\Sigma\partial^\mu\Sigma^\dagger)^k{}_i(\partial_\mu\Sigma^\dagger)^l{}_j \ , \tag{3.68}$$

$$\tilde{\Theta}_{\Delta I}^{(6,3)} = [T_{\Delta I}^{(6,3)}]_{kl}^{ij}(\Sigma\partial^\mu\Sigma^\dagger)^k{}_i(\partial_\mu\Sigma^\dagger)^l{}_j \ , \tag{3.69}$$

$$\tilde{\Theta}_{\Delta I}^{(\overline{3},15)} = [T_{\Delta I}^{(\overline{3},15)}]_{kl}^{ij}(\partial^\mu\Sigma^\dagger)^k{}_i(\Sigma^\dagger\partial_\mu\Sigma)^l{}_j \ , \tag{3.70}$$

$$\tilde{\Theta}_{\Delta I}^{(\overline{3},\overline{6})} = [T_{\Delta I}^{(\overline{3},\overline{6})}]_{kl}^{ij}(\partial^\mu\Sigma^\dagger)^k{}_i(\Sigma^\dagger\partial_\mu\Sigma)^l{}_j \ . \tag{3.71}$$

We can also construct operators with one insertion of quark masses,

$$X_\pm^L \equiv (\Sigma M) \pm (\Sigma M)^\dagger, \ \ X_\pm^R \equiv (M\Sigma) \pm (M\Sigma)^\dagger \ . \tag{3.72}$$

They transform under $SU(3)_L \times SU(3)_R$ as:

$$X_\pm^L \to L X_\pm^L L^\dagger; \ \ X_\pm^R \to R X_\pm^R R^\dagger \ . \tag{3.73}$$

With the insertion of $X_\pm$ we can build two additional sets of the dimension-7 operators at the lowest order:

$$\tilde{\Theta}'^{(L,R)}_{\Delta I,X_\pm} = [T^{(L,R)}_{\Delta I}]^{ij}_{kl}(X^L_\pm)^k{}_i(\Sigma^\dagger)^l{}_j \ , \tag{3.74}$$

for (L,R) belong to $(\overline{15},3)$ or $(6,3)$, and

$$\tilde{\Theta}'^{(L,R)}_{\Delta I,X_\pm} = [T^{(L,R)}_{\Delta I}]^{ij}_{kl}(\Sigma^\dagger)^k{}_i(X^R_\pm)^l{}_j \ , \tag{3.75}$$

for (L,R) belong to $(\overline{3},15)$ or $(\overline{3},\overline{6})$. Therefore, the dimension-6 and -7 QCD operators should be matched to hadron operators as follows,

$$\Theta^{(L,R)}_{\rm D6} \ \rightarrow \ \alpha^{(L,R)}\tilde{\Theta}^{(L,R)} \ , \tag{3.76}$$

$$\Theta^{(L,R)}_{\rm D7} \ \rightarrow \ \alpha^{(L,R)}\tilde{\Theta}^{(L,R)} + \alpha^{(L,R)}_{X_+}\tilde{\Theta}'^{(L,R)}_{X_+} + \alpha^{(L,R)}_{X_-}\tilde{\Theta}'^{(L,R)}_{X_-} \ , \tag{3.77}$$

where higher-order terms have been omitted.

In SM we need operators with X_+ only since all QCD operators obey the CPS symmetry, the CP transformation followed by an exchange of s and d quarks [78]. However, the 4-quark operators derived from new physics do not necessarily have this symmetry, and hence we can have an additional set of operators in the effective theory.

Just as the $(8,8)$ operators in SM, the $(\overline{6},6)$ dimension-6 operators will contribute at $\mathcal{O}(p^0)$ order in ChPT. This set of operators can be derived from the Higgs (or some new heavy bosons) exchange and will contribute to the CP violation phase in the same manner as Q_7, Q_8 in SM. We will consider an example of applying our result later.

Table 3.2: Tree level contributions from dimension-6 operators

	$K^0 \to Vacuum$	$K^+ \to \pi^+$	$K^0 \to \pi^0\pi^0$
$(L,R)_{\Delta I}$	b_0	c_0	d_0
$(\overline{6},6)_{3/2}$	0	-4	-8
$(\overline{6},6)_{1/2,S}$	-6	-10	16
$(\overline{6},6)_{1/2,A}$	-2	-2	0

When calculating CP conserving matrix elements, the new operators are usually negligible compared to the SM weak-interaction operators defined in Eqs.(3.58)-(3.65). The new operators are mainly responsible for the CP-violating phase, and are worth investigating as the case in [70, 79]. We observe that some of these new operators, notably $(\overline{6},6), (\overline{15},3), (6,3)$ and $(\overline{3},15)$ have contributions in $\Delta I = 3/2$ channel, in addition to $(27,1)$ and $(8,8)$ operators in SM. Furthermore, as we shall see, they all receive large chiral logarithmic corrections in one-loop ChPT. Therefore, the operators from new flavor theories beyond SM can help explain the $\Delta I = 1/2$ selection rule and the direct CP violation parameter ϵ'.

3.3.3 Results at Tree Level

In this subsection, we consider tree-level relations among the matrix elements of the QCD operators in different states. These relations reflect chiral symmetry and can also be derived using old-fashioned current algebra.

There are three processes that we are mainly interested in: $K^0 \to Vacuum$, $K^+ \to \pi^+$ and $K^0 \to \pi^0\pi^0$. For $K^0 \to \pi^+\pi^-$, one can obtained the matrix elements through angular momentum relation, as shown in Appendix. At tree level, the dimension-7 momentum operators will not contribute to $K^0 \to Vacuum$ process. For the mass-dependent operators, the result will be either proportional to $(m_s - m_d) \sim m^2_{K,0} - m^2_{\pi,0}$ or $(m_s + m_d) \sim m^2_{K,0}$, by the lowest order expansion of $X_\pm$. However, beyond tree level, the result will no longer be proportional to $(m_s - m_d)$ or $(m_s + m_d)$.

For dimension-6 operators in $(\bar{6}, 6)$, we have the tree level results:

$$\langle 0|\Theta_{D6}|K^0\rangle_{\rm Tree} = \frac{i\, b_0}{f}\alpha_{D6} \ , \tag{3.78}$$

$$\langle \pi^+|\Theta_{D6}|K^+\rangle_{\rm Tree} = \frac{c_0}{f^2}\alpha_{D6} \ , \tag{3.79}$$

$$\langle \pi^0\pi^0|\Theta_{D6}|K^0\rangle_{\rm Tree} = \frac{i\, d_0}{f^3}\alpha_{D6} \ , \tag{3.80}$$

with b_0,c_0 and d_0 coefficients listed in Table 3.2, which are different from different isospin projections. The corresponding results for $\pi^+\pi^-$ final state can be obtained from relations in Appendix. The non-perturbative coefficient α_{D6} is the same for different operators and final states.

Similarly, the tree-level matrix elements for dimension-7 operators are:

$$\begin{aligned}\langle 0|\Theta_{D7}|K^0\rangle_{\rm Tree} &= \frac{4iv}{f^3}\left[b'_{0,+}(m_s - m_d)\alpha_{D7,+} + b'_{0,-}(m_s + m_d)\alpha_{D7,-}\right] \\ &= \frac{i}{f}\left[b'_{0,+}(m^2_{K,0} - m^2_{\pi,0})\alpha_{D7,+} + b'_{0,-}m^2_{K,0}\alpha_{D7,-}\right] \ , \end{aligned} \tag{3.81}$$

$$\langle \pi^+|\Theta_{D7}|K^+\rangle_{\rm Tree} = \frac{m^2_{M,0}}{f^2}[c'_0\alpha_{D7} + c'_{0,+}\alpha_{D7,+} + c'_{0,-}\alpha_{D7,-}] \ , \tag{3.82}$$

$$\langle \pi^0\pi^0|\Theta_{D7}|K^0\rangle_{\rm Tree} = \frac{m^2_K}{f^3}[d'_0\alpha_{D7} + d'_{0,+}\alpha_{D7,+} + d'_{0,-}\alpha_{D7,-}] \ , \tag{3.83}$$

with coefficients listed in Table 3.3. Here the non-perturbative coefficients $\alpha' s$ are

Table 3.3: Tree level contributions from dimension-7 operators

	$K^0 \to Vacuum$		$K^+ \to \pi^+$			$K^0 \to \pi^0\pi^0$		
$(L,R)_{\Delta I}$	$b'_{0,+}$	$b'_{0,-}$	c'_0	$c'_{0,+}$	$c'_{0,-}$	d'_0	$d'_{0,+}$	$d'_{0,-}$
$(\overline{15},3)_{3/2}$	0	0	-8	0	2	8	-2	-2
$(\overline{15},3)_{1/2,S}$	9/2	3/2	-8	$-3/2$	2	8	-2	-2
$(\overline{15},3)_{1/2,A}$	$-1/2$	1/2	0	$-1/2$	0	8	-2	-2
$(\overline{15},3)_{1/2}$	1/2	1/2	0	$-1/2$	0	0	0	0
$(6,3)_{3/2}$	0	0	0	0	0	8	-2	-2
$(6,3)_{1/2}$	3/2	3/2	12	$-3/2$	-3	16	-4	-4
$(\overline{3},15)_{3/2,L}$	0	0	4	0	-1	0	0	0
$(\overline{3},15)_{3/2,R}$	0	0	4	0	-1	8	2	-2
$(\overline{3},15)_{1/2,L}$	$-3/2$	$-3/2$	4	3/2	-1	0	0	0
$(\overline{3},15)_{1/2,R}$	$-3/2$	3/2	4	$-3/2$	-1	-16	2	-2
$(\overline{3},\overline{6})_{1/2,L}$	3/2	$-1/2$	4	1/2	-1	0	0	0
$(\overline{3},\overline{6})_{1/2,R}$	$-1/2$	1/2	-4	$-1/2$	1	0	2	-2

different for different chiral representations. From the above equations, it is clear that one can obtained the two-pion matrix elements from the vacuum and one-pion ones, if only one of the X_+ and X_- types of operators is present, such as in the SM case.

3.4 Chiral Logarithms at One-Loop

ChPT calculations of the kaon-decay matrix elements up to higher chiral orders are needed for understanding the size of chiral corrections and for extrapolating matrix elements from unphysical quark masses to physical ones. In lattice calculations, unphysically large quark masses are usually used to make calculations feasible. Then one needs to extrapolate the matrix elements to the physical region. In this section, we calculate the large chiral logarithms of the dimension-6 and 7 operators for the process $K \to 0$, $K \to \pi$ and $K \to \pi\pi$ hoping to get the leading corrections as the function of quark masses.

In our calculations, we have made the simplifying assumption $m_u = m_d$. For $\langle 0|\mathcal{O}|K^0\rangle$ matrix element, we have kept all the Goldstone boson masses independent. For the matrix element $\langle \pi^+|\mathcal{O}|K^+\rangle$, we utilize a common mass m_M for all the mesons to conserve momentum. In the calculation of $\langle \pi^0\pi^0|\mathcal{O}|K^0\rangle$ matrix elements the pion masses are neglected. Since $m_\pi^2/m_K^2 \approx 10^{-1}$ with physical pion and kaon masses, this is a reasonable approximation for the physical processes.

3.4.1 $K^0 \to Vacuum$

The diagram we need to consider is shown in Fig. 3.4 below, where and henceforth the square dot represents an effective weak interaction operator while the round dots represent strong interaction insertions. We have not shown the wave function renormalization diagrams, but they have to be included in the final result.

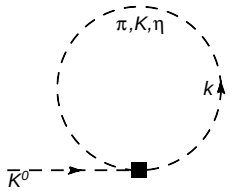

Figure 3.4: Feynman diagram for $K^0 \to Vacuum$ at one loop.

For dimension-6 operators, the results for $\langle 0|\mathcal{O}|K^0\rangle$ up to one-loop can be written as:

$$\langle 0|\Theta_{D6}|K^0\rangle = \frac{i\alpha_{D6}}{f}\left[b_0 + b_\eta L(m_\eta^2) + b_K L(m_K^2) + b_\pi L(m_\pi^2)\right] \ , \tag{3.84}$$

with coefficients listed in Table 3.4. Note that we have three different chiral logarithms corresponding to eta, kaon, and pion, respectively. The isospin-3/2 operator does contribute for the obvious reason.

For dimension-7 operators, the results are more complicated,

$$\begin{aligned}\langle 0|\Theta_{D7}|K^0\rangle \ &= \ \langle 0|\Theta_{D7}|K^0\rangle_{\rm Tree} + \frac{i}{f}\Big\{ \left[b'_\eta m_\eta^2 L(m_\eta^2) + b'_K m_K^2 L(m_K^2) + b'_\pi m_\pi^2 L(m_\pi^2)\right]\cdot\alpha_{D7} \\ &\quad + \sum_{\pm}\left[(b'_{\eta,K} m_K^2 + b'_{\eta,\pi} m_\pi^2)L(m_\eta^2) + (b'_{K,K} m_K^2 + b'_{K,\pi} m_\pi^2)L(m_K^2)\right. \\ &\quad \left. +(b_{\pi,K} m_K^2 + b'_{\pi,\pi} m_\pi^2)L(m_\pi^2)\right]\cdot\alpha_{D7,\pm}\Big\} \ , \end{aligned} \tag{3.85}$$

Table 3.4: One loop contributions from dimension-6 operators

	$K^0 \to Vacuum$			$K^+ \to \pi^+$	$K^0 \to \pi^0\pi^0$
$(L,R)_{\Delta I}$	b_η	b_K	b_π	c_M	d_K
$(\overline{6},6)_{3/2}$	0	0	0	112/3	80/9
$(\overline{6},6)_{1/2,S}$	1/2	33	57/2	196/3	−1024/9
$(\overline{6},6)_{1/2,A}$	25/6	15	3/2	28/3	−4

where each chiral logarithms now have different meson mass factors. The coefficients are listed in Tables 3.5 and 3.6.

3.4.2 $K^+ \to \pi^+$

For the $K^+ \to \pi^+$ matrix elements, we utilize a common mass for mesons $m_M^2 = m_\pi^2 = m_K^2$ in the calculation. The Feynman diagrams are shown in Fig. 3.5. The matrix elements up to the leading chiral logarithms are:

$$\langle \pi^+|\Theta_{D6}|K^+\rangle = \frac{\alpha_{D6}}{f^2}\left[c_0 + c_M L(m_M^2)\right] , \tag{3.86}$$

$$\langle \pi^+|\Theta_{D7}|K^+\rangle = \langle \pi^+|\Theta_{D7}|K^+\rangle_{\rm Tree} + \frac{m_{M,0}^2}{f^2} L(m_M^2)\Big[c'_M\alpha_{D7} + c'_{M,+}\alpha_{D7,+} + c'_{M,-}\alpha_{D7,-}\Big] , \tag{3.87}$$

for dimension-6 and 7 operators, respectively. The coefficients are listed in Tables 3.4 and 3.7.

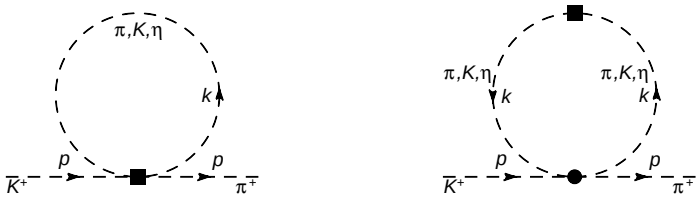

Figure 3.5: Feynman diagrams for $K^+ \to \pi^+$ at one loop.

3.4.3 $K^0 \to \pi^0\pi^0$

For $K^0 \to \pi^0\pi^0$, we neglect the pion mass in the calculation. The diagrams we need to consider for are shown in Fig. 3.6. The results are:

$$\langle \pi^0\pi^0|\Theta_{D6}|K^0\rangle = \frac{i\alpha_{D6}}{f^3}\left[d_0 + d_K L(m_K^2)\right] , \tag{3.88}$$

$$\langle \pi^0\pi^0|\Theta_{D7}|K^0\rangle = \langle \pi^0\pi^0|\Theta_{D7}|K^0\rangle_{\rm Tree} + \frac{m_K^2}{f^2}L(m_K^2)\Big[d'_M\alpha_{D7} + d'_{M,+}\alpha_{D7,+} + d'_{M,-}\alpha_{D7,-}\Big] , \tag{3.89}$$

with coefficients listed in Tables 3.4, 3.7.

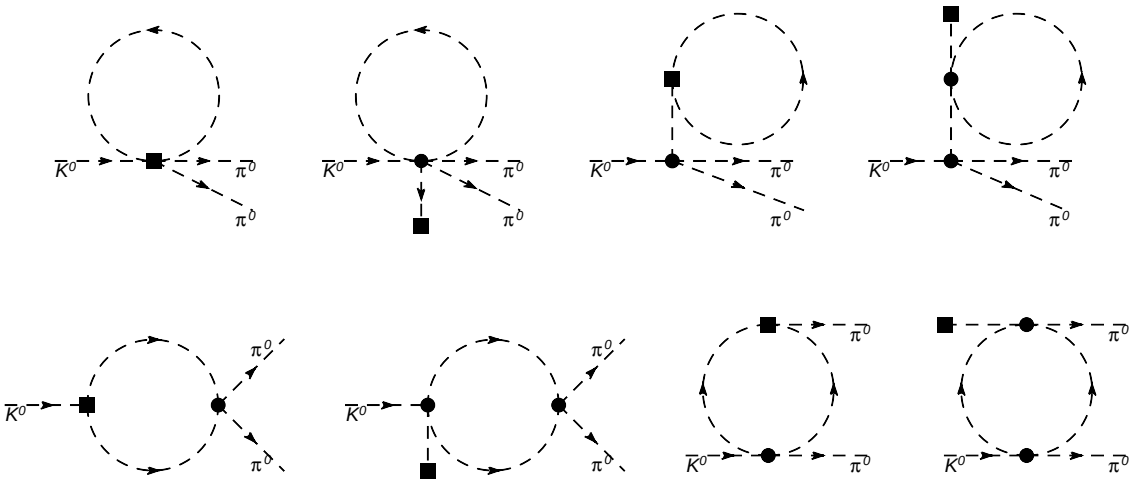

Figure 3.6: Feynman diagrams for $K^0 \to \pi^0\pi^0$ at one loop.

Table 3.5: One loop contributions from dimension-7 operators (I)

	$K^0 \to Vacuum$		
$(L,R)_{\Delta I}$	b'_η	b'_K	b'_π
$(\overline{15},3)_{1/2,S}$	0	-12	12
$(\overline{15},3)_{1/2,A}$	4	-4	0
$(\overline{15},3)_{1/2}$	-4	4	0
$(6,3)_{1/2}$	6	12	-18
$(\overline{3},15)_{1/2,L}$	18	-12	-6
$(\overline{3},15)_{1/2,R}$	6	-12	6
$(\overline{3},\overline{6})_{1/2,L}$	2	4	-6
$(\overline{3},\overline{6})_{1/2,R}$	2	4	-6

There are several comments we would like to make. First, the quark-mass-dependent operators (operators constructed with $X_\pm$) contribute in the physical process $K \to \pi\pi$, in contrary to $\Theta_2^{(8,1)}$ in the SM case. The reason is similar to that for the higher-order operators of (27,1) [69]: they cannot be expressed as a total divergence by the equations of motion. Similarly, these new operators will not act as a generator for rotation in $s-d$ plane like the $\Theta_2^{(8,1)}$ does [78, 80, 81]. Therefore the one-loop matrix elements of $K \to 0$ will no longer be proportional to $(m_s \pm m_d)$ as they did at tree level.

Second, the masses appearing in our result are either bare masses or the renor-

Table 3.6: One loop contributions from dimension-7 operators (II)

	$K^0 \to Vacuum$					
$(L,R)_{\Delta I,X\pm}$	$b'_{\eta,K}$	$b'_{\eta,\pi}$	$b'_{K,K}$	$b'_{K,\pi}$	$b'_{\pi,K}$	$b'_{\pi,\pi}$
$(\overline{15},3)_{1/2,S,X_+}$	$-43/8$	$27/8$	$-123/4$	$111/4$	$-51/8$	$99/8$
$(\overline{15},3)_{1/2,S,X_-}$	$7/8$	0	$-33/4$	0	$-33/8$	-3
$(\overline{15},3)_{1/2,A,X_+}$	$25/24$	$-17/24$	$27/4$	$-15/4$	$-21/8$	$-3/8$
$(\overline{15},3)_{1/2,A,X_-}$	$-25/24$	$1/3$	$-3/4$	0	$-27/8$	0
$(\overline{15},3)_{1/2,X_+}$	$-3/8$	$17/24$	$-15/4$	$15/4$	$-3/8$	$3/8$
$(\overline{15},3)_{1/2,X_-}$	$-3/8$	$-1/3$	$-15/4$	0	$-3/8$	0
$(6,3)_{1/2,X_+}$	$3/2$	$5/8$	$-21/4$	$9/4$	$-57/8$	$45/8$
$(6,3)_{1/2,X_-}$	$3/2$	$1/2$	$-21/4$	0	$-57/8$	$9/2$
$(\overline{3},15)_{1/2,L,X_+}$	$25/8$	$-5/8$	$45/4$	$-33/4$	$9/8$	$-45/8$
$(\overline{3},15)_{1/2,L,X_-}$	$25/8$	$1/2$	$45/4$	0	$9/8$	$-3/2$
$(\overline{3},15)_{1/2,R,X_+}$	$9/8$	$-5/8$	$33/4$	$-33/4$	$33/8$	$-45/8$
$(\overline{3},15)_{1/2,R,X_-}$	$-9/8$	$1/2$	$-33/4$	0	$-33/8$	$-3/2$
$(\overline{3},\overline{6})_{1/2,L,X_+}$	$-43/24$	$13/8$	$-45/4$	$33/4$	$-9/8$	$21/8$
$(\overline{3},\overline{6})_{1/2,L,X_-}$	$-7/24$	$1/2$	$15/4$	0	$3/8$	$-3/2$
$(\overline{3},\overline{6})_{1/2,R,X_+}$	$3/8$	$-5/24$	$3/4$	$-3/4$	$27/8$	$-15/8$
$(\overline{3},\overline{6})_{1/2,R,X_-}$	$-3/8$	$1/6$	$-3/4$	0	$-27/8$	$3/2$

Table 3.7: One loop contributions from dimension-7 operators (III)

	$K^+ \to \pi^+$			$K^0 \to \pi^0\pi^0$		
$(L,R)_{\Delta I}$	(c'_M)	$(c'_M)_{X_+}$	$(c'_M)_{X_-}$	(d'_K)	$(d'_K)_{X_+}$	$(d'_K)_{X_-}$
$(\overline{15},3)_{3/2}$	208/3	3/4	−52/3	8	−2/9	−2/9
$(\overline{15},3)_{1/2,S}$	196/3	28/3	−49/3	−640/9	214/9	160/9
$(\overline{15},3)_{1/2,A}$	−4/3	8/3	1/3	−352/9	70/9	88/9
$(\overline{15},3)_{1/2}$	−4/3	8/3	1/3	−8	2	2
$(6,3)_{3/2}$	0	0	0		8/9 −2/9	−2/9
$(6,3)_{1/2}$	−80	12	9	−848/9	212/9	212/9
$(\overline{3},15)_{3/2,L}$	−16	2/3	26/3	0	0	0
$(\overline{3},15)_{3/2,R}$	−16	2/3	26/3	−16	2/9	−2/9
$(\overline{3},15)_{1/2,L}$	0	−22/3	29/3	0	−3	−3
$(\overline{3},15)_{1/2,R}$	−32	26/3	23/3	128	−133/9	133/9
$(\overline{3},\overline{6})_{1/2,L}$	−80/3	−4	3	−8	5	−3
$(\overline{3},\overline{6})_{1/2,R}$	80/3	4	−3	0	−97/9	97/9

malized one depending on the processes. For the unphysical processes $K \to 0$ and $K \to \pi$, we use the bare masses, whereas for the physical $K \to \pi\pi$, the one-loop renormalized mass is implied. It makes the comparison to the experimental result feasible.

Third, in [82] the author claimed that infrared-sensitive terms like $m_K^2 \log m_\pi^2$, which diverges in the $m_\pi \to 0$ limit, will emerge in the $K \to \pi\pi$ matrix element. We have checked the result by keeping pion masses explicit in our calculations, and found that all such terms canceled when summing all the diagrams. Therefore it is safe to take the limit $m_\pi \to 0$.

Finally, there are a large number of unknown non-perturbative coefficients in the new operators. For dimension-6 operators, the traditional way of determining these coefficients by calculating simple processes like $K^+ \to \pi^+$ is suffice. In dimension-7 cases, however, the two simple processes $K^0 \to 0$ and $K^+ \to \pi^+$ are not enough to determine all the coefficients, unless there is the so-called CPS symmetry. Adding other simple processes like $K^0 \to \pi^0$ and $K^0 \to \eta$ will not improve the situation since they are not independent in the $SU(3)$ limit we are working on. We can in principle get more relationships when away from $SU(3)$ chiral and isospin symmetries, but many more new coefficients will enter as well, and then we need even more relationships to determine all the coefficients. Therefore we could either rely on some model-dependent assumptions or calculate more complicate processes on lattice directly. In any case, the ChPT calculations can serve as a check for relations among coefficients from lattice or other non-perturbative model calculations.

3.5 An Application of the Effective Operators: Direct CP Violation in K-decay and Minimal Left-Right Symmetry Scale

One of the much studied themes for particle physics beyond the standard model (SM) is left-right symmetry at high-energy, introduced many years ago by Mohapatra and Pati [84]. In a recent work, it has been shown that supersymmetric left-right theory arises naturally from duality cascade of a quiver in the context of intersecting D-branes [85]. The twin-Higgs model, introduced to explain the disparity between the new physics scale and the electroweak scale [86], also utilizes the idea of left-right symmetry. However, the direct collider search for the signatory right-handed W gauge boson shows that it is at least 10 times heavier than its left-handed counterpart [50]. The most stringent limit on the right-handed scale has been obtained from low-energy data, with the most well-known example being the neutral kaon mass difference [87], which gives a lower bound of at least $2.0 - 2.5$ TeV.

More recently, a general solution for the right-handed Cabibbo-Kobayashi-Maskawa (CKM) quark mixing in the minimal left-right symmetric model (LRSM) has been found [88]. Particularly interesting is the CP(charge-conjugation-parity)-violating mechanisms in the model: Apart from the usual Dirac CP phase appearing in the left-handed CKM mixing, there is also a spontaneous symmetry-breaking phase α that contributes to CP-violating observables. Using the neutral kaon mixing parameter ϵ, α can be constrained accurately. Therefore, one can make predictions on other CP-violating observables including the neutron electrical dipole moment

(EDM) and direct CP-violating parameter ϵ' in kaon decay; the experimental data can then provide new constraints on the left-right symmetric scale [89]. Unfortunately, the intermediate steps involve unknown hadronic matrix elements, and the simple factorization or large N_c (number of quark colors) assumption is usually adopted to make estimations in previous studies [89, 74]. As a consequence, the bounds suffer from unknown hadronic physics uncertainties, as exemplified in reproducing the $\Delta I = 1/2$ rule for the K to $\pi\pi$ decay.

In this section, we focus on a better estimation of the uncertainty associated with the leading hadronic matrix element, and hence a more accurate bound on the minimal left-right symmetry scale. In particular, we have found a relation between the dominating four-quark operator O_-^{LR} in the new contribution and the SM electromagnetic penguin operator O_8 through $SU(3)_L \times SU(3)_R$ chiral symmetry. We use the existing knowledge on the matrix element of the latter to get information on the former [53]. With a reasonable estimate of the O_-^{LR} matrix element, we find the lower bound for the right-handed scale in the range of 5-9 TeV, consistent with that from the neutron EDM data [89].

The direct CP-violation parameter in the neutral kaon to $\pi\pi$ decay is calculated via (3.2), where the decay amplitudes A_0 and A_2 are defined as the matrix elements of the $\Delta S = 1$ effective Hamiltonian between the neutral-K meson and the isospin $I = 0$ and 2 $\pi\pi$ states,

$$\langle (2\pi)_I | (-i)\mathcal{H}_{\Delta S=1} | K^0 \rangle = A_I e^{i\delta_I} \ . \tag{3.90}$$

δ_I is the strong phase for $\pi\pi$ scattering at the kaon mass, $\omega \equiv A_2/A_0$, and p, q are

the mixing parameters for $K^0 - \overline{K}^0$. To an excellent approximation, ω can be taken as real and $q/p = 1$. We use the experimental value for the real parts of A_0 and A_2: $\mathrm{Re}A_0 \simeq 3.33 \times 10^{-7}$ GeV and $\omega \simeq 1/22$. We focus on calculating the imaginary part of the decay amplitudes.

In the SM, the contributions to ϵ' come from both QCD and electromagnetic penguin diagrams [90]. The QCD penguin contributes exclusively to the imaginary part of $\Delta I = 1/2$ decay, whereas the electromagnetic penguin is mainly responsible for the imaginary part of $\Delta I = 3/2$ decay. Both contributions are important but have opposite signs. Therefore, the final result depends on delicate cancelations of hadronic matrix elements. The state-of-art chiral perturbation theory [**?**, 91, 72, 59] and lattice QCD calculations [83, 92] have not yet been sufficiently accurate to reproduce the experimental result [93]. On the other hand, a large-N_c approach with final-state rescattering effect taken into account seems to be able to reproduce the experimental result [94]. A nice review of the SM calculation can be found in Ref. [56, 53].

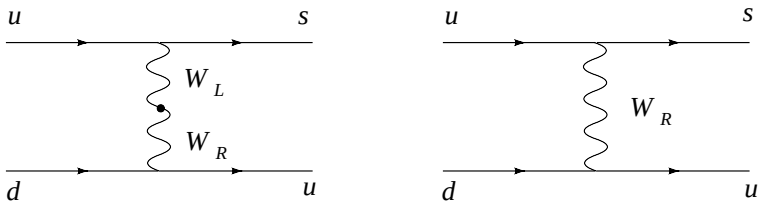

Figure 3.7: New tree-level contributions to the $\Delta S = 1$ interaction from LRSM.

In LRSM, every element in the right-handed CKM matrix has a substantial CP phase. As a consequence, there are tree-level contributions to the phases of

A_2 and A_0. Following closely the work by Ecker and Grimus [74], the tree-level Feynman diagrams in Fig. 3.7 generate

$$\begin{aligned}
\mathcal{H}^{\rm tree}_{\Delta S=1} &= \frac{G_F}{2\sqrt{2}}\lambda_u^{LL}\left[\left(\frac{\alpha_S(\mu^2)}{\alpha_S(M_L^2)}\right)^{-\frac{2}{b}} O_+^{LL}(\mu) + \left(\frac{\alpha_S(\mu^2)}{\alpha_S(M_L^2)}\right)^{\frac{4}{b}} O_-^{LL}(\mu)\right] \\
&+ \frac{G_F}{2\sqrt{2}}\frac{M_L^2}{M_R^2}\lambda_u^{RR}\left[\left(\frac{\alpha_S(\mu^2)}{\alpha_S(M_R^2)}\right)^{-\frac{2}{b}} O_+^{RR}(\mu) + \left(\frac{\alpha_S(\mu^2)}{\alpha_S(M_R^2)}\right)^{\frac{4}{b}} O_-^{RR}(\mu)\right] \\
&+ \frac{G_F}{\sqrt{2}}\sin\zeta\lambda_u^{LR}e^{i\alpha}\left[\left(\frac{\alpha_S(\mu^2)}{\alpha_S(M_L^2)}\right)^{-\frac{1}{b}} O_+^{LR}(\mu) - \left(\frac{\alpha_S(\mu^2)}{\alpha_S(M_L^2)}\right)^{\frac{8}{b}} O_-^{LR}(\mu)\right] \\
&+ \frac{G_F}{\sqrt{2}}\sin\zeta\lambda_u^{RL}e^{-i\alpha}\left[\left(\frac{\alpha_S(\mu^2)}{\alpha_S(M_L^2)}\right)^{-\frac{1}{b}} O_+^{RL}(\mu) - \left(\frac{\alpha_S(\mu^2)}{\alpha_S(M_L^2)}\right)^{\frac{8}{b}} O_-^{RL}(\mu)\right], \qquad (3.91)
\end{aligned}$$

(3.92)

where we have taken into account the leading-logarithm QCD corrections with renormalization scale μ taken to be around the charm quark mass $m_c \sim 1.3$ GeV, and $b = 11 - 2N_f/3$ with N_f the number of active fermion flavors. The left-right mixing parameter is

$$\tan\zeta = 2r\frac{m_b}{m_t}\left(\frac{M_{W_L}}{M_{W_R}}\right)^2 , \qquad (3.93)$$

where r is a parameter less than 1. The mixing coupling $\lambda_u^{AB} = V_{Aus}^{\rm CKM*}V_{Bud}^{\rm CKM}$, A, B are L, R. The right-handed CKM matrix has a form,

$$V_R = P_U\widetilde{V}_L P_D , \qquad (3.94)$$

in which $P_U = \mathrm{diag}(s_u, s_c e^{2i\theta_2}, s_t e^{2i\theta_3})$, $P_D = \mathrm{diag}(s_d e^{i\theta_1}, s_s e^{-i\theta_2}, s_b e^{-i\theta_3})$, and

$$\widetilde{V}_L = \begin{pmatrix} 1-\lambda^2/2 & \lambda & A\lambda^3(\rho - i\eta) \\ -\lambda & 1-\lambda^2/2 & A\lambda^2 e^{-2i\theta_2} \\ A\lambda^3(1-\rho-i\eta) & -A\lambda^2 e^{2i\theta_2} & 1 \end{pmatrix} , \qquad (3.95)$$

where λ, A, ρ and η are Wolfenstein parameters and the new phases θ_i are all related to spontaneous CP phase α,

$$\begin{aligned}
\theta_1 &= -\sin^{-1}[0.31(s_d s_c + 0.18 s_d s_t) r \sin\alpha] \ , \\
\theta_2 &= -\sin^{-1}[0.32(s_s s_c + 0.25 s_s s_t) r \sin\alpha] \ , \\
\theta_3 &= -\sin^{-1}[s_b s_t r \sin\alpha] \ ,
\end{aligned} \tag{3.96}$$

where experimental quark masses have been used with possible $s_i = \pm 1$ signs. The four-quark operators are

$$\begin{aligned}
O_{\pm}^{LL,RR} &= (\overline{s}_i u_i)_{V\mp A}(\overline{u}_j d_j)_{V\mp A} \pm (\overline{s}_i d_j)_{V\mp A}(\overline{u}_j u_j)_{V\mp A} \ , \\
O_{+}^{LR,RL} &= (\overline{s}_i u_i)_{V\mp A}(\overline{u}_j d_j)_{V\pm A} - \frac{1}{3}(\overline{s}_i u_j)_{V\mp A}(\overline{u}_j d_i)_{V\pm A} \ , \\
O_{-}^{LR,RL} &= -\frac{1}{3}(\overline{s}_i u_j)_{V\mp A}(\overline{u}_j d_i)_{V\pm A} \ ,
\end{aligned} \tag{3.97}$$

where i and j are color indices and the subscript $V \pm A$ refers to a quark bilinear of the form $\bar{q}\gamma_\mu(1 \pm \gamma_5)q$.

As mentioned above, one has to include the penguin contributions in the SM calculation because the CKM matrix elements have non-zero CP phases only when the third family is introduced. The only detail we would like to point out about the SM contribution is that the electromagnetic penguin involves predominantly the following operator

$$O_8 = \frac{1}{2}(\bar{s}_i d_j)_{A-V}\left[2(\bar{u}_j u_i)_{V+A} - (\bar{d}_j d_i)_{V+A} - (\bar{s}_j s_i)_{V+A}\right] \ , \tag{3.98}$$

which is an $(8,8)$ representation of the chiral $SU(3)_L \times SU(3)_R$ group. In principle, there are also new QCD penguin diagrams involving the right-handed gauge boson,

particularly with left-right gauge boson mixing. However, these contributions are suppressed by a loop factor relative to the tree contributions as well as the $\Delta I = 1/2$ rule, and hence are neglected [74].

Now we come to estimate the new contributions to the direct CP-violation parameter ϵ'. There are two types of tree contributions: the right-handed current alone and left-right interference. Both are nominally the same size, and are suppressed by $1/M_{W_R}^2$ relative to the SM contribution. In practice, however, the interference contribution dominates numerically. Let us consider the right-handed current contribution first. The relevant hadronic matrix elements can be obtained from the SM ones through parity transformation,

$$\langle \pi\pi | O_{\pm}^{RR} | K_0 \rangle = -\langle \pi\pi | O_{\pm}^{LL} | K_0 \rangle \ . \tag{3.99}$$

We use the matrix elements from a domain-wall lattice QCD calculation [83], which are consistent with the $\Delta I = 1/2$ rule,

$$\begin{aligned} \langle (\pi\pi)_{I=0} | O_{-}^{LL} | K_0 \rangle &= 0.192i \text{ GeV}^3 \\ \langle (\pi\pi)_{I=0} | O_{+}^{LL} | K_0 \rangle &= 0.064i \text{ GeV}^3 \\ \langle (\pi\pi)_{I=2} | O_{+}^{LL} | K_0 \rangle &= 0.025i \text{ GeV}^3 \end{aligned} \tag{3.100}$$

The matrix element of O_{+}^{LL} in $I = 0$ state is less important and can largely be ignored.

The dominating new contribution is from the left-right W-boson interference. Due to the QCD running effect and chiral suppression, O_{+}^{LR} operator is less important relative to O_{-}^{LR} and hence will be ignored. Therefore, we need to consider only

the matrix element of O_-^{LR} operator in the $I = 2$ state. Introduce the following $(8,8)$ operators,

$$\begin{aligned}
O_{3/2}^{(8,8)} &= (\bar{s}_i d_j)_{V-A}(\bar{u}_j u_i)_{V+A} + (\bar{s}_i u_j)_{V-A}(\bar{u}_j d_i)_{V+A} \\
&- (\bar{s}_i d_j)_{V-A}(\bar{d}_j d_i)_{V+A} \ , \\
O_{1/2A}^{(8,8)} &= (\bar{s}_i d_j)_{V-A}(\bar{u}_j u_i)_{V+A} - (\bar{s}_i u_j)_{V-A}(\bar{u}_j d_i)_{V+A} \\
&- (\bar{s}_i d_j)_{V-A}(\bar{s}_j s_i)_{V+A} \ , \\
O_{1/2S}^{(8,8)} &= (\bar{s}_i d_j)_{V-A}(\bar{u}_j u_i)_{V+A} + (\bar{s}_i u_j)_{V-A}(\bar{u}_j d_i)_{V+A} \\
&+ 2(\bar{s}_i d_j)_{V-A}(\bar{d}_j d_i)_{V+A} - 3(\bar{s}_i d_j)_{V-A}(\bar{s}_j s_i)_{V+A} \ ,
\end{aligned} \tag{3.101}$$

where subscripts 3/2 and 1/2 indicate isospin. Using the above, one can express O_-^{LR} as follows

$$O_-^{LR} = -\frac{1}{9}O_{3/2}^{(8,8)} - \frac{1}{18}O_{1/2S}^{(8,8)} + \frac{1}{6}O_{1/2A}^{(8,8)} \ . \tag{3.102}$$

On the other hand, the electromagnetic penguin operator O_8 can be expressed as

$$O_8 = \frac{1}{2}\left(O_{3/2}^{(8,8)} + O_{1/2A}^{(8,8)}\right) \ . \tag{3.103}$$

Therefore, we find the model-independent relation,

$$\langle(\pi\pi)_{I=2}|O_-^{LR}|K_0\rangle = -\frac{2}{9}\langle(\pi\pi)_{I=2}|O_8|K_0\rangle \ . \tag{3.104}$$

In the vacuum insertion approximation, one finds

$$\langle(\pi\pi)_{I=2}|O_8||K_0\rangle = \sqrt{6}f_\pi\left(\frac{m_K^2}{m_s(\mu)+m_d(\mu)}\right)^2 i \ , \tag{3.105}$$

which is about $0.95i$ GeV^3 ($f_\pi = 93$ MeV) if the strange quark mass is taken to be 120 MeV at the scale of m_c. On the other hand, the lattice QCD calculation in

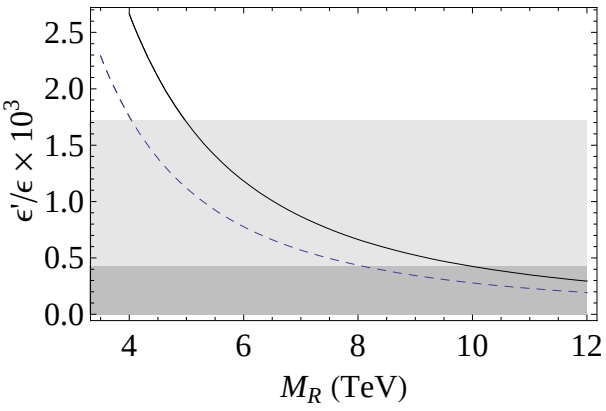

Figure 3.8: The new contribution in LRSM to ϵ'

Ref. [83] gives $1.4i$ GeV^3 at the scale of 1.9 GeV. This lattice calculation, however, does not reproduce the experimental data on ϵ'. In Ref. [53], an extensive discussion has been made about the size of this matrix element. It is expected that the variation of the matrix element is between 1 to 2 of the factorization result.

Because the phase α in the factor $e^{i\alpha}$ is dominating, ϵ' is approximately a function of $r \sin\alpha$, rather than r and $\sin\alpha$ independently. Since $r \sin\alpha$ has been fixed by ϵ and neutron EDM d_n^e [89], ϵ' is approximately a function of M_{W_R} only. In Fig. 3.8, we plot ϵ' as a function of M_{W_R} for $\sin\alpha = 0.1$, $r = 0.5$ and $s_d s_s = 1$ which is required by the neutron EDM calculation. [All other $s_i = 1$.] We choose the renormalization scale at the charm quark mass and $\Lambda_{\rm QCD} = 340$ MeV. The dashed curve shows the result with the large-N_c matrix element, whereas the solid curve shows that from the lattice QCD [83].

If one uses that factorized matrix element and following the Refs. [94, 53] for other hadronic matrix elements, the experimental data is roughly reproduced by the SM calculation. Requiring the new contribution is less than 1/4 of the experimental

data, we get a large lower bound of 8 TeV on the right-handed scale. On the other hand, if one takes the calculation in Ref. [83] seriously, the lattice QCD generates a small and negative contribution to ϵ'. If then requiring that the experimental number is entirely reproduced by the new contribution, we find a limit on M_{W_R} about 5 TeV. In any case, ϵ' gives a tighter lower bound on M_{W_R} than the well-known neutral kaon mass difference. If on the other hand, we take $r \sin \alpha = 0.15$, as required by low M_H, the bound changes to 8.5 TeV. Therefore, we take the range 5-8 TeV as our final estimate.

Finally, we have also calculated the tree-level flavor-changing neutral Higgs contributions to $\mathcal{H}_{\Delta S=1}$. Since the relevant coupling is suppressed by either the Cabibbo angle or the quark masses, their contribution is negligible.

To conclude, we have found that a robust bound on the mass of the right-handed W-boson based on a relatively well-known estimate on the strong interaction matrix element of O_-^{LR}, which is known to within a factor of 2. The result is on the order of 5-8 TeV, which is just on the border for the Large Hadron Collider detection. This situation turns out to be better than the similar calculation in SM.

3.6 Conclusion

The standard model calculations for the direct CP violation in non-leptonic kaon decay have not been entirely settled due to large cancelations between different matrix elements. Therefore, there is a considerable interest in understanding this phenomena from beyond standard model physics. However, we do not know yet

what form the new physics will take, either supersymmetry, left-right symmetry, large extra dimensions, or little Higgs, or something else. Presumably, the Large Hadron Collider will help us to identify it in the next few years.

In this chapter, we aim to study a general effective theory for non-leptonic kaon decay which has its origin from beyond SM physics. We systematically classify the dimension-5, 6 and 7 quark and gluon operators according to their chiral structures. Using chiral symmetry, we derive tree-level relations between the matrix elements involving zero, one and two pions. This is useful because lattice calculations of multiparticle matrix elements are much harder than these for few particles. We also calculate the leading chiral logarithmic behavior of these operators in ChPT. The result again will be useful for calculating matrix elements of these operators on lattice. We do not consider them in quenched QCD formulations, as the rapid progress in lattice QCD calculations has made quenched studies much less useful than the past. In the end, we apply the derived general form onto a particular model, the minimal left-right symmetric model and improve the theoretical bound for the proposed W_R boson mass.

Chapter 4

Bag model and proton spin

4.1 Backgrounds and experiment status

4.1.1 Parton helicity distributions

Similar to the quark and gluon distributions inside the proton, we can also express the *polarized* quark and gluon distributions in light-cone coordinates:

$$\begin{aligned}\Delta q(x,Q^2) &= \frac{1}{2}\int\frac{d\lambda}{2\pi}e^{i\lambda x}\langle PS|\bar{\psi}(0)U(0,\lambda n)\not{n}\gamma_5\psi(\lambda n)|PS\rangle \\ \Delta g(x,Q^2) &= \frac{i}{2}\int\frac{d\lambda}{2\pi}e^{i\lambda x}\langle PS|F^{+\alpha}(0)U(0,\lambda n)\tilde{F}^{+}_{\alpha}(\lambda n)|PS\rangle\end{aligned}$$

where $\tilde{F}_{\alpha\beta} = (1/2)\epsilon_{\mu\nu\alpha\beta}F^{\mu\nu}$ and $U(0,\lambda n)$ is the gauge link between two fields to make it gauge invariant. Here the $x<0$ part in Δq can be interpreted as the polarized anti-quark contribution.

In considering the polarized DIS process in a parton picture we can calculate the QCD corrections to the polarized proton structure function $g_1^p(x)$. The polarized gluon distribution $\Delta g(x)$ enters $g_1^p(x)$ by the diagram in Figure. 4.1. To the next-to-leading order of α_s,

$$g_1^p(x,Q^2) = \frac{1}{2}\sum_i^{2n_f} e_i^2\left[\Delta q_i(x,Q^2) + \frac{\alpha_s}{2\pi}\Delta f_q(x,Q^2)\otimes\Delta q_i(x,Q^2) + \Delta f_g(x,Q^2)\otimes\Delta g(x,Q^2)\right] \tag{4.1}$$

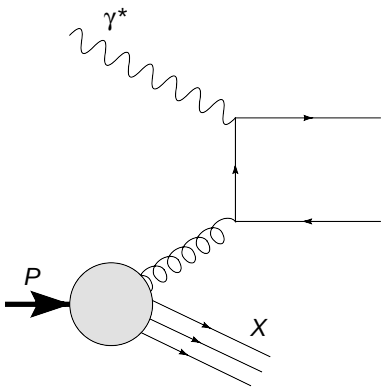

Figure 4.1: The photon-gluon scattering diagram

where i runs through all the active quarks and anti-quarks. $\otimes$ denotes the convolution

$$\int_0^1 dx\,[f(x)\otimes g(x)] = \int_0^1 dx f(x)\int_0^1 dy g(y) \tag{4.2}$$

f_q and f_g can in principle be calculated in perturbative QCD process. There are soft and collinear singularities in the calculation and both of them depend on the regularization scheme. Here we will only give out the final result of the first moment of the $g_1^p(x)$:

$$\Gamma_1^p(Q^2) \equiv \int_0^1 dx g_1^p(x,Q^2) = \frac{1}{2}\left(1-\frac{\alpha_s(Q^2)}{\pi}\right)\sum_i\left[\Delta q_i(Q^2) - \frac{\alpha_s(Q^2)}{2\pi}\Delta G(Q^2)\right] \tag{4.3}$$

On the other hand, the polarized quark and gluon distributions will obey the GLAP equations just as in the unpolarized case, but with different splitting functions[9]:

$$\frac{d}{dt}\begin{pmatrix}\Delta q_i(x,t)\\ \Delta g(x,t)\end{pmatrix} = \frac{\alpha_s(t)}{2\pi}\sum_j\begin{pmatrix}\Delta P_{q_iq_j}(x) & \Delta P_{qg}(x)\\ \Delta P_{gq}(x) & \Delta P_{gg}(x)\end{pmatrix}\otimes\begin{pmatrix}\Delta q_j(x,t)\\ \Delta g(x,t)\end{pmatrix} \tag{4.4}$$

where $t = \ln(Q^2/\Lambda^2_{\rm QCD})$. At leading order the splitting functions are

$$\begin{aligned}
\Delta P^{(0)}_{q_i q_j}(x) &= C_F \delta_{ij} \left[\frac{1+x^2}{(1-x)_+} + \frac{3}{2}\delta(1-x) \right], \\
\Delta P^{(0)}_{qg}(x) &= T_R(2x-1), \\
\Delta P^{(0)}_{gq}(x) &= C_F(2-x), \\
\Delta P^{(0)}_{gg}(x) &= C_A \left[\frac{2}{(1-x)_+} - 4x + 2 \right] + \frac{\beta_0}{2}\delta(1-x)
\end{aligned} \tag{4.5}$$

with $\beta_0 = (33 - 2n_f)/3$. In leading order $\alpha_s(Q^2) \sim 1/\ln Q^2$. By integrating over x in (4.4) using equation

$$f(x) \otimes g(x) \equiv \int_x^1 \frac{d\xi}{\xi} f\left(\frac{x}{\xi}\right) g(\xi) \tag{4.6}$$

we can easily get

$$\frac{d}{d\ln Q^2}\Delta\Sigma \sim \frac{d}{d\ln Q^2}(\alpha_s \Delta G) \sim \mathcal{O}(\alpha_s^2) \tag{4.7}$$

which indicates that $\alpha_s \Delta G$ is conserved to the leading order QCD evolution. In fact, it has a well-known solution at asymptotic limit:[10][107]

$$\begin{aligned}
\Delta\Sigma(Q^2) &= \text{const}, \\
\Delta G(Q^2) &= -\frac{4}{\beta_0}\Delta\Sigma(Q_0^2) + \frac{\ln(Q^2/\Lambda^2_{\rm QCD})}{\ln(Q_0^2/\Lambda^2_{\rm QCD})} \left(\Delta G(Q_0^2) + \frac{4}{\beta_0}\Delta\Sigma(Q_0^2) \right)
\end{aligned} \tag{4.8}$$

We can see that the first moment of the polarized gluon distribution does *not* vanish even in the asymptotic limit and will contribute to the first moment of $g_1^p(x)$. As a consequence we can understand this as what we measured in polarized DIS experiments is not Δq but rather $(\Delta q - \frac{\alpha_s}{2\pi}\Delta G)$. Hence, a large and positive ΔG may be the key to solving the problem of "spin crisis". A detailed calculation revealed that

it will need a $\Delta G \sim 2.5$ at $Q^2 = 10\text{GeV}^2$ to match the experimental result of Γ_1^p. This can be regarded as an upper limit of the gluon spin contribution since it didn't take the strange-sea polarization into account.

4.1.1.1 Quark helicity distribution

We can acquire some knowledge of the individual quark helicity distribution by assuming the $SU(3)_f$ symmetry and comparing the spin-dependent structure functions for various nucleons.

The results are shown below[7]:

$\int_0^1 \Delta q_i(x)dx$	SMC results $Q^2 = 10$ GeV^2	HERMES results $Q^2 = 2.5$ GeV^2
Δu_v	$0.77 \pm 0.10 \pm 0.08$	$0.57 \pm 0.05 \pm 0.08$
Δd_v	$-0.52 \pm 0.14 \pm 0.09$	$-0.22 \pm 0.11 \pm 0.13$
$\Delta \bar{u}$	$0.01 \pm 0.04 \pm 0.03$	$-0.01 \pm 0.02 \pm 0.03$

Table 4.1: Comparison of the first moment of separated quark spin distributions as determined from semi-inclusive DIS lepton scattering.

In RHIC with polarized high-energy $p - p$ collisions we can extract the single quark helicity distribution by detecting production rate of weak bosons since the nature of maximal parity violations in weak interactions. In tree level the single spin longitudinal asymmetry for W^+ production can be written as[8]:

$$A_L \equiv \frac{\sigma^{\uparrow\uparrow} - \sigma^{\downarrow\uparrow}}{\sigma^{\uparrow\uparrow} + \sigma^{\downarrow\uparrow}} = \frac{\Delta u(x_1)\bar{d}(x_2) - \Delta\bar{d}(x_1)u(x_2)}{u(x_1)\bar{d}(x_2) + \bar{d}(x_1)u(x_2)} \tag{4.9}$$

4.1.1.2 Gluon helicity distribution

As we can see the gluon helicity distribution plays a crucial rule in solving the "spin crisis". However, the gluon will only scatter with photon at next-to-leading order, which greatly increase the error bar of determining it in a polarized DIS scattering process. And the non-local nature of $\Delta g(x)$ in (4.1) prohibits one calculating it with a lattice approach. Now people still can't determine the sign of the first moment of $\Delta g(x)$. A recent parameter fit for $x\Delta g(x)$ with the current data are shown in Figure. 4.2[106].

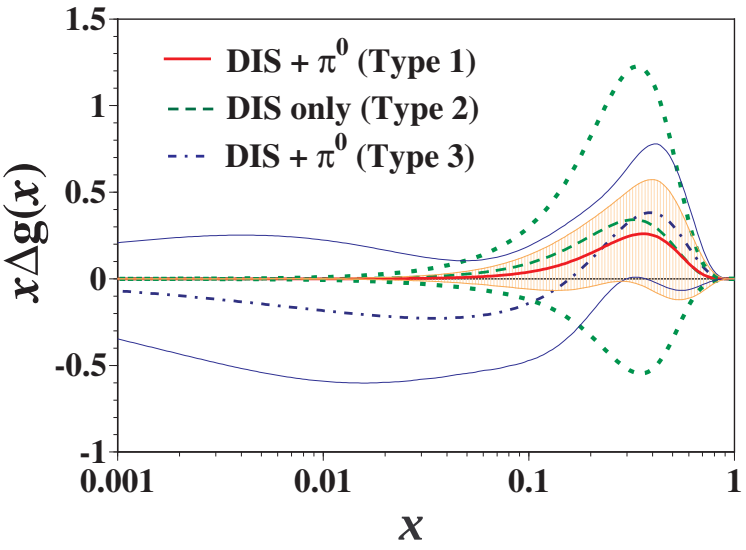

Figure 4.2: The polarized gluon distributions are shown at Q^2=1 GeV^2. The uncertainty ranges are shown by the shaded band, the dotted curves, and thin solid curves for the type 1, 2 and 3, respectively.[106]

There are various ways to measure $\Delta g(x, Q^2)$, we list them below:

a. Measure $g_1(x, Q^2)$ at various Q^2 and using NLO GLAP equation to extract $\Delta g(x, Q^2)$. There are a number of drawbacks in this method, however. The currently data with a large range of coverage of Q^2 is highly limited, and the error bars are huge. Moreover, the extracted polarized gluon distribution will strongly depend on the initial parameter set in $\Delta g(x, Q_0^2)$. A combination with method b will render but not eliminate this problem.

b. $\Delta g(x)$ from large transpose momentum hadron productions in $e - p$ scattering.

c. $\Delta g(x)$ from charm production in $e - p$ scattering .

d. $\Delta g(x)$ from di-jet production in $e - p$ scattering .

e. $\Delta g(x)$ from direct photon production in $p - p$ collisions. This is the most prominent way of measuring $\Delta g(x)$ so far and is only available in RHIC. We'll have some detailed discussion below.

At tree level, the direct photon can be produced through $q\bar{q} \to \gamma g$ and $qg \to \gamma q$, as shown in Figure. 4.3. $\hat{s}, \hat{t}$ and $\hat{u}$ are defined as:

$$\hat{s} = x_a x_b s,\ \hat{t} = x_a t,\ \hat{u} = x_b u \tag{4.10}$$

And s, t, u are the ordinary Mandelstam variables for the protons. By simple calculation we can get:

$$|M|^2_{qg\to\gamma q} = -\frac{1}{2}\frac{\hat{s}^2 - \hat{t}^2}{\hat{s}\hat{t}}; \quad |M|^2_{q\bar{q}\to\gamma g} = -\frac{8}{9}\frac{\hat{u}^2 + \hat{t}^2}{\hat{u}\hat{t}} \tag{4.11}$$

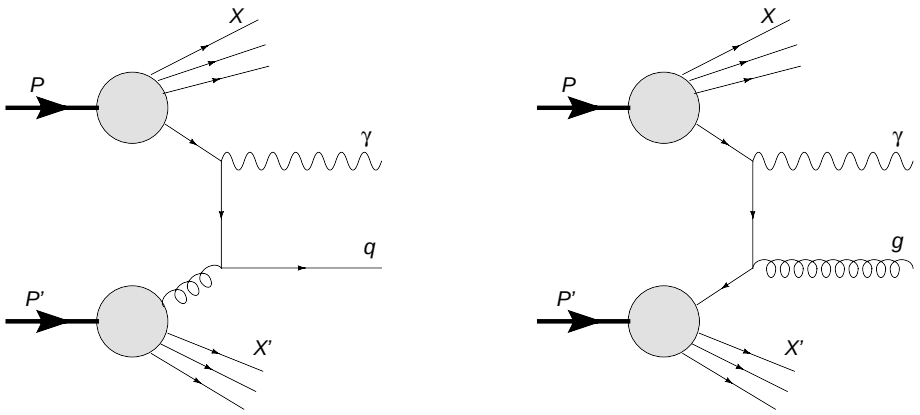

Figure 4.3: Direct photon productions

We can use factorization theorem and write the total cross section for the inclusive direct-photon production as:

$$E_\gamma \frac{d\sigma_{\rm AB}}{d^3p_\gamma} = \sum_{ab} \int dx_a dx_b f_A^a(x_a,\mu^2) f_B^b(x_b,\mu^2) E_\gamma \frac{d\hat{\sigma}_{ab}}{d^3p_\gamma} \tag{4.12}$$

The $f_{A,B}$ are the (polarized) distribution functions and μ is the factorization scale. We can choose a region where the $qg \to \gamma q$ is dominant. In this case the corresponding distribution functions will be g_1 and Δg and we can write the total cross section as

$$E_\gamma \frac{d\sigma_{\rm AB}}{d^3p_\gamma} = \int dx_a dx_b \left[\frac{2g_1(x_a,\mu^2)}{x_a} \Delta g(x_b,\mu^2) E_\gamma \frac{d\hat{\sigma}_{ab}}{d^3p_\gamma} + (x_a \leftrightarrow x_b) \right] \tag{4.13}$$

In this calculation we didn't consider the high-order QCD corrections. A complete treatment usually needs a resummation for all the soft modes and a particular choice of the method of infrared subtraction. For a detailed calculation please refer [12].

4.1.2 Experimental measurements

In recent days the $g_1(x)$ has been well measured by numerous experiments. A plot of the recent data is shown in Figure. 4.4[106]:

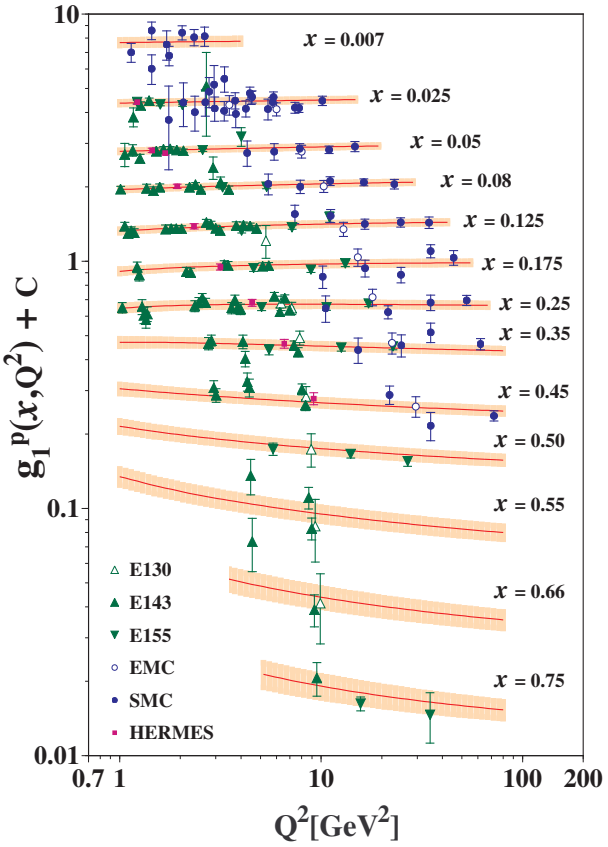

Figure 4.4: Current $g_1(x)$ result by various experiments[106]

SLAC Experiments

The SLAC program was the first experiment to measure the proton spin structure by polarized DIS process. Polarized electrons get accelerated in the SLAC linac and impinge on fixed targets in End Station A. The electron polarization is produced by Stern-Gerlach separation in an inhomogeneous magnetic field. The beam energy

could reach as much as 48GeV and the polarization could be 80%. However, due to the depolarization effects in the target the average beam currents are limited. Also the unpolarized part in the target dilute the physics asymmetry by a factor of ~ 0.15 and leads to a large error bar.

DESY Experiments

HERMES(HERa MEasurement of Spin) has been taking data at DESY since 1995. HERMES takes advantage of the stored $e^{\pm}$ beam in HERA and uses very thin gaseous targets of pure atoms(protons, deuterons, and ^{3}He). It uses Sokolov-Ternov effect[16] to make the beam transversely polarized. Then a semi-inclusive DIS with a high current($\sim$ 50mA) could be achieved. It is possible to implement a polarized proton beam in the HERA ring. This would allow it to have polarized $p-p$ collision at an energy $\sim$50GeV as supplement data to the RHIC spin program.

CERN Experiments

The famous EMC(European Muon Collaboration) was part of the CERN experiments After that the SMC(Spin Muon Collaboration) experiment bagan as an upgrade to the EMC measurements. With high energy muon beams it is able to get access to the low x regime($x < 0.01$).

The current experiment at CERN is COMPASS[17](COmmon Muon Proton Apparatus for Structure and Spectroscopy), whose goal is to get information of the polarized gluon distribution. It uses the longitudinally polarized muon beam with a energy of 160GeV^2 in the lab frame and solid polarized LiD and proton in hope

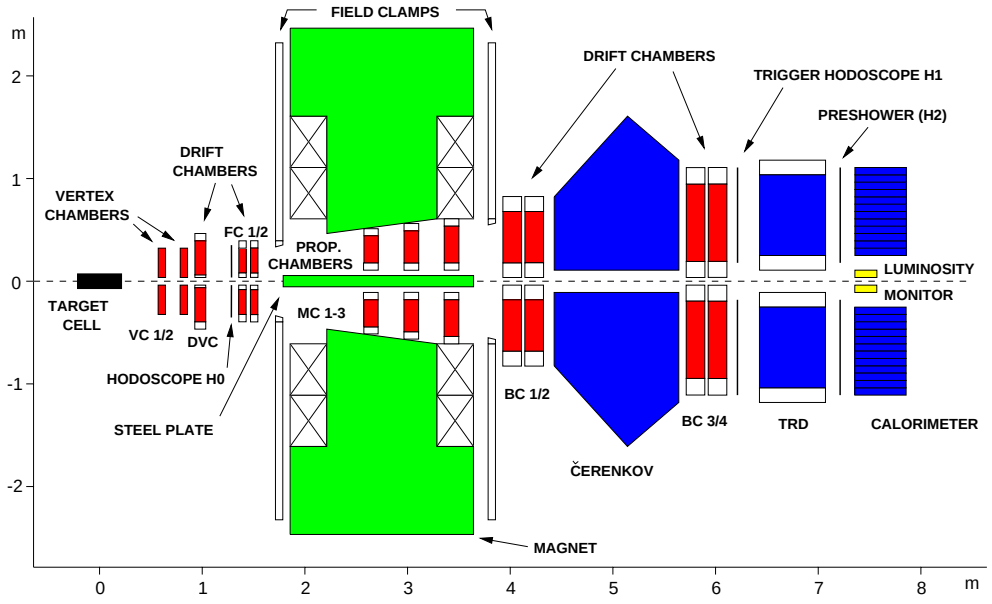

Figure 4.5: Schematic diagram of HERMES spectrometer[13]

to get the g_1 structure function of proton and deuteron.

RHIC and eRHIC Experiments

The Relativistic Heavy-Ion Collider(RHIC) is located at the Brookhaven National Laboratory. The collider mainly uses high-energy heavy ion beams to produce high luminosity collisions. With the "snake resonance" at RHIC it is able to have proton beams with 70% polarizations and a center-of-momentum energy $\sqrt{s}$ up to 500GeV.

RHIC has two large collider detectors, PHENIX and STAR, participating in the RHIC spin program. Since it's the only polarized proton-proton collider so far it owns many peculiar properties, such as a direct determination of $\Delta g(x, Q^2)$ via reaction $pp \to \gamma X$ discussed in last section.

EIC(eRHIC) is a possible upgrade for the RHIC which would allow it to pro-

duce high-luminosity polarized electrons-hadrons collisions. The aim is to reach about 70% polarization for the proton beam and a $10^{33}/(\mathrm{cm}^2 \cdot \mathrm{sec})$ luminosity at x as small as 3×10^{-4}.[14][15] A comparison of eRHIC and other lepton scattering facilities is shown in Figure. 4.6.

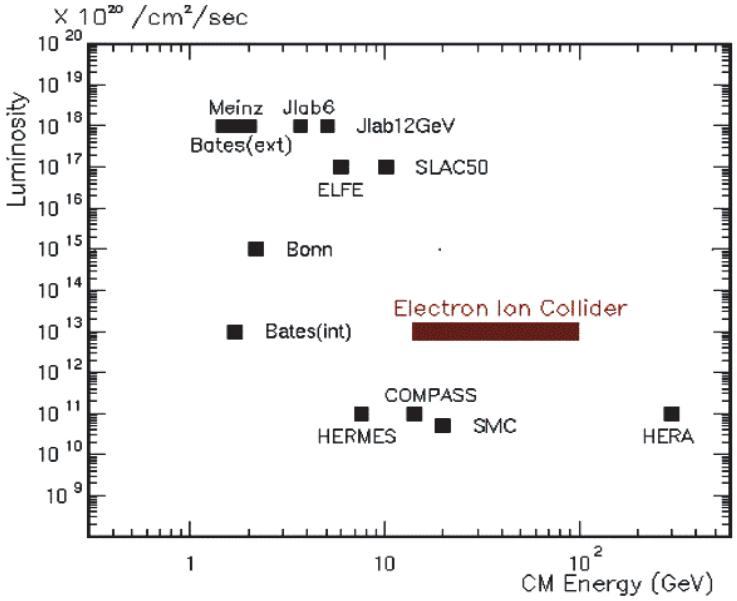

Figure 4.6: The center-of-mass energy vs. luminosity of the proposed Electron-Ion Collider eRHIC compared to other lepton scattering facilities.[14]

4.2 A Bag model calculation

The polarized gluon distribution in the proton $\Delta g(x)$ has been the focus of high-energy spin physics since the European Muon Collaboration measurement of the quark helicity distributions through polarized inclusive deep-inelastic scattering [36]. Gluons are known to play the key role in the proton's mass and momentum

[95], and it is expected that they also play a similar important role in the spin of the proton. This expectation has motivated extensive experimental programs at DESY (HERMES collaboration), CERN (COMPASS Collaboration), and polarized RHIC. Much experimental progress has been made in probing the polarized gluon distribution through leading hadron production, charm production, and neutral pions and di-jets [96]. High statistics data expected from the polarized RHIC will provide a much better picture on $\Delta g(x)$ in the near future [97].

Two fundamental questions about the gluon polarization have attracted the most attention: what it is total size $\Delta G = \int_0^1 dx \Delta g(x)$, and how does its sign vary with Feynman momentum x. Both questions are difficult to answer in practice. Since ΔG is not related to the matrix element of a local, gauge-invariant operator, it cannot be calculated directly in lattice QCD simulations, which have been the only non-perturbative approach to solve the fundamental theory so far. Experimentally, it is a challenge to measure $\Delta g(x)$ directly at a fixed-Feynman x, with the exception of few channels at tree order (e.g. direct photon production [97]). The phenomenological distributions in the literature are obtained by "educated" parametrizations and fitting of the parameters to experimental data [98][99]. The results depend on the functional forms adopted, sensitive to assumptions such as if $\Delta g(x)$ is allowed to change sign in x. Given the above situation, it is important to investigate the possibility of calculating $\Delta g(x)$ in proton models, with the hope that some key features might be shared by QCD.

Gluons are known to play the dominant role in QCD. The gluons in the QCD vacuum are responsible for, among others, color confinement and chiral symmetry

breaking. Modeling these gluons is beyond the scope of this study. On the other hand, the gluons in the unpolarized proton contribute as much as 50% of its momentum and mass [95]. These gluons are generated from the valence quarks and affect strongly the dynamics of quarks in return. Therefore they must be solved self-consistently with the motion of the quarks, which is again outside the scope of this work.

On the other hand, the polarized gluons—induced through quark polarizations in a polarized proton—is a much smaller effect. In fact, in QCD with a large number of colors N_c, the polarized gluons are suppressed by $1/N_c^2$ related to those in the QCD vacuum. As a consequence, the spin-dependent gluon potential A^μ may be solved from the chromodynamic Maxwell equation,

$$D_\mu F^{\mu\nu} = J^\nu \ , \tag{4.14}$$

with some reasonable modeling of the spin-dependent quark color current J^μ. This situation is analogous to the small-x gluons which are calculable from the valence quark color charges in the saturation region [101].

SU(6) quark models have had some reasonable successes in describing the valence quark structure of the proton. For example, they give a reasonable account of the magnetic moment of the proton. In particular, the signs and magnitudes of the magnetic moments of the up and down quarks are correlated postively with the total angular momentum carried by them ($\mu_u = 3.6$, $\mu_d = -1.0$, vs. $J_u = 4/3$ and $J_d = -1/3$). What about the proton spin for which the naive quark model prediction seems to have failed so badly? Well, in the MIT bag model, although the spin is

carried entirely by quark angular momentum in the lowest-order wave function, about 40% comes from the orbital motion of the quarks [102]. Once the gluon contribution is taken into account by the higher Fock states, the quark contribution must be renormalized from these additional wave function components. If the gluons contribute 50% of the proton spin, for example, the renormalized singlet axial charge in the bag model will be about $\Delta\Sigma = 0.60/2 = 0.30$, roughly consistent with the current experimental data. Therefore, as a first estimate, the polarized gluons may be calculated from the quark color currents in the MIT bag model.

The total gluon polarization ΔG has been studied before in quark models in Refs. [103, 104]. In Ref. [103], the calculation is incomplete because only the interference diagram has been included, and the contribution from a single quark intermediate states has been ignored. The result is a negative ΔG. In Ref. [104], the single quark contribution was taken into account in the non-relativistic quark model and ΔG is found to be positive after canceling the negative interference contribution. As we shall see, a direct calculation of $\Delta g(x)$ in non-local operator form produces actually a different total ΔG that is consistent with parton physics.

The polarized gluon distribution $\Delta g(x)$ can be calculated as a matrix element of the non-local operator [105]

$$\Delta g(x) = -\frac{i}{x}\int_{-\infty}^{\infty}\frac{d\lambda}{2\pi}e^{-i\lambda x}\langle P|F^{+\alpha}(\lambda n)W\tilde{F}^{+}{}_{\alpha}(0)|P\rangle \ , \tag{4.15}$$

where $|P\rangle$ is the proton state normalized covariantly, n is a light-like vector conjugating to an infinite momentum frame P. $F^{\mu\nu}$ is the gluon field tensor and W is a gauge link along the direction n connecting the two gluon field tensors, making the

whole operator gauge invariant. In this first calculation, we neglect the effects of the nonlinear interactions, and then the gluons fields behave as 8 independent Abelian fields. Under this approximation, the gluon field tensor is gauge invariant (as in the QED case) and the gauge link can be ignored and an equivalent expression is obtained by inserting a complete set of intermediate states between the gluon field tensors,

$$\begin{aligned}\Delta g(x) &= -i\int \frac{d^4k}{(2\pi)^4}\frac{1}{V_4}\epsilon_\perp^{\alpha\beta}(k^+ g^{\alpha\mu}g^{\beta\nu} - k^\alpha g^{+\mu}g^{\beta\nu} - k^\beta g^{+\nu}g^{\alpha\mu})\delta(x-k\cdot n) \\ &\quad \times \sum_m \langle \tilde{P}|A_\mu^*(k)|m\rangle\langle m|A_\nu(k)|\tilde{P}\rangle (V_3\cdot 2P^+)\ , \end{aligned} \tag{4.16}$$

where m sums over all possible intermediate states, and V_3 and V_4 are the space and space-time volumes, respectively. The rescaled state $|\tilde{P}\rangle$ is normalized to 1.

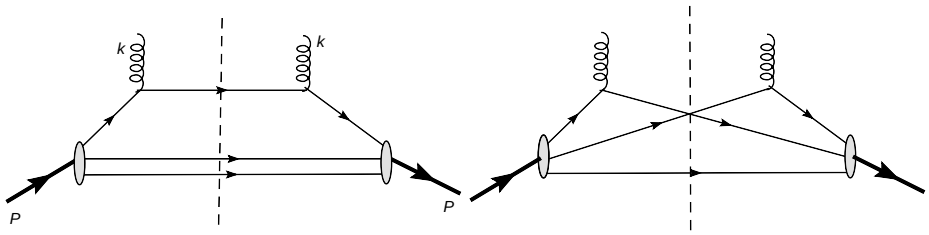

Figure 4.7: One-body and two-body contributions to the matrix element of the polarized gluon operator in the quark models of the proton.

In the quark models, the above matrix element receives contributions from one-body and two-body terms, shown schematically in Fig. 4.7. It is easy to show that the one-body term with the same quark intermediate state as the initial one cancels the two-body contribution. This cancellation is due to the color structure of the states as well as the spin property of the operator. Therefore, the net contribution

arises from one-body term with excited intermediate quark states. The matrix element in the single quark state is

$$\langle m|A_\nu(k)|\tilde{P}\rangle = 2\pi\delta\big(k^0 - (\epsilon_f - \epsilon_i)\big)\frac{-i}{k^2}(-igt^a)\langle m|j_\nu(k)|\tilde{P}\rangle \ , \qquad (4.17)$$

where the δ-function comes from the energy conservation and j_ν is the color current. For simplicity we have used the free-space gluon propagator.

The sum over all intermediate quark states produces a divergent result. This divergence is the usual ultra-violet divergence in field theory and must be regulated by cut-offs. In our case, the cut-off may be taken as the excitation energy of the intermediate states.

Shown on the left panel in Fig. 4.8 is the MIT bag result for $\Delta g(x)$ with different intermediate state cut-offs. On the left panel, the results show successive additions of s, p, d, f wave contributions. In the second panel, the result (red solid line, multiplied by an additional x) is compared with that from phenomenological fit [100] (dashed line surrounded by an uncertainty band). The bag radius R is chosen to be 1.18 fm by fitting the nucleon charge *r.m.s.* radius. The dotted curve corresponds to the s-wave contribution ($\kappa = -1$) with zero and one node wave functions included. The dash-dotted curve includes in addition the p wave contribution ($\kappa = -2, 1$); the dashed curve contains the d wave contribution ($\kappa = -3, 2$); and finally the solid curve includes up to the f wave contribution ($\kappa = -4, 3$). Two features of the result are immediately obvious. First, $\Delta g(x)$ is positive everywhere as a function of x, and vanishes quickly as $x \to 1$. Second, as more intermediate states are included, Δg gets uniformly larger. In fact, for higher intermediate states, the result shall change

with the cut-off following the perturbative QCD evolution. Therefore, $\Delta g(x)$ at different scales can be obtained approximately by limiting the excitation energy of the intermediate quarks. The solid-line result roughly corresponds to a cut-off at 1 GeV. Of course, the present cut-off scheme is different from that of the perturbative dimensional regularization and minimal subtraction. The difference can in principle be calculated in perturbation theory.

The phenomenological gluon distributions have been obtained by fitting the Q^2 evolution of the spin-dependent structure function $g_1(x)$ [98]. The result depends on the functional form assumed for $\Delta g(x)$. In a recent study, the double spin asymmetries for pion production was also included in the fits [106]. If one allows $\Delta g(x)$ to change sign, the fit generates a distribution with very large error bars. On the other hand, if one assumes that $\Delta g(x)$ is positive everywhere, the error becomes much smaller. On the right panel of Fig. 4.8, we have shown such a fit (dashed line with error band) together with our bag model result (solid line). The bag calculation is consistent with the fit, with significant strength at large and small x where the model might not be trustable.

To see that the positive $\Delta g(x)$ is a generic feature of quark models, we have shown in Fig. 4.9 the result from a non-relativistic quark model. The different curves again show successive inclusion of higher intermediate excited states. The general shape is similar to that from the MIT bag, which is shown in the thin solid line. The model artifacts at small and large x are clearly stronger.

Integrating over x, the $\kappa = -1$ intermediate state produces a result $\Delta G = 0.23\hbar$ (with $\alpha_s = 2.55$ obtained by fitting $N - \Delta$ mass splitting). Including higher

states up to $\kappa = 3, -4$, we find $\Delta G = 0.32\hbar$, from which a smaller α_s at higher excitation energy is used. Therefore, at low-energy scales, ΔG is on the order of 0.2 to $0.3\hbar$, which is considerably smaller than previous expectations inspired by the axial anomaly phenomenology [107]. Indeed, the anomaly contribution from this ΔG is negligibly small, $(\alpha_s/2\pi)\Delta G \sim 0.01$. In [104], the authors made a non-relativistic model calculation with the center-of-momentum degree of freedom explicitly excluded. The consistency between our result and that in [104] shows the single-particle approximation used in our calculation is justified.

To summarize, we have argued that the polarized gluon distribution $\Delta g(x)$ is calculable in quark models. We have carried out a first such calculation in the MIT bag, and the result shows that it is positive definite at all x. The total gluon helicity in the bag is on the order of $0.2 - 0.3\hbar$, which is substantially smaller than what has been expected in the past.

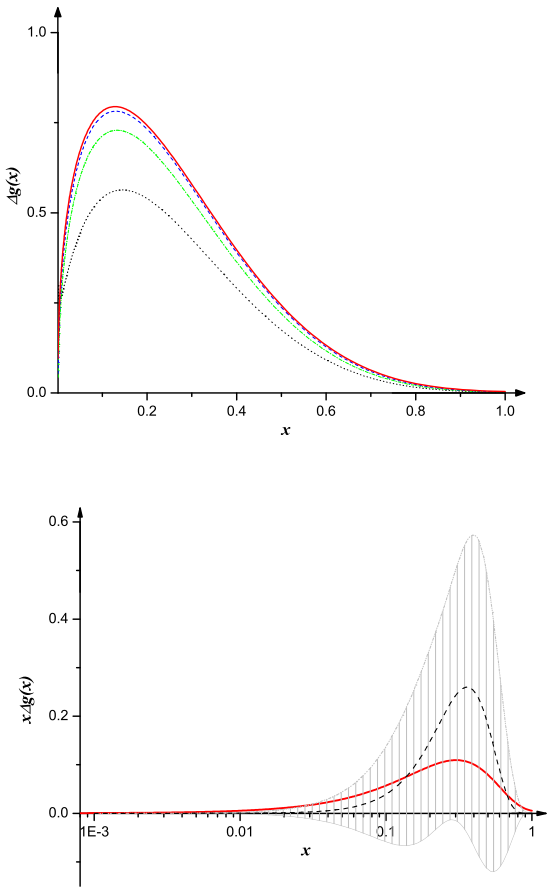

Figure 4.8: $\Delta g(x)$ and $x\Delta g(x)$ calculated in the MIT bag model.

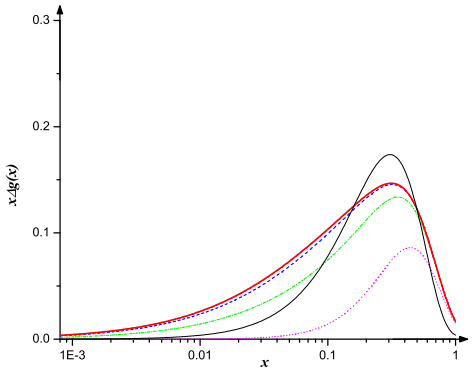

Figure 4.9: $x\Delta g(x)$ calculated in non-relativistic quark model by summing contributions from s, p, d, and f waves. The thin solid line is the MIT bag model result.

Chapter 5

SCET and Threshold Resummation

5.1 Introduction

In lepton-nucleon deep-inelastic scattering (DIS), the Bjorken regime with virtual photon mass $Q^2 \to \infty$ and $x_B = Q^2/2M\nu$ fixed presents a textbook example of perturbative QCD (pQCD) factorization [108]. In this regime, the scale $(1-x)^\alpha Q$ goes to infinity (we drop the subscript B on x henceforth), where α is any real number, or at least much larger than the soft QCD scale $\Lambda_{\rm QCD}$. An alternative DIS regime is $Q^2 \to \infty$ with $(1-x)Q \sim \Lambda_{\rm QCD}$, where the final hadron state invariant mass $(1-x)Q^2 \sim Q\Lambda_{\rm QCD}$ is still large and is distinct from the resonance region. This large-x regime has so far received little attention in theory, possibly because it covers only a small kinematic interval in real experiments. The existing QCD studies in the literature are somewhat controversial [109, 110].

In this chapter, we present a factorization study of DIS at this regime. The main point we advocate here is that the standard pQCD factorization remains valid in this new kinematic domain to leading order in $1-x$. Then we move on to discuss refactorization which factorizes the physics at scale $(1-x)Q^2$ from that at Q^2. The useful theoretical framework for this purpose is the so-called soft-collinear effective field theory (SCET) developed recently [111]. Indeed, the first treatment of the large-x region in DIS using SCET was made in [112] and followed in [109, 110] for

$(1-x)Q \sim \Lambda_{\rm QCD}$ [see also [113].] Because the scale $(1-x)Q$ does not enter in the perturbative calculation, the final result amounts to a standard pQCD factorization, with the additional benefit that the refactorization becomes manifest. One subtlety we discuss extensively in this work is the role of the soft contribution and its relation to the light-cone parton distribution. In a recent paper [109], a factorization formula for the DIS structure function is derived in SCET, which is similar to what we find here. However, because of the lack of a consistent regularization and clear separation of contributions among different factors, the result does not recover that of Ref. [112] in the limit $(1-x)Q \gg \Lambda_{QCD}$.

The traditional approach of refactorization was pioneered in [114], where a new parton distribution together with soft factor and jet function is introduced. These matrix elements are designed to absorb large logarithms generated from soft gluon radiations off on-shell lines. Evolution equations for them are derived and solved to resum the large soft-gluon logarithms. In this approach, the factorization of scales are not apparent from the start. Moreover, a spurious scale $(1-x)Q$ appears in all factors which makes them nonperturbative in the regime of our interest. After reviewing this, we present a more general factorization along this line with dependence on a rapidity cut-off ρ. Different choices of the cutoff lead to redistributions of large logarithms in different matrix elements. A particular choice yields a picture similar to that of the SCET approach.

The presentation of this chapter is as follows. In section II, we argue that the standard factorization approach remains valid in the end-point regime $x \sim 1 - \mathcal{O}(\Lambda_{\rm QCD}/Q)$. In section III, we present an effective field theory approach to

refactorization, following the previous work of Ref. [109]. The difference is that our result is consistent with that of Ref. [112], with the jet factor absorbing all physics at the intermediate scale $(1-x)Q^2$. We explain that the soft and collinear contributions combine to give the light-cone parton distribution. In section IV, we first review the traditional factorization in which various matrix elements are introduced to account for soft gluon radiations. We then show how to derive a more general factorization with a rapidity cutoff. We demonstrate explicitly that the proper soft subtractions must be made in the collinear matrix elements to avoid double counting. By choosing different cut-off, we find different pictures of factorization and large-logarithmic resummation. The effective field theory refactorization can be recovered this way.

5.2 Validity of the standard QCD factorization at $x_B \sim 1-\mathcal{O}(\Lambda_{\rm QCD}/Q)$

The standard pQCD factorization theorem is derived in the Bjorken limit in which $Q^2 \to \infty$ and x is a fixed constant between 0 and 1. To leading order in $1/Q^2$, the proton's spin-independent structure function $F_1(x, Q^2)$ can be factorized as

$$F_1(x, Q^2) = \sum_f \int_x^1 \frac{dy}{y} C_f\left(\frac{x}{y}, \frac{Q^2}{\mu^2}\right) q_f(y, \mu^2) \ , \tag{5.1}$$

where μ is a factorization scale, C_f is the coefficient function depending on scale Q^2 and μ^2 (factorization scale), and q_f is a quark distribution of flavor f. For simplicity, we omit the quark charges and gluon contribution which are inessential for our discussion. In the moment space, the factorization takes a simple product

form,

$$F_1^N(Q^2) = \sum_f C_{fN}(Q^2/\mu^2) q_{fN}(\mu^2) \ , \tag{5.2}$$

where the moments are defined the usual way, e.g., $q_N = \int_0^1 dx x^{N-1}(q(x) + \bar{q}(x))$ with N even.

The above factorization in principle is invalid in non-Bjorken regions. However, we argue that it still holds in the regime of our interest, $(1-x)Q \sim \Lambda_{\rm QCD}$, with the same physical parton distributions to leading order in $1-x$. The main point is that although we now have a new infrared scale $(1-x)Q$, it does not appear in the above factorization.

Indeed, as $x \to 1$ the coefficient function C_f can only depend on the two hard scales—invariant photon mass Q^2 and the final-hadron-state invariant mass $(1-x)Q^2$, both remain large when $(1-x)Q \sim \Lambda_{\rm QCD}$. Hence there is no emerging infrared scale entering physical observables in this new regime, and the original factorization remains valid to leading order in $1-x$.

The above observation can be seen clearly in the one-loop result. The coefficient function at order α_s in the x-space

$$C^{(1)}(x) = \frac{\alpha_s}{2\pi} C_F \left[\left(\frac{2\ln((1-x)Q^2/\mu^2) - 3/2}{1-x} \right)_+ - \left(\frac{3}{2} \ln \frac{Q^2}{\mu^2} + \frac{9}{2} + \frac{\pi^2}{3} \right) \delta(1-x) \right] \ , \tag{5.3}$$

where we have neglected higher order in $(1-x)$. The scheme we use here is the modified minimal subtraction ($\overline{\rm MS}$). In term of moments, one finds

$$C_N^{(1)}\left(\frac{Q^2}{\mu^2}, \frac{Q^2}{N\mu^2} \right) = \frac{\alpha_s}{2\pi} C_F \left[\ln^2 \frac{Q^2}{N\mu^2} - \frac{3}{2} \ln \frac{Q^2}{N\mu^2} - \ln^2 \frac{Q^2}{\mu^2} + 3 \ln \frac{Q^2}{\mu^2} - \frac{9}{2} - \frac{\pi^2}{6} \right] \ . \tag{5.4}$$

The scale dependence is manifest: The first two logarithms come from physics at scale $\mu^2 = Q^2/N$, whereas the next two logarithms come from scale Q^2. Clearly, there is no physics from scale $\mu^2 \sim (1-x)^2 Q^2 \sim Q^2/N^2$. Therefore, even when $(1-x)Q$ becomes of order $\Lambda_{\rm QCD}$, the coefficient function has no infrared sensitivity to it.

The fundamental reason for the absence of the scale $(1-x)Q$ in a physical observable is that it is not a Lorentz scalar, whereas $(1-x)Q^2$ is the invariant mass of the final hadron state. In principle, the energy of soft gluons and quarks in the Breit frame is of order $(1-x)Q$ which can appear in the factorization. However, this happens only for frame-dependent factorization. The factorization we quoted above is frame-independent and thus any non-Lorentz scalar cannot appear.

Although the above conclusion appears simple and natural, we have not seen it stated explicitly in the literature.

5.3 Refactorization: Effective Theory Approach

In the large-x region, independent of whether $(1-x)Q \gg \Lambda_{\rm QCD}$ or $\sim \Lambda_{\rm QCD}$, there is an emerging "infrared" scale $(1-x)Q^2 \ll Q^2$. Of course, we always assume $(1-x)Q^2 \gg \Lambda^2_{\rm QCD}$. The presence of this new scale suggests a further factorization in which the physics associated with scales Q^2 and $(1-x)Q^2$ is disentangled. This type of factorization was proposed by G. Sterman and others for the purpose of summing over the large double logarithms of type $\alpha_s^k[\ln^i(1-x)/(1-x)]_+$ $(i \le 2k-1)$ in the coefficient functions [114]. We consider this refactorization in this and the following

sections, commenting on its applicability in the region of our interest.

We first study refactorization in the effective field theory (EFT) approach in this section, and will discuss a more intuitive approach in the next. The EFT method is based on strict scale separation, very much like the usual QCD factorization discussed in the previous section. When the scales are separated, one can sum over large logarithms by using renormalization group evolutions between scales. Some of the basic discussions here follow Refs. [112, 115, 109].

5.3.1 EFT Refactorization

To understand the EFT factorization heuristically, we write the one-loop coefficient function in Eq. (5.4) in a factorized form,

$$C_N^{(1)}\left(\frac{Q^2}{\mu^2},\frac{Q^2}{\overline{N}\mu^2}\right) = 2C^{(1)}\left(\frac{Q^2}{\mu^2}\right) + \mathcal{M}_N^{(1)}\left(\frac{Q^2}{\overline{N}\mu^2}\right) \ , \tag{5.5}$$

where $C^{(1)}$ is N-independent and comes from physics at scale Q^2 and $\overline{N} = Ne^{\gamma_E}$ where γ_E is Euler constant. The one-loop result for C is

$$C^{(1)}\left(\frac{Q^2}{\mu^2}\right) = \frac{\alpha_s}{4\pi}C_F\left[-\ln^2\frac{Q^2}{\mu^2} + 3\ln\frac{Q^2}{\mu^2} - 8 + \frac{\pi^2}{6}\right] \ , \tag{5.6}$$

where the constant term is, in principle, arbitrary; we choose it to be consistent with the effective current below. The two-loop result for C can be found in [117, 116]. The other factor $\mathcal{M}_N^{(1)}$ comes entirely from physics at scale $(1-x)Q^2 \sim Q^2/\overline{N}$,

$$\mathcal{M}_N^{(1)}\left(\frac{Q^2}{\overline{N}\mu^2}\right) = \frac{\alpha_s}{2\pi}C_F\left[\ln^2\frac{Q^2}{\overline{N}\mu^2} - \frac{3}{2}\ln\frac{Q^2}{\overline{N}\mu^2} + \frac{7}{2} - \frac{\pi^2}{3}\right] \ , \tag{5.7}$$

and the second order result for $\mathcal{M}_N$ can also be found in [116]. The key point is that the above refactorization of scales works to all orders in perturbation theory

and EFT provides a formal approach to establish this: The physics at scale Q^2 can be included entirely in $|C|^2$ and that at the other scale is in $\mathcal{M}_N$.

To arrive at the above refactorization, we start off at the scale Q^2 at which perturbative physics involves virtual gluon corrections to the hard interaction photon vertex. Note that the soft-gluon radiations off a hard vertex are usually high-order effects in $1/Q^2$ and can be neglected. Thus the physics at Q^2 can be found from just the quark electromagnetic form factor. Integrating out physics at scale Q^2 is equivalent to matching the full QCD electromagnetic current to an effective one involving just soft-collinear physics.

$$J^\mu_{\rm QCD} = C(Q^2/\mu^2) J^\mu_{\rm eff}(Q^2/\mu^2) \ , \tag{5.8}$$

with the one-loop result given in Eq. (5.6).

We can run the effective current from scale Q^2 to scale $(1-x)Q^2$ using the renormalization group equation

$$\mu \frac{dJ_{\rm eff}(Q^2/\mu^2)}{d\mu} = -\gamma_1(\alpha_s(\mu)) J_{\rm eff}(Q^2/\mu^2) \ , \tag{5.9}$$

where the anomalous dimension can be calculated from C, $\gamma_1 = \mu d \ln C/d\mu$, and has the following generic form,

$$\gamma_1 = A(\alpha_s) \ln Q^2/\mu^2 + B_1(\alpha_s) \ , \tag{5.10}$$

in which A and B_1 are a series in strong coupling constant α_s and are now known up to three loops [118].

At scale $\mu_I^2 = (1-x)Q^2$, we follow Ref. [109], matching products of the effective currents to a product of the jet function, collinear parton contribution,

and soft distribution in SCET. Introducing a small expansion parameter λ, with $\lambda^2 Q \sim \Lambda_{\rm QCD}$, $1-x$ in the region of our interest scales like λ^2. The collinear partons at the matching scale μ_I^2 have momentum $(p^+, p^- p_\perp) \sim Q(1, \lambda^4, \lambda^2)$ [our notation for light-cone components for arbitrary four-vector l is $l \equiv (l^+, l^-, l_\perp)$ with $l^\pm = \frac{1}{\sqrt{2}}(l^0 \pm l^3)$], and the soft partons have momentum $(\lambda^2, \lambda^2, \lambda^2)Q$. The moment of the structure function F_1 after the second stage matching has the following form [109],

$$F_1^N(Q) = C^2(Q^2/\mu_I^2) J_P(N, Q^2/\mu_I^2) \phi_N(\mu_I^2) S_N(\mu_I^2) \ , \tag{5.11}$$

where various factors are defined as follows.

The jet function $J_P(N, \mu_I^2)$ is related to the absorbtive part of the hard collinear quark propagator $\mathcal{G}_P$,

$$\langle 0 | T \left[W_n^\dagger \xi_n(z) \bar{\xi}_n W_n(0) \right] | 0 \rangle = i \frac{\not{n}}{\sqrt{2}} \int \frac{d^4k}{(2\pi)^4} e^{-ikz} \mathcal{G}_P(k) \ . \tag{5.12}$$

where ξ_n is a collinear quark field and W_n is a Wilson line along the light-cone direction $\bar{n}$ ($n^2 = \bar{n}^2 = 0, \bar{n} \cdot n = 1$). A hard collinear quark has momentum $p + k$, where p is the so-called label momentum with $p^+ \sim Q$ and k is a hard residual momentum with components of order $Q(1, \lambda^2, \lambda)$. Therefore, the virtuality of the hard-collinear quark is $2p \cdot k \sim \lambda^2 Q^2$, consistent with that of the hadron final state. The jet function has no infrared divergences because the hadron final states are summed over. However, it does have light-cone divergences which are handled by the standard minimal subtraction method. An important feature of the jet function is that it is only sensitive to physics at scale μ_I^2. In fact, at one-loop order, the jet function reproduces the $\mathcal{M}_N$ function in the previous section.

The soft contribution in Eq. (12) is defined in terms of the soft Wilson lines [119]: $Y_n(x) = \mathcal{P}\exp[-ig\int_{-\infty}^{x} dsn\cdot A_{\rm us}]$ and $\widetilde{Y}_n(x) = \overline{\mathcal{P}}\exp[-ig\int_{x}^{\infty} dsn\cdot A_{\rm us}]$, where $A_{\rm us}$ are the so-called ultra-soft gluons with momentum $Q(\lambda^2,\lambda^2,\lambda^2)$ and $\mathcal{P}$ stands for path ordering [the sign convention for the gauge coupling is $D^\mu = \partial^\mu + igA^\mu$],

$$S(x,\mu_I^2) = \frac{1}{N_c}\left\langle 0\left|{\rm Tr}\left[Y_{\bar n}{}^\dagger \tilde Y_n \delta\left(1-x+\frac{n\cdot i\partial}{n\cdot p}\right)\tilde Y_n^\dagger Y_{\bar n}\right]\right|0\right\rangle\ , \tag{5.13}$$

where the ratio in the delta function fixes the momentum of the emitted gluon to be soft (of order λ^2). As such, the soft factor is a non-perturbative contribution.

The collinear contribution,

$$\phi(x,\mu_I^2) = \left\langle P\left|\bar\xi_{\bar n} W_{\bar n}\delta\left(x-\frac{n\cdot\mathcal{P}_+}{n\cdot p}\right)\frac{\not{n}}{\sqrt{2}}W_{\bar n}^\dagger\xi_{\bar n}\right|P\right\rangle \tag{5.14}$$

comes from collinear quarks and gluons with momentum $(1,\lambda^2,\lambda)Q$ and $n\cdot\mathcal{P}_+$ is the total light-cone momentum carried by the partons. In Ref. [109], the collinear contribution was identified as the usual Feynman parton distribution. This, however, is incorrect because the soft gluons with longitudinal momentum $(1-x)Q\sim\lambda^2$ in the proton cannot be included in the collinear contribution according to the definition of the collinear gluons in SCET. On the other hand, the Feynman parton distribution contains a factorizable soft contribution in the limit $x\to 1$ [120, 121]. Further discussion on this issue will be made in the next subsection as well as in the next section. The correct approach is to combine the soft and collinear contributions together to get the correct Feynman parton distribution in the $x\to 1$ limit.

Thus EFT arguments lead finally to the following refactorization, valid when $(1-x)Q\sim\Lambda_{\rm QCD}$ at leading order in $1-x$,

$$F_1^N(Q^2) = C^2(Q^2/\mu_I^2)J_P(Q^2/N\mu_I^2)q_N(\mu_I^2) + \mathcal{O}(1-x), \tag{5.15}$$

where $q_N(\mu_I^2)$ is the moment of the quark distribution, and the jet function is exactly the $\mathcal{M}_N$ function introduced in the previous section. Although formally this factorization is made at μ_I^2, the product of factors is independent of it. The claim of non-factorizability of DIS in this very regime in Ref. [110] was criticized in [123]. On the other hand, the above result seems consistent with that of Ref. [113] if used in the same regime.

The above factorization allows us to resum over large logarithms. Since the physical structure function is μ-independent, we can take μ_I in the above expression to whatever value we choose. For example, if one sets $\mu_I^2 = Q^2$, all large logarithms are now included in the jet function. One can derive a renormalization group equation for J_P [112]. Solving this equation leads to a resummation of large logarithms.

Alternatively, with the original scale μ_I^2, there are large logarithms in C, which can be resummed using the renormalization group equation and the anomalous dimension γ_1. The resulting exponential evolution can be regarded as the evolution of the jet function from scale Q^2 to μ_I^2. The parton distribution $q_N(\mu_I)$ runs from μ_I^2 to a certain factorization scale μ_F^2 using the DGLAP evolution [122]. This running generates the logarithms from initial-state parton radiations.

In the above refactorization, no scale $(1-x)Q$ appears explicitly although soft and collinear gluons in SCET do have reference to that scale. This explains that the factorization holds in the region of our interest, namely, when $(1-x)Q \sim \Lambda_{\rm QCD}$.

5.3.2 Collinear Contribution in SCET and Double Counting

SCET is an operator approach designed to take into account contributions from different regions in Feynman integrals. Calculations in SCET are sometimes formal if without a careful definition of regulators for individual contributions. Occasionally, the regulators in different parts must be defined consistently to obtain the correct answer. Otherwise, one can easily lead to double counting. The same issue has been discussed recently in Ref. [124].

To see the need of consistent regulators in SCET, let us consider the usual quark distribution in the proton. In the full QCD, the quark distribution is defined as

$$q(x) = \frac{1}{2}\int \frac{d\lambda}{2\pi} e^{i\lambda x} \langle P|\overline{\psi}(\lambda n)\ \not{n} e^{-ig\int_0^\lambda d\lambda' n\cdot A(\lambda' n)}\psi(0)|P\rangle\ , \tag{5.16}$$

where $\psi(x)$ and $A(\lambda n)$ are full QCD quark and gluon fields (here we use the vector n with mass-dimension 1). Now suppose the nucleon is moving with a high momentum Q in the z direction. The quarks and gluons in the proton, in general, have large k^+, and small momentum k^- and $k_\perp$, in the sense that they are collinear to the proton momentum. Therefore, one may match the full QCD fields in the above expression to the corresponding collinear fields in SCET.

However, the procedure is incomplete for wee gluons with $(1-x) \sim \Lambda/Q$. Such a gluon has a soft longitudinal momentum and is definitely included in the above gauge link. The QCD factorization theorem shows that soft gluons do not make a singular contribution to the parton density, but it does not exclude the non-singular wee gluon contributions of type $[\ln^k(1-x)/(1-x)]_+$. In fact, the wee gluon effect in

the $x \to 1$ limit can be factorized out into a soft factor $S(x)$, which is responsible for the large-x behavior of the parton distribution [120, 121]. Therefore, in SCET it is natural to express $q(x)$ in terms of the product of the soft factor and true collinear gluon contribution.

In Ref. [109], the evolution equation was derived for the collinear contribution $\phi(x)$ and is found to be the same as the DGLAP evolution, even in the $x \to 1$ limit. This could be the main motivation to identify $\phi(x)$ as $q(x)$. However, the collinear gluons in the one-loop Feynman diagrams can no longer be considered as "collinear" if $(1-x)Q \sim \Lambda_{\rm QCD}$, and must be subtracted explicitly. This subtraction was not made through certain regulators and hence there is a double counting. In fact, once the soft-gluons are subtracted, a collinear parton jet shall not have singularity in the limit $x \to 1$. Likewise, the calculation of the soft-factor in Ref. [109] should have a soft transverse-momentum cutoff to include just the true soft gluons. Thus, the regulators in the soft and collinear contributions must be made consistently to avoid double counting. A consistent scheme of defining the soft and collinear contributions for a parton distribution defined with off light-cone gauge link can be found in Ref. [120]. We will present another example of a consistent regularization in the following section.

5.4 ReFactorization: Intuitive Approach

The EFT approach for refactorization is gauge-invariant and all factors are defined at separate scales. The resummation is of the simple renormalization-group

type. However, the physical origin of the large logarithms is not entirely transparent. For example, it is well known in QED that the double infrared logarithms are generated from soft radiations from jet-like lines. This is not obvious in the EFT approach.

In the approach introduced by Sterman and others [114], the structure functions are factorized into different factors which have clear physical significance, although each factor now contains multi-scales. Explicit equations can be derived to bridge the scales within these factors, which allow one to resum large logarithms. The main shortcoming of this intuitive approach is the introduction of a spurious scale $(1-x)Q$ in each factor, which make them nonperturbative in the kinematic region of our interest.

In this section, we first briefly review Sterman's approach in subsection A. We then introduce in subsection B a more general factorization approach along this direction, which involves a rapidity cutoff. With an appropriate cutoff, we arrive at a picture similar to that of EFT. The example also shows that a consistent soft subtraction must be made to obtain a correct factorization.

5.4.1 Sterman's Method

Consider the lepton-nucleon DIS process in the Breit frame in which the initial and final partons have similar momentum but move in opposite directions. In the region $x \to 1$, the final hadron state consists of a high-energy jet plus soft gluon radiations. A so-called reduced diagram is shown in Fig. 1, showing the space-time

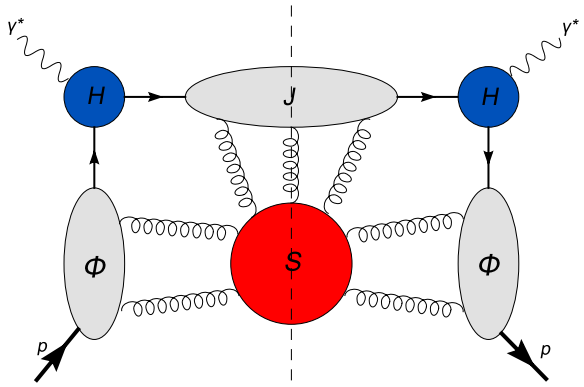

Figure 5.1: The leading reduced diagram contributing to the deep-inelastic structure function in $x \to 1$ regime.

picture of the process. There are in principle four different scales which are relevant: virtual photon mass Q^2, final-hadron invariant mass $(1-x)Q^2$, the soft parton energy radiated off the proton $(1-x)Q$, and finally the genuine nonperturbative QCD scale $\Lambda_{\rm QCD}$.

According to the analysis in Ref. [114], the reduced diagram can be factorized into various physically intuitive contributions, and the structure function can be expressed as a product of a soft factor, a final-state jet function, and a parton distribution,

$$F_1(x,Q^2) = H(Q^2)\int_x^1 \frac{dy}{y}\phi(y)\int_0^{y-x}\frac{dw}{1-w}S(w)J(x,y,w)\ . \tag{5.17}$$

The parton distribution $\phi(x)$ is not the usual gauge-invariant one on the light-cone. Rather it is defined as

$$\phi(y) = \frac{1}{2p^+}\int\frac{d\lambda}{2\pi}e^{-iy\lambda}\langle P|\overline{q}(\lambda n)\gamma^+ q(0)|P\rangle\ , \tag{5.18}$$

in $A^z = 0$ gauge, or equivalently there are gauge links along the z direction going from the quark positions to infinity. Because it is not truly gauge-invariant, it is

frame-dependent. In particular, it can depend on the soft parton energy $(1-x)Q$. This parton distribution contains contributions of both collinear and soft gluon radiations form the initial state quark, thus involving double logarithms.

Likewise, the jet function is defined as

$$J \sim \text{Disc} \int \frac{d^4x}{(2\pi)^4} e^{-ixl} \langle 0|T\left[\overline{q}(x)q(0)\right]|0\rangle \tag{5.19}$$

and normalized to $\delta(1-x)$ at the leading order. Once again the jet is defined in the axial gauge and is frame dependent. In particular, it depends on the infrared scale $(1-x)Q$ as well. However, this jet function contains no true infrared divergences. It accounts for the collinear and soft radiations from the jet final state.

Finally, the soft function S is defined as the matrix element of Wilson lines first going along the $\bar{n}$ direction from $-\infty$ along the light-cone, then going along n direction to $+\infty$. The collinear divergences are regularized by $A^z = 0$ gauge. Therefore, it contains no true infrared divergences.

In the moment space, the refactorization appears in a simple form,

$$F_1^N(Q^2) = H(Q^2/\mu^2)\phi_N(Q^2/\mu^2)S_N(Q^2/\mu^2)J_N(Q^2/\mu^2)\ , \tag{5.20}$$

and H stands for the hard contribution which comes only from virtual diagrams. Again, we emphasize that the factorization follows intuitively from the space-time picture of the reduced diagrams. However, one pays a price for this: the breaking of Lorentz invariance and introduction of a new scale $(1-x)Q$. When this scale becomes of order $\Lambda_{\rm QCD}$, as this is the main interest of the paper, all factors becomes nonperturbative in principle. On the other hand, the scale $(1-x)Q$ is spurious, it

should be cancelled out. It is unclear how this is achieved at the nonperturbative level.

The physics of the above factorization is best seen through a one-loop calculation. The parton distribution is

$$\phi(x) = \frac{\alpha_s}{\pi} C_F \left\{ -\frac{1}{\epsilon} P_{qq}(x) + \left[\left(2D_1 + D_0 \ln \frac{Q^2}{\mu^2} \right) - D_0 - \left(\frac{\pi^2}{6} + 1 \right) \delta(1-x) \right] \right\} , \tag{5.21}$$

where $P_{qq}(x)$ is the quark splitting function and

$$D_i \equiv \left[\frac{\ln^i (1-x)}{1-x} \right]_+ \quad i = 0, 1, 2.... \tag{5.22}$$

Apart from the divergent term which is the same as the Feynman parton distribution, there are extra constant terms which absorb the soft-collinear gluon contribution. Some of these come from the scale $(1-x)^2 Q^2$. In moment space, we have

$$\phi_N(x) = 1 + \frac{\alpha_s}{4\pi} C_F \left[-\frac{1}{\epsilon} (3 - 4 \ln \overline{N}) + \ln^2 \frac{Q^2}{\overline{N}^2 \mu^2} - 2 \ln \frac{Q^2}{\overline{N}^2 \mu^2} - \ln^2 \frac{Q^2}{\mu^2} + 2 \ln \frac{Q^2}{\mu^2} - 4 \right] . \tag{5.23}$$

One may view the double logarithmic terms as from the initial state radiation. The large logarithms resulting from large scale differences can be summed through an x-space evolution equation [114].

The one-loop jet function is explicit finite,

$$\begin{aligned} J(x) &= \delta(1-x) + \frac{\alpha_s}{4\pi} C_F \left[4 \left(D_1 + D_0 \ln \frac{Q^2}{\mu^2} \right) - 4 \left(2D_1 + D_0 \ln \frac{Q^2}{\mu^2} \right) - 7 D_0 \right. \\ &\quad \left. + \left(3 - 3 \ln \frac{Q^2}{\mu^2} \right) \delta(1-x) \right] , \end{aligned} \tag{5.24}$$

which involves physics at both scales $(1-x)^2 Q^2$ and $(1-x) Q^2$. Both type terms generate double logarithms, corresponding to the radiations from the jet. In moment

space, the jet function becomes,

$$J_N = 1 + \frac{\alpha_s}{4\pi} C_F \left[-\ln^2 \frac{Q^2}{\overline{N}^2 \mu^2} + 2 \ln \frac{Q^2}{\overline{N}^2 \mu^2} + 2 \ln^2 \frac{Q^2}{\overline{N} \mu^2} - 3 \ln \frac{Q^2}{\overline{N} \mu^2} \right.$$
$$\left. -4 \ln \frac{Q^2}{\overline{N}^2 \mu^2} - \ln^2 \frac{Q^2}{\mu^2} + 3 - \frac{\pi^2}{3} \right] . \tag{5.25}$$

Again the large logs can be resummed through an evolution equation for J [114].

The soft function is also finite and at one-loop;

$$S(x) = \delta(1-x) + \frac{\alpha_s}{\pi} C_F \left[2D_0 + \left(\ln \frac{Q^2}{\mu^2} \right) \delta(1-x) \right] , \tag{5.26}$$

which contains physics at scale $(1-x)^2 Q^2$, generating a single logarithm. In the moment space, it is

$$S_N = 1 + \frac{\alpha_s}{\pi} C_F \ln \frac{Q^2}{\overline{N}^2 \mu^2} . \tag{5.27}$$

Here the collinear singularity is regulated by gauge fixing.

When summing over the jet, parton distribution and soft contribution, the soft scale $(1-x)^2 Q^2$ dependence cancels. We are left with only the physical scale $(1-x)Q^2$. All the factors introduced above are sufficient to factor away the singular contributions in the structure function at $x \to 1$ limit. In fact, at one-loop

$$F_1^{(1)}(x, Q^2) - (\phi^{(1)}(x) + J^{(1)}(x) + S^{(1)}(x)) = \frac{\alpha_s}{2\pi} C_F \left[-4 + \ln \frac{Q^2}{\mu^2} \right] \delta(1-x) , \tag{5.28}$$

which contains only the δ-function singularity. Therefore, the large double logarithms have been absorbed either into the parton distribution or the jet function. This is, in fact, the purpose of the intuitive refactorization approach: The double logarithms from the initial and final state radiations are made explicit through factorization.

However, because of the presence of the extra scale $(1-x)Q$, the above refactorization is not very useful in the region of our interest because all factors, except H, become nonperturbative.

5.4.2 Alternative Regulator, Consistent Subtraction and Relation to SCET Factorization

In defining various contributions in Sterman's approach, the gauge choice $A^z = 0$ is made, or equivalently gauge links along the z-direction are added to operators to make them gauge invariant. This choice of a non-light-like gauge can serve in addition as a regulator for collinear divergences arising from gauge links going along the light-cone direction, as can be seen from the one-loop the soft factor, Eq. (5.27).

In this subsection we present an alternative method to arrive at the correct factorization formula with factors that are manifestly gauge invariant. We regulate collinear divergences by choosing gauge links slightly off the light-cone (for more discussion of off-light-cone gauge links see [120, 125, 121].) The direction of a gauge link supports a finite rapidity which can serve as a rapidity cutoff, thereby avoiding light-cone singularities which appear in calculations of scaleless quantities like the parton distribution and which cannot be regularized by dimensional regularization [126]. We show that the factorization theorem proposed here is obtained only after proper subtractions of soft factors are made. By choosing the rapidity parameter ρ appropriately, we can eliminate the intermediate scale $(1-x)Q$ and arrive at a factorization similar to that of EFT.

Let $\tilde{v} = (\tilde{v}^+, \tilde{v}^-, 0)$ with $\tilde{v}^+ \gg \tilde{v}^-$ and $v = (v^+, v^-, 0)$ with $v^- \gg v^+$ with $\rho \equiv \tilde{v}^+/\tilde{v}^- = v^-/v^+$. It is assumed below that the incoming quark is collinear in the z direction with momentum $p_1 = (Q/\sqrt{2}, 0, 0)$ and the outgoing quark is collinear in the $-z$ direction with $p_2 = (0, Q/\sqrt{2}, 0)$, and we denote $p^+ = p_1^+ = p_2^- = Q/\sqrt{2}$. We define the soft factor as

$$\begin{aligned} S(1-x) &= \int \frac{d\lambda}{2\pi} e^{i\lambda(1-x)p^+} \langle 0|\mathrm{Tr}[Y_{\tilde{v}}^\dagger(0,-\infty;\lambda\tilde{v}) Y_v^\dagger(\infty,0;\lambda v) \\ &\quad \times Y_v(\infty,0;0) Y_{\tilde{v}}(0,-\infty;0)]|0\rangle \frac{1}{N_c} \end{aligned} \tag{5.29}$$

where Y_v is

$$Y_v(a,b;\xi) = \mathcal{P}\exp\left(-ig\int_b^a d\lambda' v\cdot A(\lambda' v+\xi)\right) , \tag{5.30}$$

Similar definition holds for $Y_{\tilde{v}}$. Thus the soft factor depends on two off-light-cone Wilson lines in the directions of v and $\tilde{v}$. This definition of the soft factor has no collinear divergences. On the other hand, if we take one of the Wilson lines on the light-cone, the resulting light-cone divergence may be considered as the collinear divergence. Then the S factor will include a collinear contribution as discussed in [125]. However, here we are interested in the soft factor that is not contaminated with collinear divergences.

The final state jet function is defined as follows:

$$\tilde{J}(x,Q) = \int \frac{d\lambda}{2\pi} e^{i\lambda(1-x)p^+} \langle 0|W_v^\dagger(\infty,0;\lambda\tilde{v})\psi(\lambda\tilde{v})\overline{\psi}(0)W_v(\infty,0;0)|0\rangle , \tag{5.31}$$

where it involves a Wilson line in the $\tilde{v}$ direction which is taken to be in the (almost) conjugate direction to the out-going partons. It is given by:

$$W_v(a,b;\xi) = \mathcal{P}\exp\left(-ig\int_b^a d\lambda'\tilde{v}\cdot A(\lambda'\tilde{v}+\xi)\right) . \tag{5.32}$$

Finally we define the parton distribution function as

$$\begin{aligned}\tilde{\phi}(x) &= \frac{1}{2p^+}\int\frac{d\lambda}{2\pi}e^{i\lambda xp^+}\langle P|\overline{\psi}(\lambda v)W_{\tilde{v}}^{\dagger}(\infty,0;\lambda v)\\ &\quad\times\gamma^+W_{\tilde{v}}(\infty,0;0)\psi(0)|P\rangle\ ,\end{aligned}\tag{5.33}$$

where the Wilson line is taken along the (almost) conjugate direction of the incoming partons, i.e., in the v direction. Both the jet and parton distribution are in principle defined to absorb just the collinear gluon contributions. Although this can be done by cutoffs in loop integrals, it is difficult to achieve in an operator approach. In fact, it will be clear later that both $\tilde{J}(x)$ and $\tilde{\phi}(x)$ do contain soft contributions as well, which must be subtracted explicitly.

Let us consider the factorization of the DIS structure function at one-loop using the above definitions of the factors. We first calculate the soft factor, jet function, and parton distribution in pQCD. The one-loop soft factor is

$$\begin{aligned}S(1-x) &= \delta(1-x)+\frac{\alpha_s}{2\pi}C_F\left(-2+\frac{\rho^2+1}{\rho^2-1}\ln\rho^2\right)\left(2D_0+\ln\frac{Q^2}{\mu^2}\delta(1-x)\right)\\ &\approx \delta(1-x)+\frac{\alpha_s}{2\pi}C_F\left(-2+\ln\rho^2\right)\left(2D_0+\ln\frac{Q^2}{\mu^2}\delta(1-x)\right)\ ,\end{aligned}\tag{5.34}$$

where the second line is obtained by taking the large ρ^2 limit. The result does not have any soft and collinear divergences. It does have an ultraviolet divergence coming from the cusp of the Wilson lines, which has been subtracted minimally in dimensional regularization. In moment space,

$$S_N = 1+\frac{\alpha_s}{2\pi}C_F\left[2-\ln\rho^2\right]\ln\frac{\mu^2\overline{N}^2}{Q^2}\ .\tag{5.35}$$

The UV-subtracted soft factor obeys the following renormalization group equation

(RGE),

$$\mu\frac{\partial S(1-x,\mu^2)}{\partial\mu} = 2\gamma_S\ S(1-x,\mu^2)\ , \tag{5.36}$$

where the anomalous dimension is

$$\gamma_S = \frac{\alpha_s}{2\pi}C_F(2-\ln\rho^2)\ , \tag{5.37}$$

which depends on the rapidity cutoff ρ and is related to the so-called cusp anomalous dimension [127].

The jet function has no infrared divergences either. At one-loop,

$$\begin{aligned}\tilde{J}(x,Q) &= \delta(1-x)+\frac{\alpha_s}{4\pi}C_F\left[\left(3-2\pi^2-3\ln\frac{Q^2}{\mu^2}+4\ln\rho-2\ln^2\rho\right)\delta(1-x)\right.\\ &\left.-7D_0-4D_1+4\ln\rho\,D_0\right]\ .\end{aligned} \tag{5.38}$$

In moment space, it has a particularly simple form,

$$\tilde{J}_N = 1+\frac{\alpha_s}{4\pi}C_F\left\{3\ln\frac{\overline{N}\mu^2}{Q^2}-2[\ln(\overline{N}\rho)-1]^2+5-\frac{7}{3}\pi^2\right\}\ . \tag{5.39}$$

The wave function renormalization brings in the scale-dependence of the jet function, which therefore obeys the following RGE,

$$\mu\frac{\partial\tilde{J}_N}{\partial\mu} = \gamma_{J,\mu}\tilde{J}_N\ , \tag{5.40}$$

with

$$\gamma_{J,\mu} = \frac{3\alpha_s}{2\pi}C_F\ , \tag{5.41}$$

which is the anomalous dimension of the quark field in axial gauge [128].

The parton distribution at one-loop is,

$$\begin{aligned}\tilde{\phi}(x) &= \delta(1-x)+\frac{\alpha_s}{4\pi}C_F\left\{-\frac{1}{\epsilon}P_{qq}(x)-\left(4+\frac{2\pi^2}{3}\right)\delta(1-x)\right.\\ &\left.+\left(4\ln\frac{Q^2}{\mu^2}+4\ln\rho-4\right)D_0+8D_1\right\}\ ,\end{aligned} \tag{5.42}$$

where the $1/\epsilon$ pole comes from collinear divergences. In moment space we have

$$\tilde{\phi}_N = \frac{\alpha_s}{4\pi}\left\{-\frac{1}{\epsilon}\left[3-4\ln\overline{N}\right]+4\left[-1+\ln\overline{N}+\ln^2\overline{N}-\ln\overline{N}\ln\rho-\ln\overline{N}\ln\frac{Q^2}{\mu^2}\right]\right\} . \tag{5.43}$$

Its UV divergences come from wave function corrections and have been subtracted minimally, and therefore its evolution in μ^2 is the same as that for the jet function.

Because $\tilde{\phi}$ and $\tilde{J}$ contain the soft contribution as well, the structure function F_1 cannot be factorized into $\tilde{\phi}\otimes\tilde{J}\otimes S$ multiplied by a hard contribution, where $\otimes$ is a convolution operator in x-space. Instead, one must define the soft-subtracted version of the parton distribution $\phi=\tilde{\phi}/S$ and jet $J=\tilde{J}/S$. Then the factorization reads:

$$\begin{aligned} F_1(x,Q^2) &= H(Q^2)\otimes J(x,Q^2/\mu^2)\otimes\phi(x,Q^2/\mu^2)\otimes S(x,Q^2/\mu^2)+\mathcal{O}(1-x) \\ &= H(Q^2)\otimes\tilde{J}(x,Q^2/\mu^2)\otimes\tilde{\phi}(x,Q^2/\mu^2)/S(x,Q^2/\mu^2)+\mathcal{O}(1-x) , \end{aligned} \tag{5.44}$$

where $H(Q^2)$ is hard contribution independent of x. This can be easily checked at one-loop level by calculating H,

$$\begin{aligned} H^{(1)}(Q^2) &= F_1^{(1)}(x,Q^2)-\tilde{J}^{(1)}(x,Q^2)-\tilde{\phi}^{(1)}(x,Q^2)+S^{(1)}(x,Q^2) \\ &= \left[1+\frac{\alpha_s}{4\pi}\left(2\ln\frac{Q^2}{\mu^2}+4\ln\frac{Q^2}{\mu^2}\ln\rho+2\ln^2\rho-4\ln\rho-8+2\pi^2\right)\right]\delta(1-x) \end{aligned} \tag{5.45}$$

which is indeed independent of $D_i(x)$. All singular contributions of type $1/(1-x)_+$ have been subtracted from the structure function F_1 by the jet, soft factor and parton distribution. We emphasize that this is possible only when the soft contributions

to the jet and parton distributions have been subtracted first. The anomalous dimension of the hard part is

$$\gamma_H \equiv \frac{\mu}{H}\frac{dH}{d\mu} = -\frac{\alpha_s}{\pi}C_F\big(2\ln\rho+1\big)\ , \tag{5.46}$$

which is ρ-dependent.

The above factorization uses the rapidity cutoff parameter ρ, which has the similar role as the renormalization scale μ^2: Every factor is a function of it, but the product has no dependence. Therefore, one can get different pictures of refactorization by choosing different value of ρ. For instance, if one takes $\rho \to \infty$, all gauge links move back to the light-cone. Here collinear divergences shows up in different factors which have to be subtracted beforehand to yield a meaningful factorization. Distribution $\tilde{\phi}$ corresponds to the physical quark distribution $q(x)$. The subtraction of the soft contribution in $\tilde{J}(x)$ ensures $J(x)$ have collinear contributions only. Thus factorization can be written as

$$F_1(x,Q^2) = H(Q^2)\otimes J(x,Q^2/\mu^2)\otimes\tilde{\phi}(x,Q^2/\mu^2)+\mathcal{O}(1-x) \tag{5.47}$$

which is heuristically similar to Eq. (15)

One can also take $\rho = -1$. Then $\tilde{J}(x) = J_{\rm st}(x)$, and $\tilde{\phi}(x) = \phi_{\rm st}(x)$ and $S(x) = S_{\rm st}^{-1}(x)$, where quantities with subscripts "st" refer to those in the previous subsection. Eq. (44) then reproduces the factorization Eq. (20) from Ref. [114].

We can also make contact with the EFT approach by taking ρ to be small although it shall be considered as large in principle. Consider the moment of $\phi(x) =$

$\tilde{\phi}(x)/S$,

$$\phi_N = 1 + \frac{\alpha_s}{4\pi} C_F \left\{ -\frac{1}{\epsilon} \left[3 - 4 \ln \overline{N} \right] + 4 \left[1 - \ln(\overline{N}\rho) \right] \ln \frac{Q^2}{\overline{N}\mu^2} - 4 \right\} , \qquad (5.48)$$

where the finite part depends on a single logarithm $\ln \frac{Q^2}{\overline{N}\mu^2}$, i.e., the scale $(1-x)Q$. In the leading-logarithmic approximation, if ρ is taken to be $1/\overline{N}$, the distribution $\phi(x)$ no longer depends on scale $(1-x)Q$. The anomalous dimension of the distribution $\phi(x)$ is

$$\gamma_{\phi,\rho} \equiv \frac{\mu}{\phi_N} \frac{d\phi_N}{d\mu} = \frac{\alpha_s}{2\pi} C_F (-1 + 4 \ln \rho) . \qquad (5.49)$$

With $\rho \sim 1/\overline{N}$, the evolution equation for $\phi(x)$ is similar to that of the light-cone quark distribution $q(x)$.

Now let us examine the refactorization in the following form,

$$F_1^N(Q^2) = H(Q^2/\mu^2, \rho) \otimes \tilde{J}_N(Q^2/\mu^2, \rho) \otimes \phi_N(Q^2/\mu^2, \rho)|_{\rho \sim 1/\overline{N}} + \mathcal{O}(1-x) , \quad (5.50)$$

Taking $\mu^2 = \mu_I^2 = Q^2/N$, the jet factor $\tilde{J}_N$ in Eq. (39) does not contain any large logarithms. The hard factor $H(Q^2/\mu^2)$ contains large logarithms that can be resummed. The resummation generates exactly the evolution of the matching coefficient C^2 for the product of effective currents in SCET. Therefore, the above form of factorization exactly reproduces the SCET result in Eq. (15).

5.5 Summary

In this paper, we considered deep-inelastic scattering in a region $(1-x)Q \sim \Lambda_{\rm QCD}$ where the standard pQCD factorization is not supposed to work. We argued, however, there is nothing that invalidates it in the new regime in leading order $1-x$

because the Lorentz invariant factorization does not involve this soft scale in the sense that there are no new infrared divergences associating with this scale.

We then discussed refactorization of the coefficient function. The EFT approach maintains Lorentz invariance and hence allows a form of refactorization which is valid in the new regime. However, in the traditional approach in which jets and parton distributions are defined to take into account explicitly the double-logarithmic soft radiations, the scale $(1-x)Q$ does appear in various factors, making them nonperturbative in nature. We consider a more general factorization in this spirit which involves a rapidity cutoff. We showed how the EFT result can be reproduced through choices of this cutoff. The example also shows how to make consistent subtraction of the soft contribution in collinear matrix elements.

Appendix A

Noether Current with Higher Order Derivatives

The effective theory Lagrangian usually contains higher order derivatives of the field and is not suitable to apply the well-known Euler-Lagrangian equation and Noether current formulas immediately, since they all imply that the Lagrangian is a function of the field and its first order derivatives only. One can get the modified equation of motion and Noether current formula by defining $\partial\phi$ as an auxiliary field or work from the basics. We give out the general result for $\mathcal{L} = \mathcal{L}(\phi, \partial^\mu\phi, \partial^\mu\partial^\nu\phi)$ here since it is most relevant to our calculation.

We will use a shorthand notation defined as:

$$\mathcal{L}_\alpha \equiv \frac{\partial\mathcal{L}}{\partial\phi^\alpha}; \;\; [\mathcal{L}_\alpha]^\mu \equiv \frac{\partial\mathcal{L}}{\partial(\partial_\mu\phi^\alpha)}; [\mathcal{L}_\alpha]^{\mu\nu} \equiv \frac{\partial\mathcal{L}}{\partial(\partial_\mu\partial_\nu\phi^\alpha)}; \tag{A.1}$$

The equation of motion will be:

$$\mathcal{L}_\alpha - \partial_\mu[\mathcal{L}_\alpha]^\mu + \frac{1}{2}\partial_\mu\partial_\nu[\mathcal{L}_\alpha]^{\mu\nu} = 0 \tag{A.2}$$

The symmetric energy-momentum tensor $T^{\mu\nu}$ has the form:

$$T^{\mu\nu} = -\mathcal{L}g^{\mu\nu} + [\mathcal{L}_\alpha]^\mu\partial^\nu\phi^\alpha - \frac{1}{2}\partial_\eta[\mathcal{L}_\alpha]^{\mu\eta}\partial^\nu\phi^\alpha + \frac{1}{2}[\mathcal{L}_\alpha]^{\mu\eta}\partial_\eta\partial^\nu\phi^\alpha - \partial_\sigma f^{\mu\sigma\nu}, \tag{A.3}$$

with $f^{\mu\sigma\nu}$ defined as:

$$\begin{aligned} f^{\mu\sigma\nu} \;\equiv\; & \frac{1}{2}\left[([\mathcal{L}_\alpha]^\mu\phi_\beta - \frac{1}{2}\partial_\eta[\mathcal{L}_\alpha]^{\mu\eta}\phi_\beta + \frac{1}{2}[\mathcal{L}_\alpha]^{\mu\eta}\partial_\eta\phi_\beta)(S^{\alpha\beta})^{\sigma\nu} - (\mu \leftrightarrow \sigma) + (\mu \leftrightarrow \nu)\right] \\ & -\frac{1}{2}[\mathcal{L}_\alpha]^{\mu\nu}\partial^\sigma\phi^\alpha + \frac{1}{2}[\mathcal{L}_\alpha]^{\sigma\nu}\partial^\mu\phi^\alpha, \end{aligned} \tag{A.4}$$

in which $(S^{\alpha\beta})^{\sigma\nu}$ is the generator of the Lorentz transformation.

Therefore the angular momentum tensor can be written as:

$$\begin{aligned} \mathcal{M}^{\mu\nu\lambda} &= T^{\mu\lambda}x^{\nu} - T^{\mu\nu}x^{\lambda} \\ M^{ij} &= \int d^3x \mathcal{M}^{0ij}. \end{aligned} \tag{A.5}$$

Appendix B

Leading Chiral-Logarithms in SM Operators

The leading chiral-logarithms in SM operators have been calculated by many authors [66, 65, 69, 70, 79], and for completeness we list the result here. Notice that the results quoted in Eqs. (80) and (81) in [83] contain sign errors. The result for $K^0 \to \pi^0\pi^0$ here is different from that in [66], as pointed out in [82]. Results for $K^0 \to$ *Vacuum* and $K^+ \to \pi^+$ are presented in terms of bare masses and couplings, while for $K^0 \to \pi^0\pi^0$ we use the physical mass.

The operators we use are defined in the main body of the paper (Eqs. 3.58 - 3.65). We first consider the matrix elements between K^0 and the vacuum,

$$\begin{aligned}
\langle 0|\Theta^{(8,1)}|K^0\rangle &= \frac{2i\alpha_1^{(8,1)}}{f}\left[m_\eta^2 L(m_\eta) + 2m_K^2 L(m_K) - 3m_\pi^2 L(m_\pi)\right] \\
&\quad + \frac{4i\alpha_2^{(8,1)}}{f}(m_{K,0}^2 - m_{\pi,0}^2)\left[1 - \frac{1}{12}L(m_\eta) - \frac{3}{2}L(m_K) - \frac{3}{4}L(m_\pi)\right] \qquad \text{(B.1)} \\
\langle 0|\Theta_{1/2}^{(27,1)}|K^0\rangle &= \frac{6i\alpha^{(27,1)}}{f}\left[3m_\eta^2 L(m_\eta) - 4m_K^2 L(m_K) + m_\pi^2 L(m_\pi)\right] , \qquad \text{(B.2)} \\
\langle 0|\Theta_{1/2,A}^{(8,8)}|K^0\rangle &= \frac{12i\alpha^{(8,8)}}{f}\left[L(m_K) - L(m_\pi)\right] , \qquad \text{(B.3)} \\
\langle 0|\Theta_{1/2,S}^{(8,8)}|K^0\rangle &= -\frac{12i\alpha^{(8,8)}}{f}\left[1 - \frac{3}{4}L(m_\eta) - \frac{13}{2}L(m_K) - \frac{7}{4}L(m_\pi)\right] , \qquad \text{(B.4)} \\
\langle 0|\Theta^{(\overline{3},3)}|K^0\rangle &= -\frac{2i\alpha^{(\overline{3},3)}}{f}\left[1 - \frac{1}{12}L(m_\eta) - \frac{3}{2}L(m_K) - \frac{3}{4}L(m_\pi)\right] \qquad \text{(B.5)}
\end{aligned}$$

where f is the bare meson decay constant, and $m_{\pi,0}$,$m_{K,0}$ are bare masses of mesons. Due to the isospin conservation, only $I = 1/2$ part of the operator can contribute.

For $K^+ \to \pi^+$ matrix elements, we apply a common mass m_M for all the

mesons. Therefore the momentum is conserved in the process.

$$\begin{aligned}
\langle\pi^+|\Theta^{(8,1)}|K^+\rangle &= \frac{4m_{M,0}^2}{f^2}\left\{\alpha_1^{(8,1)}\left[1+\frac{1}{3}L(m_M)\right]-\alpha_2^{(8,1)}\left[1+2L(m_M)\right]\right\} \quad \text{(B.6)}\\
\langle\pi^+|\Theta_{3/2}^{(27,1)}|K^+\rangle &= \langle\pi^+|\Theta_{1/2}^{(27,1)}|K^+\rangle\\
&= -\frac{4m_{M,0}^2\alpha^{(27,1)}}{f^2}\left[1-\frac{34}{3}L(m_M)\right]\ , \quad \text{(B.7)}\\
\langle\pi^+|\Theta_{3/2}^{(8,8)}|K^+\rangle &= \frac{4\alpha^{(8,8)}}{f^2}\left[1-8L(m_M)\right]\ , \quad \text{(B.8)}\\
\langle\pi^+|\Theta_{1/2,A}^{(8,8)}|K^+\rangle &= \frac{8\alpha^{(8,8)}}{f^2}\left[1-5L(m_M)\right]\ , \quad \text{(B.9)}\\
\langle\pi^+|\Theta_{1/2,S}^{(8,8)}|K^+\rangle &= \frac{4\alpha^{(8,8)}}{f^2}\left[1-8L(m_M)\right]\ , \quad \text{(B.10)}\\
\langle\pi^+|\Theta^{(\overline{3},3)}|K^+\rangle &= \frac{2\alpha^{(\overline{3},3)}}{f^2}\left[1+2L(m_M)\right]\ . \quad \text{(B.11)}
\end{aligned}$$

This result is useful in lattice calculations where the pion mass can be adjusted through quark mass parameters. The $K^0 \to \pi^0$ matrix elements can be obtained from the above by using,

$$\begin{aligned}
\langle\pi^0|\mathcal{O}_{\Delta I=1/2}|K^0\rangle &= -\sqrt{\frac{1}{2}}\langle\pi^+|\mathcal{O}_{\Delta I=1/2}|K^+\rangle\ ,\\
\langle\pi^0|\mathcal{O}_{\Delta I=3/2}|K^0\rangle &= \sqrt{2}\langle\pi^+|\mathcal{O}_{\Delta I=3/2}|K^+\rangle\ . \quad \text{(B.12)}
\end{aligned}$$

Finally, for $K \to \pi\pi$, we take the limit $m_\pi \to 0$ and keep the kaon mass

dependency only,

$$\langle\pi^0\pi^0|\Theta^{(8,1)}|K^0\rangle = \frac{4i\alpha_1^{(8,1)}m_K^2}{f^3}\left[1-\frac{5}{4}L(m_K)\right] , \tag{B.13}$$

$$\langle\pi^0\pi^0|\Theta_{3/2}^{(27,1)}|K^0\rangle = \frac{8i\alpha^{(27,1)}m_K^2}{f^3}\left[1-\frac{3}{2}L(m_K)\right] , \tag{B.14}$$

$$\langle\pi^0\pi^0|\Theta_{1/2}^{(27,1)}|K^0\rangle = -\frac{4i\alpha^{(27,1)}m_K^2}{f^3}\left[1-15L(m_K)\right] , \tag{B.15}$$

$$\langle\pi^0\pi^0|\Theta_{3/2}^{(8,8)}|K^0\rangle = \frac{8i\alpha^{(8,8)}}{f^3}\left[1+L(m_K)\right] , \tag{B.16}$$

$$\langle\pi^0\pi^0|\Theta_{1/2,A}^{(8,8)}|K^0\rangle = -\frac{8i\alpha^{(8,8)}}{f^3}\left[1-\frac{7}{2}L(m_K)\right] , \tag{B.17}$$

$$\langle\pi^0\pi^0|\Theta_{1/2,S}^{(8,8)}|K^0\rangle = \frac{8i\alpha^{(8,8)}}{f^3}\left[1-\frac{19}{2}L(m_K)\right] . \tag{B.18}$$

Here the physical mass of kaon is used. Note that the weak mass operator, $\Theta_2^{(8,1)}$, will not contribute to the $K\to\pi\pi$ matrix element as being pointed out in [77, 78, 80, 81].

The matrix elements for the final state $|\pi^+\pi^-\rangle$ is related to the above ones simply by

$$\begin{aligned} A_{+-} &= \frac{1}{\sqrt{3}}(A_2+\sqrt{2}A_0) , \\ A_{00} &= \sqrt{\frac{2}{3}}(-\sqrt{2}A_2+A_0) . \end{aligned} \tag{B.19}$$

Compared with the angular momentum relation, the A_0 amplitude has a factor of $-\sqrt{2}$. The minus sign arises from the definition of $\pi^+=(\pi^1+i\pi^2)/\sqrt{2}$ which has a different sign from the usual spherical tensor definition. The $\sqrt{2}$ accounts for the identical particle nature of two π^0's, which is usually accounted from by a factor of $1/2$ in the final state phase space. From the above relation, we derive:

$$\begin{aligned} \langle\pi^+\pi^-|\mathcal{O}_{\Delta I=1/2}|K^0\rangle &= \langle\pi^0\pi^0|\mathcal{O}_{\Delta I=1/2}|K^0\rangle , \\ \langle\pi^+\pi^-|\mathcal{O}_{\Delta I=3/2}|K^0\rangle &= -\frac{1}{2}\langle\pi^0\pi^0|\mathcal{O}_{\Delta I=3/2}|K^0\rangle . \end{aligned} \tag{B.20}$$

Using the relation (B.12) and (B.20), it is easy to check that the result for (8,8) operators is consistent with that in Ref. [70].

Bibliography

[1] E. Rutherford, Phil. Mag. **21**, 669 (1911).

[2] M. Gell-Mann, Phys. Lett. **8**, 214 (1964). G. Zweig, CERN Preprint, number 8182/TH401 (1964) 24p

[3] G. Baum *et al.*, Phys. Rev. Lett. **51**, 1135 (1983).

[4] J. Ashman *et al.* [European Muon Collaboration], Phys. Lett. B **206**, 364 (1988).

[5] J. R. Ellis and R. L. Jaffe, Phys. Rev. D **9**, 1444 (1974) [Erratum-ibid. D **10**, 1669 (1974)].

[6] J. D. Bjorken, Phys. Rev. **148**, 1467 (1966).

[7] B. W. Filippone and X. D. Ji, Adv. Nucl. Phys. **26**, 1 (2001) [arXiv:hep-ph/0101224].

[8] C. Bourrely and J. Soffer, Nucl. Phys. B **445**, 341 (1995) [arXiv:hep-ph/9502261].

[9] G. Altarelli and G. Parisi, Nucl. Phys. B **126**, 298 (1977).

[10] P. G. Ratcliffe, Phys. Lett. B **192**, 180 (1987).

[11] G. Altarelli and G. G. Ross, Phys. Lett. B **212**, 391 (1988); R. D. Carlitz, J. C. Collins and A. H. Mueller, Phys. Lett. B **214**, 229 (1988).

[12] S. Frixione and W. Vogelsang, Nucl. Phys. B **568**, 60 (2000) [arXiv:hep-ph/9908387].

[13] K. Ackerstaff *et al.* [HERMES Collaboration], Nucl. Instrum. Meth. A **417**, 230 (1998) [arXiv:hep-ex/9806008].

[14] A. Deshpande, R. Milner, R. Venugopalan and W. Vogelsang, Ann. Rev. Nucl. Part. Sci. **55**, 165 (2005) [arXiv:hep-ph/0506148].

[15] F. Wang *et al.*, PAC-2005-TPPP022, *Prepared for Particle Accelerator Conference (PAC 05), Knoxville, Tennessee, 16-20 May 2005*

[16] A. A. Sokolov and I. M. Ternov, Phys. Dokl. **8**, 1203 (1964).

[17] G. K. Mallot [COMPASS Collaboration], arXiv:hep-ex/9611016.

[18] W. E. Caswell and G. P. Lepage, Phys. Lett. B **167**, 437 (1986).

[19] P. Chen, X. Ji, Y. Xu and Y. Zhang, arXiv:0909.1560 [hep-ph].

[20] G. T. Bodwin, E. Braaten and G. P. Lepage, Phys. Rev. D **51**, 1125 (1995) [Erratum-ibid. D **55**, 5853 (1997)] [arXiv:hep-ph/9407339].

[21] M. Beneke and V. A. Smirnov, Nucl. Phys. B **522**, 321 (1998) [arXiv:hep-ph/9711391].

[22] P. Labelle, Phys. Rev. D **58**, 093013 (1998) [arXiv:hep-ph/9608491].

[23] A. V. Manohar, Phys. Rev. D **56**, 230 (1997) [arXiv:hep-ph/9701294].

[24] B. Grinstein and I. Z. Rothstein, Phys. Rev. D **57**, 78 (1998) [arXiv:hep-ph/9703298].

[25] T. Kinoshita and M. Nio, Phys. Rev. D **53**, 4909 (1996) [arXiv:hep-ph/9512327].

[26] R. L. Jaffe and A. Manohar, Nucl. Phys. B **337**, 509 (1990).

[27] X. D. Ji, Phys. Rev. Lett. **78**, 610 (1997) [arXiv:hep-ph/9603249].

[28] X. D. Ji, J. Tang and P. Hoodbhoy, Phys. Rev. Lett. **76**, 740 (1996) [arXiv:hep-ph/9510304].

[29] A. Pineda and J. Soto, Phys. Rev. D **59**, 016005 (1999) [arXiv:hep-ph/9805424]; Phys. Rev. D **58**, 114011 (1998) [arXiv:hep-ph/9802365]; N. Brambilla, A. Pineda, J. Soto and A. Vairo, Nucl. Phys. B **566**, 275 (2000) [arXiv:hep-ph/9907240].

[30] M. E. Luke and A. V. Manohar, Phys. Rev. D **55**, 4129 (1997) [arXiv:hep-ph/9610534]; M. E. Luke, A. V. Manohar and I. Z. Rothstein, Phys. Rev. D **61**, 074025 (2000) [arXiv:hep-ph/9910209].

[31] A. H. Hoang, [arXiv:hep-ph/0204299]; N. Brambilla *et al.* [Quarkonium Working Group], [arXiv:hep-ph/0412158].

[32] A. Pineda and J. Soto, Phys. Lett. B **420**, 391 (1998) [arXiv:hep-ph/9711292].

[33] N. Brambilla, D. Gromes and A. Vairo, Phys. Lett. B **576**, 314 (2003) [arXiv:hep-ph/0306107].

[34] A. O. Barut, *Electrodynamics And Classical Theory of Fields And Particles* (Dover Publications, New York 1980).

[35] M. I. Eides, H. Grotch and V. A. Shelyuto, Phys. Rept. **342**, 63 (2001) [arXiv:hep-ph/0002158].

[36] J. Ashman et al., Phys. Lett. B206, 364 (1989); Nucl. Phys. B328, 1.

[37] N. Brambilla, A. Pineda, J. Soto and A. Vairo, Rev. Mod. Phys. **77**, 1423 (2005) [arXiv:hep-ph/0410047].

[38] A. H. Hoang, A. V. Manohar and I. W. Stewart, Phys. Rev. D **64**, 014033 (2001) [arXiv:hep-ph/0102257].

[39] A. V. Manohar and I. W. Stewart, Phys. Rev. Lett. **85**, 2248 (2000) [arXiv:hep-ph/0004018].

[40] G. P. Lepage, L. Magnea, C. Nakhleh, U. Magnea and K. Hornbostel, Phys. Rev. D **46**, 4052 (1992) [arXiv:hep-lat/9205007].

[41] G. Bunce, N. Saito, J. Soffer and W. Vogelsang, Ann. Rev. Nucl. Part. Sci. **50**, 525 (2000) [arXiv:hep-ph/0007218].

[42] D. de Florian, R. Sassot, M. Stratmann and W. Vogelsang, Phys. Rev. Lett. **101**, 072001 (2008) [arXiv:0804.0422 [hep-ph]].

[43] P. Chen and X. Ji, Phys. Lett. B **660**, 193 (2008) [arXiv:hep-ph/0612174].

[44] P. Y. Chen, X. Ji, and Y. Zhang, to be published.

[45] R. L. Jaffe, Phys. Lett. B **365**, 359 (1996) [arXiv:hep-ph/9509279].

[46] A. Manohar, private commmunication.

[47] B. R. Holstein, Am. J. Phys. **73**, 333 (2004).

[48] J. H. Christenson, J. W. Cronin, V. L. Fitch and R. Turlay, Phys. Rev. Lett. **13**, 138 (1964).

[49] A. Alavi-Harati *et al.* [KTeV Collaboration], Phys. Rev. D **67**, 012005 (2003) [Erratum-ibid. D **70**, 079904 (2004)] [arXiv:hep-ex/0208007]; J. R. Batley *et al.* [NA48 Collaboration], Phys. Lett. B **544**, 97 (2002) [arXiv:hep-ex/0208009]; G. D. Barr *et al.* [NA31 Collaboration], Phys. Lett. B **317**, 233 (1993); L. K. Gibbons *et al.*, Phys. Rev. Lett. **70**, 1203 (1993).

[50] W.-M.Yao et al. (Particle Data Group), J. Phys. G 33, 1 (2006) and 2007 partial update for the 2008 edition

[51] L. Wolfenstein, Phys. Rev. Lett. **13**, 562 (1964).

[52] M. Kobayashi and T. Maskawa, Prog. Theor. Phys. **49**, 652 (1973).

[53] A. J. Buras and M. Jamin, JHEP **0401**, 048 (2004) [arXiv:hep-ph/0306217].

[54] M. Ciuchini and G. Martinelli, Nucl. Phys. Proc. Suppl. **99B**, 27 (2001) [arXiv:hep-ph/0006056].

[55] M. Ciuchini, Nucl. Phys. Proc. Suppl. **59**, 149 (1997) [arXiv:hep-ph/9701278].

[56] S. Bertolini, J. O. Eeg and M. Fabbrichesi, Phys. Rev. D **63**, 056009 (2001) [arXiv:hep-ph/0002234].

[57] E. Pallante, A. Pich and I. Scimemi, Nucl. Phys. B **617**, 441 (2001) [arXiv:hep-ph/0105011].

[58] T. Hambye, G. O. Kohler, E. A. Paschos and P. H. Soldan, Nucl. Phys. B **564**, 391 (2000) [arXiv:hep-ph/9906434].

[59] S. Bosch, A. J. Buras, M. Gorbahn, S. Jager, M. Jamin, M. E. Lautenbacher and L. Silvestrini, Nucl. Phys. B **565**, 3 (2000) [arXiv:hep-ph/9904408].

[60] L. Maiani and M. Testa, Phys. Lett. B **245**, 585 (1990).

[61] C. W. Bernard, T. Draper, G. Hockney and A. Soni, Nucl. Phys. Proc. Suppl. **4**, 483 (1988).

[62] S. Aoki *et al.* [JLQCD Collaboration], Phys. Rev. D **58**, 054503 (1998) [arXiv:hep-lat/9711046].

[63] C. Dawson, G. Martinelli, G. C. Rossi, C. T. Sachrajda, S. R. Sharpe, M. Talevi and M. Testa, Nucl. Phys. B **514**, 313 (1998) [arXiv:hep-lat/9707009].

[64] M. F. L. Golterman and K. C. L. Leung, Phys. Rev. D **58**, 097503 (1998) [arXiv:hep-lat/9805032].

[65] J. Bijnens, H. Sonoda and M. B. Wise, Phys. Rev. Lett. **53**, 2367 (1984).

[66] J. Bijnens, Phys. Lett. B **152**, 226 (1985).

[67] M. F. L. Golterman and K. C. L. Leung, Phys. Rev. D **57**, 5703 (1998) [arXiv:hep-lat/9711033].

[68] M. Golterman and E. Pallante, "On the determination of nonleptonic kaon decays from $K \to \pi$ matrix JHEP **0008**, 023 (2000) [arXiv:hep-lat/0006029].

[69] J. Bijnens, E. Pallante and J. Prades, Nucl. Phys. B **521**, 305 (1998) [arXiv:hep-ph/9801326].

[70] V. Cirigliano and E. Golowich, Phys. Lett. B **475**, 351 (2000) [arXiv:hep-ph/9912513].

[71] S. Bertolini, M. Fabbrichesi and J. O. Eeg, Rev. Mod. Phys. **72**, 65 (2000) [arXiv:hep-ph/9802405].

[72] G. Buchalla, A. J. Buras and M. E. Lautenbacher, Rev. Mod. Phys. **68**, 1125 (1996) [arXiv:hep-ph/9512380].

[73] A. J. Buras, arXiv:hep-ph/9806471.

[74] G. Ecker and W. Grimus, Nucl. Phys. B **258**, 328 (1985). J. M. Frere, J. Galand, A. Le Yaouanc, L. Oliver, O. Pene and J. C. Raynal, Phys. Rev. D **46**, 337 (1992).

[75] C. W. Bernard and M. F. L. Golterman, Phys. Rev. D **46**, 853 (1992) [arXiv:hep-lat/9204007]; C. W. Bernard and M. F. L. Golterman, Phys. Rev. D **49**, 486 (1994) [arXiv:hep-lat/9306005].

[76] J. Gasser and H. Leutwyler, Nucl. Phys. B **250**, 465 (1985).

[77] J. Bijnens and M. B. Wise, Phys. Lett. B **137**, 245 (1984).

[78] C. W. Bernard, T. Draper, A. Soni, H. D. Politzer and M. B. Wise, Phys. Rev. D **32**, 2343 (1985).

[79] V. Cirigliano and E. Golowich, Phys. Rev. D **65**, 054014 (2002) [arXiv:hep-ph/0109265].

[80] J. Kambor, J. Missimer and D. Wyler, Nucl. Phys. B **346**, 17 (1990).

[81] R. J. Crewther, Nucl. Phys. B **264**, 277 (1986).

[82] M. Buchler, Phys. Lett. B **633**, 497 (2006) [arXiv:hep-ph/0511087].

[83] T. Blum *et al.* [RBC Collaboration], Phys. Rev. D **68**, 114506 (2003) [arXiv:hep-lat/0110075].

[84] R. N. Mohapatra and J. C. Pati, Phys. Rev. D **11**, 566 (1975); R. N. Mohapatra and J. C. Pati, Phys. Rev. D **11**, 2558 (1975); G. Senjanovic and R. N. Mohapatra, Phys. Rev. D **12**, 1502 (1975); Phys. Rev. D **23**, 165 (1981); For a review, Rabindra N. Mohapatra, *CP Violation*, World Scientific Publ. Co., C. Jarlskog, Ed., 1989.

[85] J. J. Heckman, C. Vafa, H. Verlinde and M. Wijnholt, JHEP **0806**, 016 (2008) [arXiv:0711.0387 [hep-ph]].

[86] Z. Chacko, H. S. Goh and R. Harnik, Phys. Rev. Lett. **96**, 231802 (2006) [arXiv:hep-ph/0506256]. Z. Chacko, H. S. Goh and R. Harnik, JHEP **0601**, 108 (2006) [arXiv:hep-ph/0512088].

[87] G. Beall, M. Bander and A. Soni, Phys. Rev. Lett. **48**, 848 (1982).

[88] Y. Zhang, H. An, X. Ji and R. N. Mohapatra, Phys. Rev. D **76**, 091301 (2007) [arXiv:0704.1662 [hep-ph]].

[89] Y. Zhang, H. An, X. Ji and R. N. Mohapatra, Nucl. Phys. B **802**, 247 (2008) [arXiv:0712.4218 [hep-ph]].

[90] M. A. Shifman, A. I. Vainshtein and V. I. Zakharov, Sov. Phys. JETP **45**, 670 (1977) [Zh. Eksp. Teor. Fiz. **72**, 1275 (1977)].

[91] G. Buchalla, A. J. Buras and M. K. Harlander, Nucl. Phys. B **337**, 313 (1990).

[92] D. Pekurovsky and G. Kilcup, Phys. Rev. D **64**, 074502 (2001) [arXiv:hep-lat/9812019].

[93] H. Burkhardt *et al.* [NA31 Collaboration], Phys. Lett. B **206**, 169 (1988); V. Fanti *et al.* [NA48 Collaboration], Phys. Lett. B **465**, 335 (1999) [arXiv:hep-

ex/9909022]; A. Alavi-Harati *et al.* [KTeV Collaboration], Phys. Rev. Lett. **83**, 22 (1999) [arXiv:hep-ex/9905060].

[94] E. Pallante and A. Pich, Phys. Rev. Lett. **84**, 2568 (2000) [arXiv:hep-ph/9911233]. E. Pallante, A. Pich and I. Scimemi, Nucl. Phys. B **617**, 441 (2001) [arXiv:hep-ph/0105011].

[95] J. Pumplin, D. R. Stump, J. Huston, H. L. Lai, P. Nadolsky and W. K. Tung, QCD JHEP **0207**, 012 (2002); X. D. Ji, Phys. Rev. Lett. **74**, 1071 (1995).

[96] B. Adeva *et al.* [Spin Muon Collaboration (SMC)], Phys. Rev. D **70**, 012002 (2004); E. S. Ageev *et al.* [COMPASS Collaboration], Phys. Lett. B **633**, 25 (2006); A. Airapetian *et al.* [HERMES Collaboration], high Phys. Rev. Lett. **84**, 2584 (2000); K. Boyle [PHENIX Collaboration] arXiv:nucl-ex/0606008; B. Abelev [STAR Collaboration] arXiv:hep-ex/0608030.

[97] G. Bunce, N. Saito, J. Soffer and W. Vogelsang, Ann. Rev. Nucl. Part. Sci. **50**, 525 (2000) [arXiv:hep-ph/0007218].

[98] J. Blumlein and H. Bottcher, Nucl. Phys. B **636**, 225 (2002) [arXiv:hep-ph/0203155].

[99] M. Gluck, E. Reya, M. Stratmann and W. Vogelsang, Phys. Rev. D **63**, 094005 (2001) [arXiv:hep-ph/0011215].

[100] M. Hirai, S. Kumano and N. Saito [Asymmetry Analysis Collaboration], Phys. Rev. D **69**, 054021 (2004) [arXiv:hep-ph/0312112].

[101] J. Jalilian-Marian and Y. V. Kovchegov, Prog. Part. Nucl. Phys. **56**, 104 (2006) [arXiv:hep-ph/0505052].

[102] R. L. Jaffe and A. Manohar, Nucl. Phys. B **337**, 509 (1990).

[103] R. L. Jaffe, Phys. Lett. B **365**, 359 (1996) [arXiv:hep-ph/9509279].

[104] V. Barone, T. Calarco and A. Drago, Phys. Lett. B **431**, 405 (1998) [arXiv:hep-ph/9801281].

[105] A. V. Manohar, Phys. Rev. Lett. **66**, 289 (1991).

[106] M. Hirai, S. Kumano and N. Saito, data Phys. Rev. D **74**, 014015 (2006) [arXiv:hep-ph/0603213].

[107] G. Altarelli and G. G. Ross, Phys. Lett. B **212**, 391 (1988); R. D. Carlitz, J. C. Collins and A. H. Mueller, Phys. Lett. B **214**, 229 (1988).

[108] J. C. Collins, D. E. Soper and G. Sterman, Perturbative Quantum Chromodynamics, in A. H. Mueller (Ed.), World Scientific, Singapore, 1989, p. 1.

[109] J. Chay and C. Kim, [arXiv:hep-ph/0511066].

[110] B. D. Pecjak, JHEP **0510**, 040 (2005).

[111] C. W. Bauer, S. Fleming, D. Pirjol and I. W. Stewart, Phys. Rev. D **63**, 114020 (2001); C. W. Bauer, D. Pirjol and I. W. Stewart, Phys. Rev. D **65**, 054022 (2002); C. Chay, C. Kim, Phys. Rev. D **65**, 114016 (2002).

[112] A. V. Manohar, Phys. Rev. D **68**, 114019 (2003).

[113] T. Becher and M. Neubert, [arXive:hep-ph/0605050].

[114] G. Sterman, Nucl. Phys. B **281**, 310 (1987).

[115] A. Idilbi, X. Ji, J-P. Ma, and F. Yuan, Phys. Rev. D **73**, 077501 (2006).

[116] A. Idilbi, X. Ji, and F. Yuan, [arXive:hep-ph/0605068].

[117] A. Idilbi, X. Ji, and F. Yuan, Phys. Lett. B **625**, 253 (2005).

[118] A. Vogt, S. Moch, and J. A. M. Vermaseren, Nucl. Phys. B **691**, 129 (2004).

[119] J. Chay, C. Kim, Y. G. Kim, and J. Lee, Phys. Rev. D **71**, 056001 (2005).

[120] G. P. Korchemsky, Mod. Phys. Lett. A**4** 1257 (1989).

[121] X. Ji, J-P. Ma, and F. Yuan, Phys. Rev. D **71**, 034005 (2005).

[122] L. N. Lipatov, Sov. J. Nucl. Phys. **20**, 95 (1975); V. N. Gribov abd L. N. Lipatov, Sov. J. Nucl. Phys. **15**, 438 (1972); G. Altraelli and G. Parisi, Nucl. Phys. B **126**, 298 (1977); Yu. L. Dokshitzer, Sov. Phys. JETP **46**, 641 (1977).

[123] A. V. Manohar, Phys. Lett. B **633**, 729 (2006) [arXiv:hep-ph/0512173].

[124] A. V. Manohar and I. W. Stewart, [arXiv:hep-ph/0605001].

[125] J. C. Collins and F. Hautmann, Phys. Lett. B **472**, 129 (2000).

[126] J. C. Collins and F. V. Tkachov, Phys. Lett. B **294**, 403 (1992).

[127] G. P. Korchemsky and A. .V. Radyushkin, Nucl. Phys. B bf 283, 342 (1987).

[128] E. G. Florates, D. A. Ross, and C. T. Sachrajda,Nucl. Phys. B **129**, 66 (1977).

[129] G. Altarelli, R. K. Ellis, and G. Marinelli, Nucl. Phys. B **157**, 461 (1979).